The Effects of Multiple Retention Basins on the Hydrodynamics in Convergent Tidal Channels

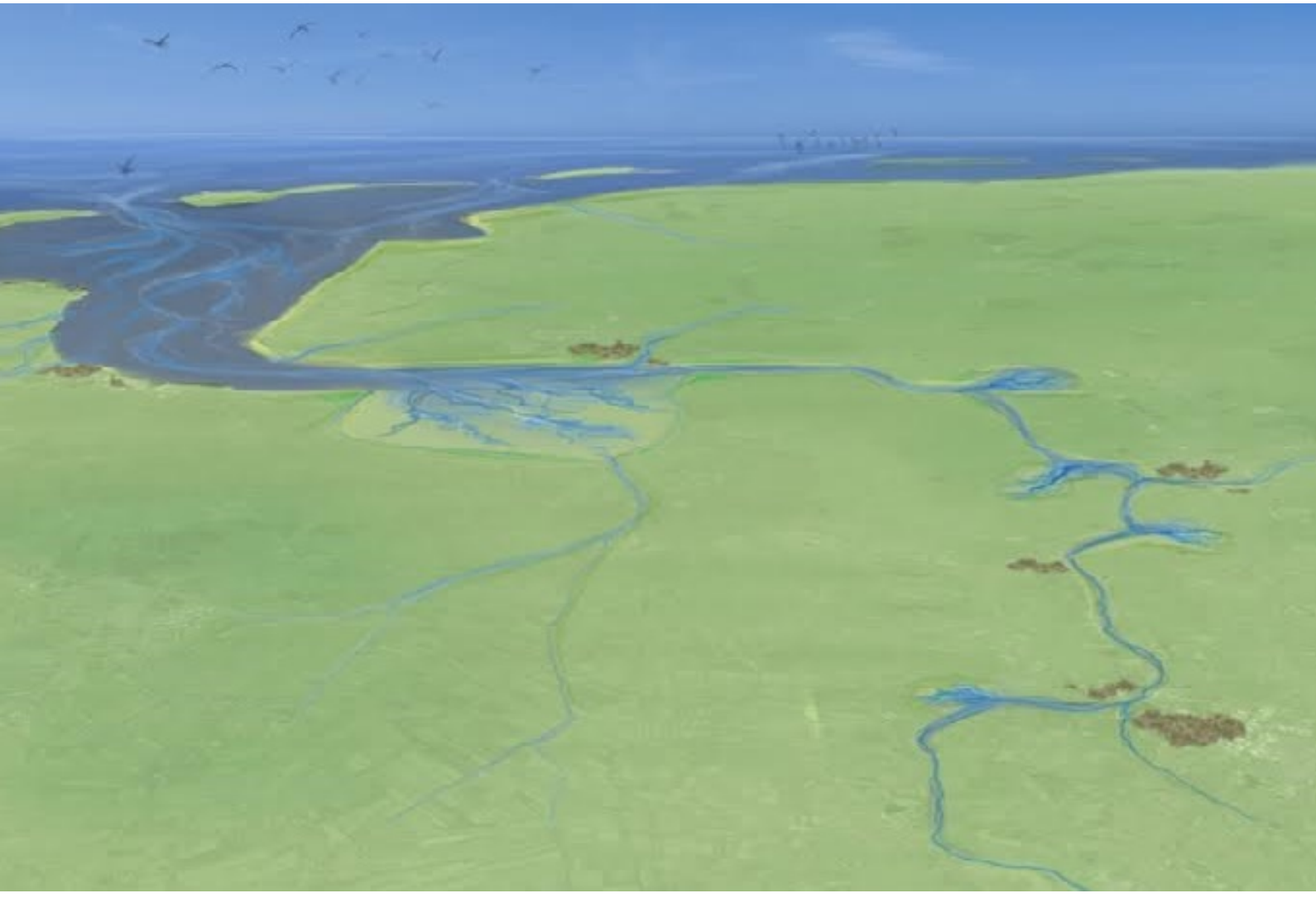

J.H. Damveld BSc

July 2015

Cover illustration: courtesy of Elias van Hoek

UNIVERSITY OF TWENTE.

Faculty of Engineering Technology
Water Engineering & Management
Master's Thesis

The Effects of Multiple Retention Basins on the Hydrodynamics in Convergent Tidal Channels

Author: **J.H. Damveld BSc**
Contact: j.h.damveld@alumnus.utwente.nl

Graduation supervisor: **Prof. dr. S.J.M.H. Hulscher**
(University of Twente)
Daily supervisor: **Dr. ir. P.C. Roos**
(University of Twente)
External supervisor: **Dr. H.M. Schuttelaars**
(Delft University of Technology)

Enschede, 03-07-2015

Abstract

This thesis presents a study into the effects of retention basins in a convergent tidal channel. Such measures are currently considered to be implemented in the Ems-Dollard estuary in order to reduce the tidal range, which has increased dramatically over the past decades. Therefore, the goal of this study is stated as follows.

To explain the effects of multiple retention basins on the tidal dynamics of a convergent tidal channel by analysing the underlying physical mechanisms and to explore the effects of implementing the proposed plans of these basins in the Ems-Dollard estuary.

Model In order to accomplish this, the cross-sectionally averaged linear shallow water equations are used to develop an idealised model. This model consists of subsequent convergent channel sections, while depth is allowed to vary in a stepwise manner between these sections. Forcing is described by a prescribed elevation at the channel mouth. Secondary basins are represented as Helmholtz basins, i.e. basins with a certain area connected to the main channel by a short and narrow linear inlet channel.

Results The effects are presented in terms of the amplitude gain at the channel head, which may show amplification, reduction, or no change at all. The results show that for a single basin in a convergent channel, which is placed increasingly farther away from the channel mouth, more amplitude reduction occurs. Moreover, for basins in supercritically convergent channels, amplification may only occur if placed near the channel mouth. In this regime, channel length is not influencing the response any more. Also in supercritically convergent channels, basins that placed in close proximity of each other will amplify each other's response response.

The difference between various basin sizes is independent of channel convergence, a similar pattern for convergent channels is found as for prismatic channels. However, in the frictional case, 'negative' (supercritically forced) basins can not be observed any more, while 'large' basins shown an amplitude reduction at nearly all locations.

Physical mechanism To explain these results, the physical mechanism has been unravelled. It appears that for convergent channels, the well known quarter wavelength resonance, as seen in prismatic channels, deforms. For increasing convergence, the wavelength for which resonance occurs increases as well, until they become infinitely long for critical convergence. Further increasing convergence will lead to supercritically convergent channels, where only an oscillatory behaviour can be seen, which is in phase with the forcing amplitude.

The mechanism that is responsible for the response of basins is overall similar to that in prismatic channels. Additional waves develop due to a volume transport through the inlet channel, which may trigger waves at either side of the vertex point. For supercritically convergent channels this is not the case, since no 'real' waves can be distinguished in this regime.

Ems-Dollard estuary The model has been calibrated according to historical water levels in order to test its applicability to real world estuaries. The result of the calibration shows that the model is overall well capable of predicting these water levels. However, the analysis of the proposed scenarios shows only some minor changes to the elevation amplitude. This is in contrast to results of other complex numerical studies, where significant amplitude reductions were achieved. Since this is an idealised model, not developed for such detailed predictions, it is likely that other excluded processes play an important role in the effects of retention basins in tidal channels.

Although there is a large difference between the models, this model proves to be very useful for exploring possible alternatives to current scenarios. Regarding the Ems River, the placement of basins more towards the channel head showed a significant increase in amplitude reduction.

Preface

These pages contain the result of a half year hard work as part of my graduation from my Master 'Water'. It presents the result of a research into retention basins in convergent estuaries, a subject what I have found very challenging and interesting. This thesis marks the end of my study period and I can say that I am very eager to put all this knowledge into practice.

First of all, I would like to thank the members of my graduation committee, Suzanne Hulscher and Henk Schuttelaars, for their valuable input during my graduation and, in particular, my daily supervisor Pieter Roos. Due to his critical view and comments I could really challenge myself and therefore I feel I that have learned a lot during the last six months. But most of all, it was a very enjoyable time and our meetings were always fun.

Of course, I would like to thank my parents for their support over the years and the interest they have shown in my study.

Also, I would like to thank those that supported me during some difficult periods. For a few years, my study has not always been that smoothly and in my experience it was very important that during this period the people close to me have shown their faith and trust. I hope that the people I am talking about know how much this helped me and I want you to know that I am very grateful for that!

Furthermore, many thanks to my fellow graduation students for a very nice time in our room, but also the fruitful discussions and comments about my thesis.

Last, but certainly not least, I would like to thank Jansje Schurer. Not only for being a great girlfriend, but also for all her help during my graduation period.

Rests me nothing than to wish everyone who is about to continue to the next pages much pleasure with reading this thesis.

Johan Damveld,
Enschede, July '15

Contents

Chapter 1

Introduction

The Ems-Dollard estuary is part of the 600 km long Wadden Sea, a shallow intertidal sea, protected by several barrier islands. The estuary is located at the border of Germany and The Netherlands and stretches over almost 500 km^2, including a fresh water zone of ca. 40 km^2. An overview map of the estuary can be found in figure 1.1,

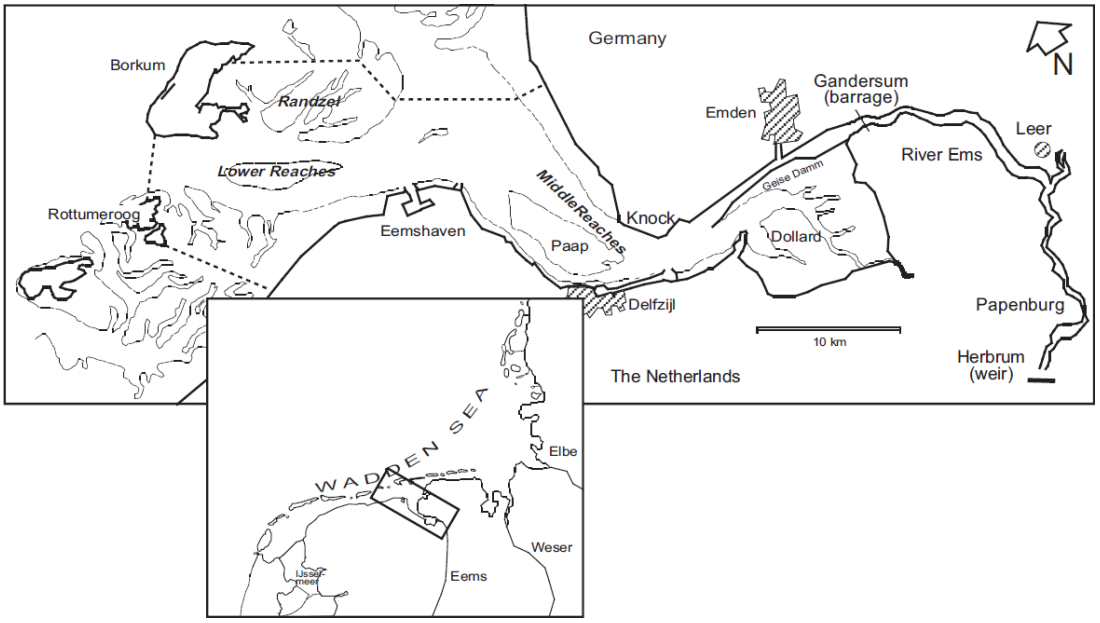

FIGURE 1.1: Map of the Ems estuary, where four areas can be distinguished; the lower and middle reaches, the Dollard and the Ems River (Schuttelaars et al., 2013).

where a subdivision in four main sections can be distinguished; the lower reaches, the middle reaches, the Dollard and Ems River. The weir at Herbrum, located 65 km upstream, is the landward boundary of the Ems estuary. The river is convergent,

with a width of around 1000 m near the river mouth, decreasing down to 150 m at Papenburg and 60 m at the weir.

1.1. Problem definition

Over the past centuries the Ems has faced many natural and anthropogenic changes. In the Medieval times, increased storm surges led to the formation of the Dollard, after which the inhabitants tried to reclaim the lost land until the 20th century. With the Ems River becoming increasingly important to shipping, channels were developed in order to maintain navigability. Large amounts of sediments have been dredged from the estuary and it has been proven that these changes are related to the increased tidal range. Other important measures that have influenced the dynamics in the estuary are the construction of several hard barriers, namely the weir at Herbrum, the Geiseleitdamm and the Emssperwerk at Pogum (Talke and de Swart, 2006). With this increase in ship traffic, harbours have been expanded as well. Although several harbours are present in the estuary, the driving force behind the mentioned changes is the Meyerwerft at Papenburg. These docks are producing increasingly larger cruise ships (figure 1.2), demanding increasingly larger water depths.

As mentioned, due to the changes in the estuary, the tidal range has dramatically increased over the past decades. The tidal range at Herbrum has more than doubled since the 1950's. This is visible in the mean high water (MHW), as well as the mean low water (MLW). Originally, the MLW in the tidal river was unrelated to the MLW at the German coast, while nowadays these are fully coupled (Jensen and Mudersbach, 2005). The increased tidal range, combined with an asymmetrical tide has made the Ems River highly susceptible to sediment trapping. Suspended sediment concentrations have increased in the whole estuary and the turbidity maximum has shifted into the fresh water zone of the tidal river (Chernetsky et al., 2010). Fluid mud layers caused by high sedimentation processes can be observed nowadays, causing a decrease in hydraulic roughness, which again can be related to the increased tidal range. As a result of the high turbidity, the Ems River has been marked as highly polluted. This is for instance reflected in the oxygen concentrations, which have decreased to almost 0 mg/l for major parts of the tidal river. Many species in these areas have almost totally disappeared (Bioconsult, 2006; Jager and Vorberg, 2008).

Recent studies have shown that the construction of secondary channels along the tidal river may influence the tidal dynamics; see chapter 2. Currently, it is considered to construct up to nine retention basins along the Ems River in order to reduce the tidal range (DHI-WASY, 2012). Various researchers have tried model to the effects of these retention basins (Alebregtse et al., 2013; Alebregtse and de Swart, 2014; Roos and Schuttelaars, 2015). In the most recent of these studies, Roos and Schuttelaars (2015)

FIGURE 1.2: Cruise ship in the Ems River, transported from the Meyer Werft towards the Eemshaven (Hallas, 2015).

developed an idealised model in an effort to explain the effects of multiple retention basins on tidal dynamics in prismatic channels. However, estuaries are usually not prismatic, but are often convergent in landward direction, as also observed in the Ems-Dollard estuary. Since bottom friction and channel convergence are theoretically counteracting each other, these are important factors that should be understood well.

Although Roos and Schuttelaars (2015) successfully explained the effects of retentions basins in tidal channels, they limited their analysis to prismatic channels and only two basins. These issues will be addressed in this study, where the focus will be on the effects of channel convergence, as well as an arbitrary number of basins, in order to explain the physical mechanism underlying these processes.

1.2. Research goal and questions

The goal of this study is stated as follows.

To explain the effects of multiple retention basins on the tidal dynamics of a convergent tidal channel by analysing the underlying physical mechanisms and to explore the effects of implementing the proposed plans of these basins in the Ems-Dollard estuary.

Based on the problem definition and research goal, the following main research questions have been formulated.

1. *What are the main problems that can be observed in the Ems-Dollard estuary nowadays and which model studies focus on addressing these problems through the use of retention basins?*
2. *What are the effects of multiple retention basins on the hydrodynamics in convergent tidal channels?*
3. *To what extent can the acquired knowledge be applied to the Ems-Dollard estuary?*

To further specify the course of this study, the second research question has been divided into sub-questions. These are as follows.

2.1. *What is the effect of channel convergence on the hydrodynamics of tidal rivers?*

2.2. *Which hydrodynamic effects can be observed when adding one or more retention basins along the main channel?*

2.3. *How does the basin geometry influence the hydrodynamics in convergent channels?*

2.4. *To what extent does bottom friction counteract the effects of the channel convergence?*

1.3. Methodology

Background This part of the study will focus on the main events in the estuary which have led to its current state, as well as the steps that are being taken to address the problems faced nowadays. Therefore, three subjects are reviewed here:

- As already stated in the problem statement, the events that have led to the current state of the estuary date back many years. Here, a detailed overview of these events will be given. In addition, the problems faced nowadays will be reviewed, with the main focus on hydro- and morphodynamics.
- This part will zoom in on the proposed solutions in the Ems-Dollard estuary, with a clear focus on retention basins along the tidal river.
- Here, an overview will be given of the most important model studies into the effects of retention basins on tidal resonance, of which some already have been mentioned in the problem statement.

Model set-up To simulate the dynamics in estuaries, often extensive 3D numerical models are applied. These models generally are highly detailed and include many processes, such that they are computationally expensive. Thus, it becomes difficult to focus on the magnitude and importance of certain processes and analyse the sensitivity of the included parameters. This motivates the choice of using idealised models, in which specific physical processes can be isolated. Therefore, the idealised model by Roos and Schuttelaars (2015) will be used as a starting point for this study, since it is detailed enough to describe various important processes in an estuary, while it avoids high computational processing time. As a result, it allows for an extensive sensitivity analysis into the model parameters and hence, channel convergence.

Parameter analysis In order to further understand the physics underlying the system of the tidal channel, an assessment of the parameters is necessary. As a first step in analysing the parameters, two reference cases will have to be formulated, which serve as the basis for the remainder of the assessment. The first case will be represented with a prismatic channel, similar to the one as specified by Roos and Schuttelaars (2015), the second includes a convergent channel. To assess the different parameters on their influence, two indicators will be used here:

- The first is the ratio between the tidal range at the mouth and the tidal range at the channel head, with the purpose of revealing the tidal amplification in the channel.

- The second and most important indicator, is the *amplitude gain* at the channel head. This is the relative effect of the adjusted case compared to the reference case.

The following steps will present the remainder of the analysis in which the above indicators will be used:

- As one of the novelties in this study, width convergence will play an important role in this sensitivity analysis. As one of the reference cases includes a convergent channel, this will be the first feature to be analysed. To understand the impact of a convergent channel, two parameters have to be varied, the length of the channel and the channel convergence itself.
- Previous studies have shown that the basin geometry is very important for the way the basins interact with the main channel. To analyse the effects of varying basin geometry, the responsible parameters will be systematically increased. Since this has already been addressed by Roos and Schuttelaars (2015) for prismatic channels, the main interest here is the effect in convergent channels.
- Another important aspect of this study is the effect of multiple retention basins on convergent tidal channels. In this part of the analysis, these effects will be assessed. In previous studies, cases with one or two basins have already been discussed, a further analysis will be given by systematically increasing the number of basins in various locations using both reference cases.
- The final part of the analysis will focus on the effects of bottom friction on the system. It is effective to discard friction in order to adequately explain the dynamics in tidal rivers. However, it is interesting to see how bottom friction interacts with the channel convergence for instance, as these phenomena theoretically counteract each other. To analyse this, bottom friction will be systematically varied for each of the above cases.

Physical mechanism To further extend the analysis of the interaction between retention basins and the width convergence, the objective in this part is to unravel the physical mechanism behind convergent channels with and without retention basins. As Roos and Schuttelaars (2015) successfully explained the mechanisms in prismatic channels, a similar approach will be used here. Analogous to the parameter analysis, the role of bottom friction to the physical mechanism will also be discussed here.

Ems Case As the last part of this study, the Ems river will be discussed. This case will explore the effects of retention basins along the channel. Since the model in this

study is used in an idealised setting, it is only possible to roughly approximate the geometry of the Ems. To this end, gometric and bathymetric data will be obtained from various sources in order to model the estuary as detailed as the idealised model allows for. Next, the model will be calibrated using historical data of water levels in the tidal river. As a third step, the effect of the proposed retention basins will be investigated for their effectiveness and the results will be compared to that of other studies.

1.3.1. Research overview

Figure 1.3 presents a schematic overview for this study. It gives an indication of the major steps which are discussed in this section.

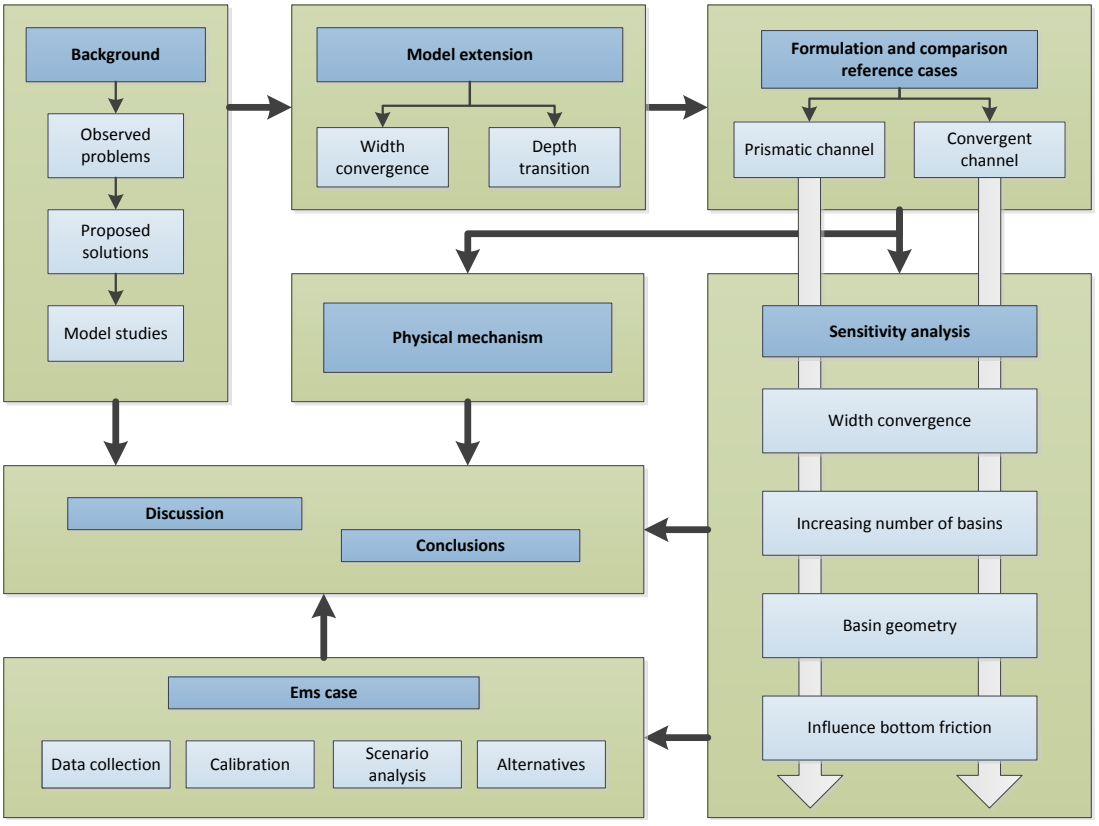

FIGURE 1.3: Study roadmap.

1.4. Thesis outline

Chapter 2 will go into the background of the problem. Next, chapter 3 will present the model formulation, where after an overall solution method is presented in chapter 4. Chapter 5 will discuss the main channel convergence. Then, the results of the parameters analysis are given in chapter 6 and the physical mechanism in the system will be presented in chapter 7. The application to the Ems-Dollard estuary will be discussed in chapter 8. Discussion and conclusions will be presented in chapters 9 and 10, respectively.

Chapter 2

Background

Over the last centuries, the Ems-Dollard estuary has experienced major changes of its shape by both natural dynamics and human intervention. Coastal retreat due to storm surges and reclaimed land by inhabitants illustrate the course of the last centuries. The subsequent deepening and streamlining of the shipping lines in the middle and lower reaches changed the long-term morphodynamical processes, which causes many problems along the river nowadays. Many studies have linked these changes to the current state of the estuary and since a few years various plans have been introduced to deal with these problems.

In the following chapter, an overview will be given of the most important factors which have contributed to the current state of the estuary, together with an overview of the latest plans and model studies that are used.

2.1. History of the Ems-Dollard estuary

2.1.1. Origin

The part of the estuary displaying the most visible changes is certainly the Dollard. A few hundred years ago, during the medieval period, the Dollard was formed as a result of frequent storm surges and the cultivation of peat layers. At first, only a shallow bay was formed which was only flooded a few times per year. Due to progressive erosion, mainly due to the cultivation of peat layers, the bay reached its maximum dimension in the 16th century (Groenendijk and Bärenfänger, 2008; Stratingh and Venema, 1855).

At the beginning of the 16th century, a period of intensive land reclamation started, which continued until the 20th century. Sedimentation due to floods, combined with

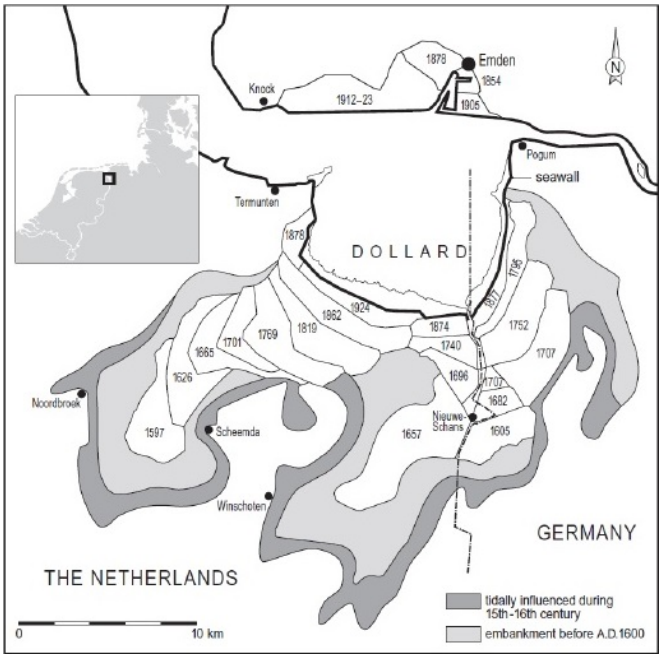

FIGURE 2.1: The maximum extent of the Dollard at the beginning of the 16th century and the phases of land reclamation in the centuries after (Esselink et al., 2012).

the construction of levees, led to the seaward migration of the coastline. Figure 2.1 shows the history of this process. Currently, only 35% of the maximum size of the bay has remained (Groenendijk and Bärenfänger, 2008; Stratingh and Venema, 1855).

Not only the Dollard was subject to land reclamation, also in the area around Emden levees were constructed contributing to the current topography, as depicted in figure 2.1. In the outer estuary, north of Delfzijl and along the northern Dutch coast, similar processes of land reclamation were ongoing (Talke and de Swart, 2006). These changes may not have had a direct effect on the history of the Dollard itself, but they do influence the properties of the estuary as a whole. After World War II, the land reclaiming projects came slowly to an end and only 63 hectares have been reclaimed from the Dollard basin since. Some additional (small) surface area was lost due to dike stabilization measures and the growth of forelands in front of the dikes (Steen, 2003).

2.1.2. Recent developments

These final episodes of land reclamation near Emden were carried out for navigation purposes (Talke and de Swart, 2006). This illustrates the shift from land reclamation in favour of for instance agriculture, towards a more industrial point of view, where shipping became the main priority.

Maintenance of fairways increasingly dominated the activities in the Ems estuary since the late 19^{th} century. Several interventions have influenced the physics of the Ems estuary over the years, amongst others the construction of dams and the straightening of river bends.

Weir Herbrum The first large interventions to improve navigation in the estuary were the construction of the Ems – Dortmund canal and the weir at Herbrum (Steen, 2003). This weir constitutes the landward boundary of the estuary nowadays, where before the construction the tidal wave could propagate further upstream. As suggested by Habermann (2003), reflection off the weir could have influenced the dynamics of the tide in the rest of the estuary.

Geiseleitdamm Also in the beginning of the 20th century, the German government started with the reinforcement of the natural boundary between the Ems and the Dollard, the Geiserücken. As a result, flow speeds and depth increased in the fairway of the Ems. By 1961, the Geiseleitdamm had a total length of 12 km west of Pogum, constructed at the level of the MHW. Finally, a stretch of 2 km called 'Leitdamm Seedeich' was created in the outer estuary, which was the final expansion of the dam (Steen, 2003). Since these last activities, the dam has not been maintained anymore. The result is that the dam has become more and more porous due to ground subsidence and sea level rise, as well as natural weathering. By 1979 the dam had decayed so much already, that a clear separation of the Ems and Dollard was not present anymore and that water and sediment could flow through the dam. The western part of the dam had settled so much by 2000, that it is now flooded for 4 hours during high tide (Werkgroep Dollard, 2001).

Channel development To improve navigability, the German government straightened a large number of rivers in the 20th century. Between 1900 and 1928 tributary channels and river bends were cut off and the course of the riverbed was streamlined. Together with the construction of other measures, such as groynes and dykes, this led to a shortening of about 15% of the former length of the lower part of the estuary (Höpner, 1994). Besides the straightening of the river course, the river was deepened as well. In the first part of the 20th century, this mainly focused on maintaining the shipping lines in the outer estuary. According to de Jonge (1983), after the 60s, these shipping lines were deepened and straightened between Knock and Borkum to ensure a single channel instead of several coexisting channels, where the depth of the stretch between Pogum and Knock was already influenced by the Geiseleitdamm.

Emssperwerk The increased tidal range has made the Ems more prone to storm surges (Siefert and Lassen, 1986). From 1998 until 2002 the Emssperwerk has been constructed near Gandersum, a storm barrier which protects against water levels up to 3.7 m when closed (Niemeyer and Kaiser, 2000). Additionally, it is used to temporarily increase the upstream water levels for the passage of large ships being built in the docks in Papenburg (see figure 1.2). The barrier is closed about twice a year for several days, where water from the downstream part is pumped into the river in order to let the water rise quickly. During this period, it has been shown that due to density driven currents, saline water can intrude up to 20 km upstream. After reopening the barrier, the effect on the tides is visible for only a few days (Talke and de Swart, 2006).

Harbours Several harbours exist in the Ems-Dollard estuary, leading to a high density of shipping traffic. The main harbours in the upper estuary are Emden, Delfzijl and the Eemshaven. As already illustrated in figure 1.2, a large dock is located along the tidal river near Papenburg. This Meyerwerft dock is the driving force for the increased interventions over the past decades. Increasingly large ships are being constructed, demanding higher water depths. Jensen et al. (2002) relate these measures to the changing tidal dynamics and the increase of the tidal range in the Ems River over the years.

Other impacts Over the years, significant volumes of sediment were dredged in the estuary to maintain the shipping lines and harbours. Even in the beginning of the 20th century, parts of the estuary were dredged. However, the volume of dredged sediment greatly increased after the 1960's, partly facilitated by the introduction of the suction dredger (Talke and de Swart, 2006). Already in the 1980's awareness increased about the effects of dredging on the estuary. The relation between concentration of suspended matter and yearly dredging amounts was described by de Jonge (1983). He showed that with an increasing amount of dredging volume, the concentration of suspended matter increased as well. The dredging activities in the lower part of the estuary occurred mainly in the past 30 years. In those years, the Ems River between Pogum and Papenburg has been deepened several times, to 5.7 m in 1996, to 6.8 m in 1992 and to 7.3 m in 1994 (Jensen et al., 2002).

Europe's largest natural gas field is located over a large part of the outer estuary. Since 1959, the field has been developed and as a result of the extractions, ground subsidence has occurred. By 2008, the subsidence was over 20 cm near Delfzijl (NAM, 2010); see figure 2.2. It is expected that in 2070 the ground will be subsided as much as 38 cm for the Dutch coast, while for the Dollard this will be 10 cm. However, according to Cleveringa (2008), strong sediment depositions will counteract the subsidence in the estuary itself.

FIGURE 2.2: Illustration of the ground subsidence since the start of the gas extractions in 1964 (NAM, 2010).

2.1.3. Current problems

The Ems-Dollard estuary has faced major changes in the last century. Nowadays the river is categorized as highly polluted (NLWKN, 2012). This indicates the poor state the river currently is in. In the following paragraphs, an overview will be given of some of the most important problems faced in the estuary, ranging from hydro- and morphodynamics to ecological problems.

Hydrodynamics Many of the anthropogenic changes to the estuary have caused the hydrodynamics to change. The tidal rage is increasing in the Ems due to both sea level rise and channel deepening (Jensen and Mudersbach, 2005). Since the 1960's, the mean tidal range increases linearly with 33 cm/century. This trend echoes through in the Ems-Dollard estuary, where the tidal range is even more amplified than at the coast. At Emden for instance, tidal range has increased with an average rate of 57 cm/century (Jensen and Mudersbach, 2002).

More upstream in the brackish regions of the river, Jensen et al. (2003) determined that the tidal range is increasing due to both sea level rise and channel deepening. These changes are illustrated in figure 2.3, where the tidal range has been plotted over

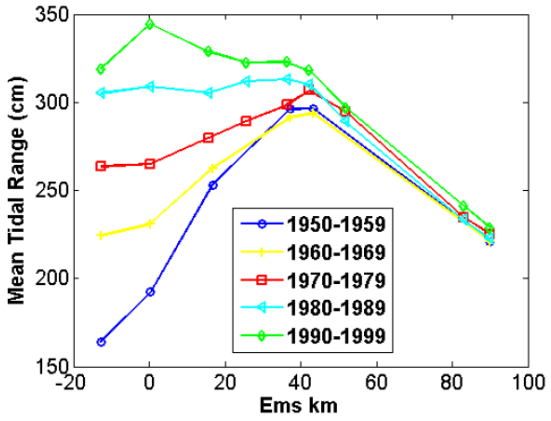

FIGURE 2.3: Longitudinal tidal range for over 5 decades between 1950 and 2000 (Schuttelaars et al., 2011). The x-axis ranges from the upstream to downstream, where Ems km 0 denotes Papenburg.

the total length of the river. The data show that the changes were already present before the 1960's suggesting the relation between the earlier changes to the estuary (weir at Herbrum) and the changes in hydrodynamics. This is further explained by Schuttelaars et al. (2011), who showed that the length of the estuary has a large effect on hydrodynamics.

When analysing the properties of the tide, it becomes clear that the tide in the Ems-Dollard estuary is clearly asymmetrical. Amongst others, Rollenhagen (2011) studied the combination of different tidal constituents in the river. Due to the presence of the M4 and M6 tide, the time between high water and low water is much longer than the other way around.

Morphodynamics Tidal asymmetry can be related to the changes in morphodynamics, one of the problems faced in the estuary. Over the past decades, the turbidity of the Ems-Dollard estuary has significantly increased. It was shown by de Jonge (1983) that sediment concentration in the turbidity maximum of the river has increased with almost 400% between the 1960's and 1980's. Also, visibility decreased as the turbidity increased with 5-10 times (Kuehl and Mann, 1973). Currently, near-surface concentrations up to 1 g/l can be observed, which exemplifies the hyperturbid system (Esselink et al., 2012).

Healthy estuaries have their turbidity maximum around the head of the salinity intrusion, while the maximum in the Ems River can be observed far into the fresh water zone (Winterwerp, 2011). This is further illustrated by Chernetsky et al. (2010), who modelled sediment concentration in the river in 1980 and 2005 (figure 2.4). Over these years a clear upstream migration of the turbidity maximum can be seen.

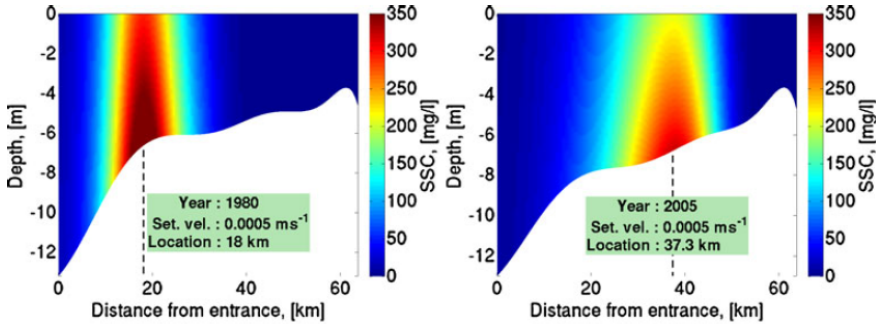

FIGURE 2.4: Tidally averaged suspended sediment concentration for 1980 and 2005 (Chernetsky et al., 2010). Note the difference x-axis compared to figure 2.3; it is reversed, while Ems km 0 denotes the mouth.

In a study by Schrottke and Bartholomä (2008), it was shown that highly dynamic fluid mud layers, measuring up to 2 m in thickness around slack water, were present in the Ems River. Winterwerp (2011) explained that the occurrence of fluid mud layers is caused by an exceedance of the maximum load of sediment which can be hold in capacity. As the presence of fluid mud decreases the hydraulic roughness, this will only lead to more tidal amplification.

Ecology As a result of the increased turbidity, the water quality of the Ems-Dollard estuary has deteriorated. Over the years, oxygen concentrations depleted and the area over which this occurred increased. According to van der Welle and Meire (1999), the oxygen concentration were still 8 mg/l in 1980, while they decreased to around 0 mg/l nowadays (Bos et al., 2012).

The decreased water quality has major influences on the habitat of species in the estuary. The fish population was analysed by Bioconsult (2006) and they showed a clear relation between the oxygen concentrations and the fish density. Moreover, migratory species are experiencing barriers in their route from the river towards the sea (Jager and Vorberg, 2008).

2.2. Proposed solutions in the Ems-Dollard estuary

Several solutions have been proposed to be implemented in the Ems-Dollard estuary in order to address the distorted tidal dynamics. Amongst those are plans for the construction of up to nine retention basins along the tidal river (DHI-WASY, 2012; Donner et al., 2011, 2012). The goal of this project is "*to adjust the hydro- and morphodynamics of the river in order to restore the tidal dynamics and increase the*

sustainability of the estuary". The next paragraphs will present the different scenarios in this project, while a detailed description of all the basins can be found in chapter 8.

Scenario A: flattening plus three retention basins This measure consists of two combined solutions, A1(s) and A2(s). The basis for these solutions is a flattening of a part of the river, namely the section Leer – Papenburg. As an extension to the A1 scenario, the A2 scenario adds three retentions basins just south of Papenburg with a total volume of 29 Mm^3. Of special interest is the width of the inlet channel, which is designed to be 30-50% of the local width of the Ems and ranges from 60 meters at Herbrum, up to 1000 meters at the channel mouth. Additionally, an extension of this scenario is an adjustment of the bed roughness. The standard scenarios use the bed roughness of the original model settings, while with the $-s$ extension indicates an increased roughness.

Scenario B: shift of the weir plus two retention basins The second scenario focuses on the weir at Herbrum. While the tidal dynamics are influenced by the length of the channel, an upstream shift of the weir may lead to a dampening of the system. As an additional measure, two retention basins are added between Gandersum and Papenburg and have a total volume of 18 Mm^3.

Scenario C1: six retention basins This scenario explores the effects of several retention basins along the Ems between Terborg and Herbrum. Six retention basins with a total volume of 29 Mm^3 are designed here, including the areas from the previous B scenario. The bed roughness and width of the inlet channel is equal to the previous case seen above, with the exception of the retention basin at Rhede. Here, the width of the inlet channel is as wide as the river width itself.

Scenario C2: nine retention basins The idea for the C2 scenario is basically the same as for the C1 scenario. Retention basins are used to store a part of the volume of the tidal wave, in order to lower the tidal range. Here, nine retention basins are designed with a total volume of 14 Mm^3. The locations of the retention basins are all upstream of Leer. Bed roughness and inlet channel width are again equal to the previous scenarios, whereas the most downstream area at Brahe has an inlet channel width of 100% of the river width.

2.3. Model studies on retention basins

The Ems-Dollard estuary has been extensively studied over the past 50 years. Several models have been used to simulate hydro- and morphodynamics in the river, with the goal of tracing back the changes which occurred in the past as well as testing proposed solution to the problems faced. A complete overview of these studies is given by Talke and de Swart (2006). Since then, researchers have tried to keep improving their understanding of the processes in the estuary and several solutions have been formulated. Since 6/7 years, many model studies have focused on the tidal response of the estuary. These studies can be distinguished in complexity, where the complex models are often focusing on long-term morphological processes, while idealised models are used to focus on isolated processes in order to improve the understanding of those processes.

Complex models The idea to use retention basins as a measure to counter the tidal resonance in the Ems River was introduced by Rollenhagen (2011), who arbitrarily chose two locations to simulate the effects of those basins in the Delft3D model. Her findings were that the dominant flood wave would decrease in strength and that the upstream transport of sediment would decrease as well. In a more extensive study, DHI-WASY (2012) proposed to construct several basins along the lower and middle Ems River. Using the complex model MIKE 3 FM, they formulated different scenarios and they analysed those scenarios for the effects on the hydro- and morphodynamics. They found similar results as Rollenhagen (2011) did, where almost every scenario in where they included retention basins showed to be an improvement to the current system. A comprehensive analysis of this project was given in two follow-up studies (Donner et al., 2011, 2012).

The results showed that these scenarios only have a low to moderate effect and are sometimes even aggravating the observed problems. A basin near the mouth of the river resulted in an increased sediment import in the estuary. However, the basins placed in the lower part of the Ems exemplified better results, where in all the scenarios an improvement was visible in the hydro- and morphodynamics. It is notable that there were reasonable differences between the outcomes of the scenarios, which shows that arbitrary placement of retention basins may not be an effective solution. This clearly emphasizes the need for a better understanding of the physical processes behind secondary basins in estuaries.

Idealised models The idea of retention basins has an analogy in acoustics, where side branches are used as acoustic filters (Lighthill, 1978), which has inspired more

researchers to look into this phenomenon. Alebregtse et al. (2013) developed an idealised model, which described the tidal motion using a one-dimensional model. They found that if a channel was placed between a node and a successive landward located antinode, the secondary channel would weaken the tide. On the other hand, if it were placed between a node and a successive seaward located antinode, the tide would be amplified.

In a follow up study, Alebregtse and de Swart (2014) used a non-linear model to include the effects of tidal asymmetry on the influence of retention basins on the tide. Their findings were in line with those of Alebregtse et al. (2013), confirming that a secondary channel could lead to a weakening of the tide in the rest of the system when placed correctly, which was later confirmed again in a study by Kumar et al. (2014). They used a three-dimensional model to explain the tidal and sediment dynamics in both longitudinal and lateral direction, in which they considered a prismatic channel with one retention basin.

In one of the most recent studies on this topic, Roos and Schuttelaars (2015) studied the effects of multiple basins in a prismatic channel. They used the *basin admittance* to describe the basins response, by which they showed that a supercritical basin (positive basin admittance) has a reversed response compared to a subcritical basin (negative basin admittance). Moreover, in case of multiple basins, large basins were found to have stronger interactions than smaller basins.

Another important novelty in the study of Roos and Schuttelaars (2015), compared to previous studies, is the formulation of the conditions at the mouth of the channel. The limitations in the formulation of the boundary conditions used by Alebregtse et al. (2013) and Alebregtse and de Swart (2014) are the fact that they rule out the possibility of a resonating system as a whole due to the presence of a secondary channel. Since they treat the channel as infinitely long, no interference is possible at the transition between the channel and the sea. Analogous to the basin admittance, Roos and Schuttelaars (2015) used the *radiative impedance* to represent the effects of the chosen boundary formulation. They found large differences in amplification, which occur due to different sea representations.

Although Roos and Schuttelaars (2015) successfully explained the effects of retentions basins in tidal channels, they limited their analysis to prismatic channels and only two basins. Estuaries can usually not be depicted as prismatic channels, since they are often convergent in landward direction. As bottom friction and channel convergence are theoretically counteracting each other, these are an important factors that should be understood well. Second, as the proposed plans have shown, up to nine basins are currently considered to be implemented. Since the previous (idealised) studies have only analysed up to two basins, more research is needed in this matter.

Chapter 3

Model formulation

To analyse the effects of retention basins on the tide, the model developed by Roos and Schuttelaars (2015) will be extended to include a variable width, while depth is allowed to vary in a stepwise manner. The model represents a convergent estuary which is constrained by a weir at the landward side. The estuary is considered to be a channel of length l_j, width $b_j(x)$ and uniform depth h_j, with any number of secondary basins. A Cartesian coordinate system is used, with x the along channel coordinate directed landwards and y the cross channel coordinate pointed upwards, as illustrated in figure 3.1. The model can be divided into multiple channel sections, each with their own properties, in order to describe the course of the channel as detailed as necessary.

The channel is assumed to be exponentially convergent, so the width of the estuary can be described as

$$B(x) = B_{0,j} \exp(-x/L_{b,j}), \tag{3.1}$$

with $B_{0,j}$ the width of the j^{th} channel section at the seaward side and $L_{b,j}$ the e-folding convergence length of that section.

3.1. Main channel

In the main channel, $u(x,t)$ and $\eta(x,t)$ denote the flow velocity and surface elevation respectively. The following cross-sectionally averaged linear shallow water equations

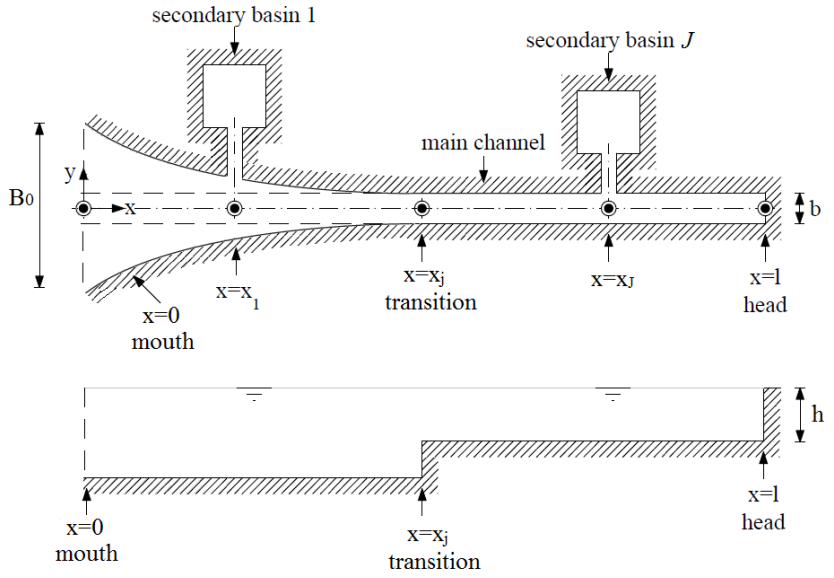

FIGURE 3.1: Top and side view of the model with a convergent main channel of length l_j, width b_j, uniform depth h_j and J secondary basins. The main channel can be divided into j multiple convergent sections, this is an example with two sections, with the transition at $x = x_j$.

are used to describe conservation of mass and momentum in the main channel:

$$\frac{\partial \eta}{\partial t} + h\frac{\partial u}{\partial x} + \frac{hu}{b}\frac{\partial b}{\partial x} = 0, \tag{3.2}$$

$$\frac{\partial u}{\partial t} + \frac{ru}{h} = -g\frac{\partial \eta}{\partial x}. \tag{3.3}$$

Here, g is the gravitational acceleration, while r denotes a linear bottom friction coefficient, specified according to Lorentz's linearisation (Lorentz, 1922; Zimmerman, 1982) in appendix A. Combining equations (3.1) and (3.2) leads to the following mass balance for the main channel including width convergence:

$$\frac{\partial \eta}{\partial t} + h\frac{\partial u}{\partial x} - \frac{hu}{L_b} = 0. \tag{3.4}$$

To effectively describe the landward boundary condition in the main channel, it is required to assume zero flow at the closed end. The elevation at the mouth is required to match that of the forcing amplitude Z, while the elevation and volume transport at the transitions is required to match those of the subsequent channel section:

$$\eta = Z\cos\omega t \qquad \text{at } x = 0, \tag{3.5}$$

$$\eta^{\oplus} = \eta^{\ominus} \quad \text{and} \quad b^{\oplus}hu^{\oplus} = b^{\ominus}hu^{\ominus} \qquad \text{at } x = x_j, \tag{3.6}$$

$$u = 0 \qquad \text{at } x = l. \tag{3.7}$$

Here, the superscripts $\oplus$ and $\ominus$ represent the limits on the left and right hand side of the transition ($x = x_j$), respectively. Other types of forcing, as described by Roos and Schuttelaars (2015), are not considered here.

3.2. Secondary basins

As illustrated in figure 3.1, J secondary basins can be located anywhere along the main channel, where the j^{th} basin is located at $x = x_j$. The basins are represented as Helmholtz basins, which are characterized by a short inlet channel, with length $l_{b,j}$, width $b_{b,j}$ and depth $h_{b,j}$ and a basin with surface area A_j. The flow velocity in the channel is denoted by $v_j(t)$ and is positive when pointed towards the basin. A linear slope in the surface elevation in the channel is assumed, making the uniform basin level $\zeta_j(t)$ the other unknown here. The model equations that describe the water motion in this system are given by the following expressions:

$$A_j \frac{d\zeta_j}{dt} = b_{b,j} h_{b,j} v_j, \tag{3.8}$$

$$\frac{dv_j}{dt} + \frac{r_{b,j} v_j}{h_{b,j}} = -g \frac{\zeta_j - \eta_j}{l_{b,j}}. \tag{3.9}$$

Here, $r_{b,j}$ is a friction coefficient and η_j is the surface elevation in the main channel at $x = x_j$. Possible other basin types, as described by Alebregtse et al. (2013), are not considered here.

At the J vertex points, the connection between the main channel and the secondary channel, continuity of elevation is guaranteed by the linear slope in the channel, while continuity of volume will be satisfied as follows:

$$b_j h_j \left[u_j^{\oplus} - u_j^{\ominus} \right] = b_{b,j} h_{b,j} v_j \quad \text{at } x = x_j. \tag{3.10}$$

Here superscripts $\oplus$ and $\ominus$ represent the limits on the left and right hand side of the vertex point $x = x_j$, respectively.

Chapter 4

Solution method

We will seek solutions in dynamic equilibrium with the periodic forcing of angular frequency ω. For the main channel, the following can thus be stated:

$$\eta(x,t) = \Re\{N(x)\exp(i\omega t)\}, \tag{4.1}$$

$$u(x,t) = \Re\{U(x)\exp(i\omega t)\}, \tag{4.2}$$

with complex amplitudes $N(x)$ and $U(x)$. For the secondary channels, V_j denotes the complex amplitude of the inlet channel velocity. In the model, $J+1$ complex elevation amplitudes can be defined, where N_0 and N_J denote the elevation amplitudes at the mouth and head respectively. The solution will result from a set of linear equations for each of these $J+1$ unknowns.

4.1. Main channel

As a first step, the solution in the main channel will be obtained. The model equations, as described in equations (3.2) and (3.3), can be rewritten to the following general equation for η:

$$\frac{\partial^2\eta}{\partial t^2} + \frac{r}{h}\frac{\partial\eta}{\partial t} + \frac{gh}{L_{b,j}}\frac{\partial\eta}{\partial x} - gh\frac{\partial^2\eta}{\partial x^2} = 0. \tag{4.3}$$

Substituting equation (4.1) into equation (4.3) leads to the following single expression for $N(x)$:

$$\frac{d^2N}{dx^2} - \frac{2\beta_j}{\mu_j\gamma_j}k_j\frac{dN}{dx} + k_j^2N = 0. \tag{4.4}$$

In here, $k_j = \gamma_j k_{0,j}$ is the complex wavenumber in the main channel, $\gamma_j = \sqrt{1 - \frac{ir_j}{\omega h_j}}$ the frictional correction factor, $k_{0,j} = \frac{\omega}{\sqrt{gh_j}}$ the frictionless shallow water wavenumber and $\mu_j = k_{0,j}/k_{0,m}$ a coefficient which controls the depth transitions. Subscripts j and m denote the j^{th} channel section and the conditions at the channel mouth, respectively.

Finally, the dimensionless parameter β_j describes the convergence of the main channel, which is formulated to facilitate solution:

$$\beta_j = \frac{1}{2k_{0,m}L_{b,j}}. \tag{4.5}$$

Depending on the e-folding convergence length L_b, four different regimes for β can be distinguished:

- No convergence, which can be expressed with $L_b = \infty$, so that $\beta = 0$.
- Subcritical convergence, which occurs when $\frac{1}{2k} < L_b < \infty$, so that $0 < \beta < 1$.
- Critical convergence, this is when $L_b = \frac{1}{2k}$, so that $\beta = 1$.
- Supercritical convergence, which occurs when $L_b < \frac{1}{2k}$, so that $\beta > 1$.

For each of these regimes a unique solution can be obtained, which will be discussed in detail in chapter 5. Here, the focus will be on a general solution which is valid throughout the whole domain, with any number of basins.

Equation (4.4) can be solved by obtaining fundamental solutions of the form $N(x) = \exp(\Lambda x)$, which results in the following characteristic polynomial equation:

$$p(\Lambda) = \Lambda^2 - \frac{2\beta_j}{\mu_j\gamma_j}k_j\Lambda + k_j^2 = 0. \tag{4.6}$$

This results in two roots, $\Lambda_{1,2} = k_j\left(\frac{\beta_j}{\mu_j\gamma_j} \pm \sqrt{\left[\frac{\beta_j}{\mu_j\gamma_j}\right]^2 - 1}\right)$, so the solution to equation (4.4) is a superposition of two waves/oscillations travelling in opposite directions, $N(x) = \hat{A}_j \exp(\Lambda_1 x) + \hat{B}_j \exp(\Lambda_2 x)$, i.e. a partially standing wave with coefficients $\hat{A}_j$ and $\hat{B}_j$. It is convenient to write this with wavenumbers

$$k_{1,j} = k_j\left(i\frac{\beta_j}{\mu_j\gamma_j} - \sqrt{1 - \left[\frac{\beta_j}{\mu_j\gamma_j}\right]^2}\right), \quad k_{2,j} = k_j\left(-i\frac{\beta_j}{\mu_j\gamma_j} - \sqrt{1 - \left[\frac{\beta_j}{\mu_j\gamma_j}\right]^2}\right). \tag{4.7}$$

This results in a new expression for $N(x)$, which can be written as

$$N(x) = \hat{A}_j \exp(-ik_{1,j}x) + \hat{B}_j \exp(ik_{2,j}x). \tag{4.8}$$

In each of the J main channel sections $x_{j-1} < x < x_j$, $N_{j-1}^{\oplus}$ and $N_j^{\ominus}$ represent the right and left elevation limit in the j^{th} channel section. Solving for $N(x_{j-1})$ and $N(x_j)$ gives the following coefficients:

$$\hat{A}_j = \frac{N_{j-1}\exp(ik_{2,j}x_j) - N_j\exp(ik_{2,j}x_{j-1})}{\exp(i[k_{2,j}x_j - k_{1,j}x_{j-1}]) - \exp(i[k_{2,j}x_{j-1} - k_{1,j}x_j])}, \tag{4.9}$$

$$\hat{B}_j = \frac{N_j\exp(-ik_{1,j}x_{j-1}) - N_{j-1}\exp(-ik_{1,j}x_j)}{\exp(i[k_{2,j}x_j - k_1x_{j-1}]) - \exp(i[k_{2,j}x_{j-1} - k_{1,j}x_j])}. \tag{4.10}$$

The velocities follow from substituting equations (4.1) and (4.2) into the momentum equation (equation (3.3)), which leads to $i\omega\gamma_j^2 U = -gdN/dx$, such that

$$U(x) = \frac{i}{\gamma_j}\sqrt{\frac{g}{h_j}}\left(\frac{ik_{2,j}}{k_j}\hat{B}_j\exp[ik_{2,j}x] - \frac{ik_{1,j}}{k_j}\hat{A}_j\exp[-ik_{1,j}x]\right). \tag{4.11}$$

Here, $U_j^{\oplus}$ and $U_j^{\ominus}$ represent the right and left velocity limit at each vertex point $x = x_j$. From equation (4.11) the following is found:

$$b_jh_{j+1}U_j^{\oplus} = \frac{i\omega b_m}{k_{0,m}}\left(\frac{i\alpha_jk_{2,j+1}}{k_{j+1}\mu_{j+1}\gamma_{j+1}}\hat{B}_{j+1}\exp[ik_{2,j+1}x_j] - \frac{i\alpha_jk_{1,j+1}}{k_{j+1}\mu_{j+1}\gamma_{j+1}}\hat{A}_{j+1}\exp[-ik_{1,j+1}x_j]\right), \tag{4.12}$$

$$b_jh_jU_j^{\ominus} = \frac{i\omega b_m}{k_{0,m}}\left(\frac{i\alpha_jk_{2,j}}{k_j\mu_j\gamma_j}\hat{B}_j\exp[ik_{2,j}x_j] - \frac{i\alpha_jk_{1,j}}{k_j\mu_j\gamma_j}\hat{A}_j\exp[-ik_{1,j}x_j]\right), \tag{4.13}$$

with coefficient $\alpha_j = b_j/b_m$, which expresses the ratio of the local width to the width at the mouth.

Next, imposing the boundary condition at the channel head ($x_J = l$) implies $U_J^{\ominus} = 0$, which, by using equation (4.13), leads to the following expression:

$$\frac{k_{1,J}}{\mu_J\gamma_J}\hat{A}_J\exp(-ik_{1,J}x_J) - \frac{k_{2,J}}{\mu_J\gamma_J}\hat{B}_J\exp(ik_{2,J}x_J) = 0. \tag{4.14}$$

Further specifying leads to an expression for N_J:

$$N_J = N_{J-1}\frac{\sigma_J^{\ominus}}{\tau_J^{\ominus}}, \tag{4.15}$$

with factors $\sigma_J^{\ominus}$ and $\tau_J^{\ominus}$ (for arbitrary j), which are defined as

$$\sigma_j^{\ominus} = \frac{i}{k_j\mu_j\gamma_j}\frac{k_{1,j}\exp(i[k_{2,j}x_j - k_{1,j}x_j]) + k_{2,j}\exp(i[k_{2,j}x_j - k_{1,j}x_j])}{\exp(i[k_{2,j}x_j - k_{1,j}x_{j-1}]) - \exp(i[k_{2,j}x_{j-1} - k_{1,j}x_j])}, \tag{4.16}$$

$$\tau_j^{\ominus} = \frac{i}{k_j\mu_j\gamma_j}\frac{k_{1,j}\exp(i[k_{2,j}x_{j-1} - k_{1,j}x_j]) + k_{2,j}\exp(i[k_{2,j}x_j - k_{1,j}x_{j-1}])}{\exp(i[k_{2,j}x_j - k_{1,j}x_{j-1}]) - \exp(i[k_{2,j}x_{j-1} - k_{1,j}x_j])}. \tag{4.17}$$

4.2. Retention basins

For the retention basins, we will seek solutions in dynamic equilibrium with the periodic forcing of angular frequency ω:

$$v(t) = \Re\{V(x)\exp(i\omega t)\}, \tag{4.18}$$

with complex amplitude $V(x)$.

The expressions for conservation of mass and momentum in the basins (equations (3.8) and (3.9)) can be rewritten as

$$\frac{1}{\omega_{0,j}^2}\frac{d^2v_j}{dt^2} + \frac{r_{b,j}}{h_{b,j}}\frac{1}{\omega_{0,j}^2}\frac{dv_j}{dt} + v_j = \frac{d\eta_j}{dt}, \tag{4.19}$$

where $\omega_{0,j} = \sqrt{b_{b,j}h_{b,j}g/(A_j l_j)}$ represents the eigenfrequency. Substituting equations (4.1) and (4.18) into this expression leads to

$$N_j\frac{i\omega A_j}{b_{b,j}h_{b,j}} = V_j\left[1 - \left(\frac{\gamma_{b,j}\omega}{\omega_{0,j}}\right)^2\right], \tag{4.20}$$

using the frictional correction factor $\gamma_{b,j} = \sqrt{1 - \frac{ir_{b,j}}{\omega h_{b,j}}}$.

Combining equation (4.20) with the vertex condition in equation (3.10) gives the following expression:

$$Y_j N_j = b_{b,j}h_{b,j}V_j = b_j\left[h_j U_j^{\oplus} - h_{j+1}U_{j+1}^{\ominus}\right]. \tag{4.21}$$

Here, the proportionality coefficient Y_j represents the *basin admittance*:

$$Y_j = \frac{i\omega b_m}{k_m}\tilde{Y}_j, \tag{4.22}$$

with the dimensionless admittance $\tilde{Y}_j$, which is used in order to facilitate interpretation:

$$\tilde{Y}_j = \frac{A_j k_m}{b_{0,m}}\left[1 - \left(\frac{\gamma_{b,j}\omega}{\omega_{0,j}}\right)^2\right]^{-1}. \tag{4.23}$$

Finally, it should be stated that with the result of equation (4.21) continuity of mass at each vertex point is automatically satisfied, which is independent of the main channel convergence.

4.3. Forcing

The forcing of the system can be represented as stated below:

$$N(0) = N_{\text{forc}}. \tag{4.24}$$

This is similar to the expression for deep sea conditions, as presented by Roos and Schuttelaars (2015).

4.4. Solution

By combining the vertex transport equations (4.12) and (4.13) and the conditions in equations (4.15), (4.21) and (4.24), a set of linear equations is found. These can be presented in matrix form, here for cases with two, three and four vertex points:

$$\begin{bmatrix} 1 & 0 \\ -\sigma_1^{\ominus} & \tau_1^{\ominus} \end{bmatrix} \begin{bmatrix} N_0 \\ N_1 \end{bmatrix} = \begin{bmatrix} N_{\text{forc}} \\ 0 \end{bmatrix}, \tag{4.25}$$

$$\begin{bmatrix} 1 & 0 & 0 \\ -\sigma_1^{\ominus} & \tau_1^{\ominus} + \tau_1^{\oplus} - \alpha_1 \tilde{Y}_1 & -\sigma_1^{\oplus} \\ 0 & -\sigma_2^{\ominus} & \tau_2^{\ominus} \end{bmatrix} \begin{bmatrix} N_0 \\ N_1 \\ N_2 \end{bmatrix} = \begin{bmatrix} N_{\text{forc}} \\ 0 \\ 0 \end{bmatrix}, \tag{4.26}$$

$$\begin{bmatrix} 1 & 0 & 0 & 0 \\ -\sigma_1^{\ominus} & \tau_1^{\ominus} + \tau_1^{\oplus} - \alpha_1 \tilde{Y}_1 & -\sigma_1^{\oplus} & 0 \\ 0 & -\sigma_2^{\ominus} & \tau_2^{\ominus} + \tau_2^{\oplus} - \alpha_2 \tilde{Y}_2 & -\sigma_2^{\oplus} \\ 0 & 0 & -\sigma_3^{\ominus} & \tau_3^{\ominus} \end{bmatrix} \begin{bmatrix} N_0 \\ N_1 \\ N_2 \\ N_3 \end{bmatrix} = \begin{bmatrix} N_{\text{forc}} \\ 0 \\ 0 \\ 0 \end{bmatrix}. \tag{4.27}$$

The factors $\sigma_j^{\oplus}$ and $\tau_j^{\oplus}$ are specified below. Factors $\sigma_j^{\ominus}$ and $\tau_j^{\ominus}$ are as in equations (4.16) and (4.17), $\tilde{Y}_j$ as in equation (4.23).

$$\begin{aligned} \sigma_j^{\oplus} = {} & \frac{i}{k_{j+1}\mu_{j+1}\gamma_{j+1}} \\ & \times \frac{k_{1,j+1}\exp(i[k_{2,j+1}x_j - k_{1,j+1}x_j]) + k_{2,j+1}\exp(i[k_{2,j+1}x_j - k_{1,j+1}x_j])}{\exp(i[k_{2,j+1}x_{j+1} - k_{1,j+1}x_j]) - \exp(i[k_{2,j+1}x_j - k_{1,j+1}x_{j+1}])}, \end{aligned} \tag{4.28}$$

$$\begin{aligned} \tau_j^{\oplus} = {} & \frac{i}{k_{j+1}\mu_{j+1}\gamma_{j+1}} \\ & \times \frac{k_{1,j+1}\exp(i[k_{2,j+1}x_{j+1} - k_{1,j+1}x_j]) + k_{2,j+1}\exp(i[k_{2,j+1}x_j - k_{1,j+1}x_{j+1}])}{\exp(i[k_{2,j+1}x_{j+1} - k_{1,j+1}x_j]) - \exp(i[k_{2,j+1}x_j - k_{1,j+1}x_{j+1}])}. \end{aligned} \tag{4.29}$$

For a constant width in a single channel section ($b_j = b_m$ and $k_j = k_{1,j;2,j} = k_m$), these factors reduce to the result found by Roos and Schuttelaars (2015), i.e. $\sigma_j^{\oplus} = 1/\sin(k[x_{j+1} - x_j])$ and $\tau_j^{\oplus} = 1/\tan(k[x_{j+1} - x_j])$.

Chapter 5

Main channel convergence

To understand the mechanism behind convergent channels, this chapter will go into the physics behind this system. Through the mathematical explanation, the physical mechanism will be revealed. The focus will be on a single convergent channel, in order to unravel the specific effect of convergence on the tidal motions. Second, the effects of friction on this mechanism will be investigated.

5.1. Four regimes

In this section the physical mechanism in a frictionless convergent channel will be discussed. Revisiting chapter 4 gives the following differential problem, which describes the elevation amplitude in the channel:

$$\frac{d^2N}{dx^2} - \frac{2\beta_j}{\mu_j\gamma_j}k_j\frac{dN}{dx} + k_j^2N = 0. \tag{5.1}$$

For the application here, it is convenient to describe the channel by only one (frictionless) section, such that $\gamma_j = 1, \mu_j = 1$. These terms will be left out of the equations from now on to facilitate the solution. Equation (5.1) can be solved by finding fundamental solutions of the form $N(x) = \exp(\Lambda x)$, which results in:

$$p(\Lambda) = \Lambda^2 - 2\beta k\Lambda + k^2 = 0, \tag{5.2}$$

with two roots $\Lambda_{1,2}$, given by

$$\Lambda_1 = k(\beta + \sqrt{\beta^2 - 1}), \quad \Lambda_2 = k(\beta - \sqrt{\beta^2 - 1}). \tag{5.3}$$

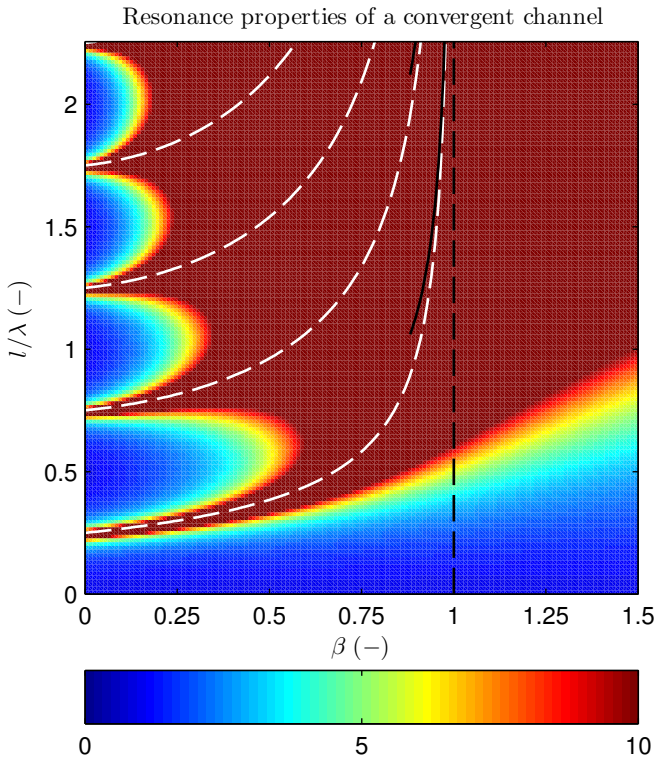

FIGURE 5.1: Dimensionless elevation amplitude at the channel head $|N_{\text{head}}/N_{\text{forc}}|$ for increasing channel lengths (scaled against the shallow water wavelength λ) and increasing convergence. The *black* dashed line represents critical convergence, the *white* dashed lines represent the locations at which resonance occurs, while the solid *black* lines represent an approximation of the resonance locations around $\beta = 1$.

Depending on the dimensionless parameter β, four different regimes can be distinguished. The overall solution used in chapter 4 is valid throughout the whole domain and allows for both real and complex amplitudes in all of these regimes. To further analyse the behaviour of the free surface elevation in these regimes, four different solutions will be used.

No convergence This regime can be expressed with $L_b = \infty$, so that $\beta = 0$, which can be characterised as a prismatic channel. The resulting waves in the channel will display resonance at $l/\lambda = \frac{1}{4}, \frac{3}{4}, ...$, the well known quarter wavelength resonance. This situation can be seen in figure 5.1.

Subcritical convergence This situation occurs when $\frac{1}{2k} < L_b < \infty$, so that $0 < \beta < 1$. This solution is associated with two complex conjugate roots $\Lambda_{1,2} = \Lambda_r \pm i\Lambda_i$, consisting of a positive real part $\Lambda_r = \beta k$ and an imaginary part $\Lambda_i = k\sqrt{1-\beta^2}$.

The general solution to this problem reads $N(x) = \exp(\Lambda_r x)\left[\hat{A}\cos(\Lambda_i x) + \hat{B}\sin(\Lambda_i x)\right]$, with possible complex constants $\hat{A}$ and $\hat{B}$. Applying the boundary conditions $N(0) = N_0$ and $\frac{dN(l)}{dx} = 0$ results in the following solution:

$$N(l) = N_0 \frac{\Lambda_i \exp(\Lambda_r l)}{\Lambda_i \cos(\Lambda_i l) + \Lambda_r \sin(\Lambda_i l)}. \tag{5.4}$$

From this equation the channel length can be found for which resonance occurs. If the denominator is zero, the surface elevation will go to infinity, i.e. resonance:

$$\frac{l}{\lambda} = \frac{n\pi - \arctan\frac{\sqrt{1-\beta^2}}{\beta}}{2\pi\sqrt{1-\beta^2}} \qquad \text{with } n = 0, 1, 2, ... \tag{5.5}$$

This result is represented by the *white* dashed lines in figure 5.1.

To further describe the behaviour of the resonance peaks, the situation is analysed when β is approaching one. A striking property of the tangents is that around zero, $\tan(x) \approx x$. Since this is valid for every channel length, equation (5.5) simplifies as:

$$\frac{l}{\lambda} = \frac{n\pi - \frac{\sqrt{1-\beta^2}}{\beta}}{2\pi\sqrt{1-\beta^2}} \qquad \text{with } n = 0, 1, 2, ... \tag{5.6}$$

In case $n = 0$, this can further be simplified to $\frac{l}{\lambda} = -\frac{1}{2\pi\beta}$, which means that this situation does not occur, since negative β-values indicate channel divergence. Furthermore, $n \neq 0$ simplifies to $\frac{l}{\lambda} = \frac{n}{2\sqrt{1-\beta^2}}$. This situation does occur, where the solid *black* lines in figure 5.1 represent the situation where β approaches one for $n = 1$.

For resonance in combination with subcritical values for β, this is described by a combination of the cosine and the sine in the denominator of equation (5.4). It can be seen that when β approaches zero, the roots become $\Lambda_r = 0$ and $\Lambda_i = k$. The result of this is that the cosine becomes increasingly important with a decreasing β, which thus eventually leads to a prismatic channel, for which the familiar result reads:

$$N(l) = \frac{N_0}{\cos kl} \tag{5.7}$$

Critical convergence At the boundary between sub- and supercritical convergence, critical convergence occurs. This boundary represent a transition for which no resonance peaks are visible any more. This is when $L_b = \frac{1}{2k}$, so that $\beta = 1$. From equation (5.3) now two double real valued roots are found at $\Lambda = k$. The general solution for this problem reads $N(x) = (A + Bx)\exp(\Lambda x)$. Applying the boundary conditions gives the following expression:

$$N(x) = N_0\left(1 - \frac{kx}{1+kl}\right)\exp(kx). \tag{5.8}$$

It directly follows that resonance occurs when

$$\frac{l}{\lambda} = -\frac{1}{2\pi}. \tag{5.9}$$

And since the interest here is only in positive values for the channel length, no resonance is observed in figure 5.1.

Supercritical convergence Finally, supercritical convergence occurs when $L_b < \frac{1}{2k}$, so that $\beta > 1$. This situation is associated with two roots which are both real, as found in equation (5.3). The general solution reads $N(x) = A\exp(\Lambda_1 x) + B\exp(\Lambda_2 x)$, with constants A and B. By applying the boundary conditions it follows that

$$N(x) = N_0 \frac{\Lambda_2 \exp[\Lambda_1 x] - \Lambda_1 \exp(l[\Lambda_1 - \Lambda_2])\exp[\Lambda_2 x]}{\Lambda_2 - \Lambda_1 \exp(l[\Lambda_1 - \Lambda_2])}. \tag{5.10}$$

Again, resonance occurs when the denominator is zero, which leads to the following expression:

$$\frac{l}{\lambda} = \frac{\ln\left(\frac{\beta-\sqrt{\beta^2-1}}{\beta+\sqrt{\beta^2-1}}\right)}{4\pi\sqrt{\beta^2-1}}. \tag{5.11}$$

And analogous to the previous case, resonance only occurs for negative values of the channel length. Hence, no resonance is observed in figure 5.1 to the right of the *black* dashed line.

Furthermore, it can be observed that in the limit $\beta \to \infty$ the roots simplify to $\Lambda_{1,2} = k(\beta \pm \beta)$, so that equation (5.10) becomes $N(x) = N_0$. The physical interpretation for this is that the channel elevation is moving uniformly with the forcing amplitude. This can be observed in figure 5.1, where the blue area increases linearly with an increasing β.

5.2. Velocities

To determine what happens to the oscillations around the landward boundary, the velocities will be analysed. Therefore, the reflected and incoming wave are described separately and can be written as

$$N(x) = A_{\text{refl}}\exp(\Lambda_1[x-l]) + A_{\text{inc}}\exp(\Lambda_2[x-l]), \tag{5.12}$$

with roots $\Lambda_{1,2} = \Lambda_r \pm i\Lambda_i$ and $\Lambda_r = \beta k$, $\Lambda_i = k\sqrt{1-\beta^2}$ for the subcritical part and $\Lambda_{1,2} = k(\beta \pm \sqrt{\beta^2-1})$ for the supercritical part. Now, the velocities around the

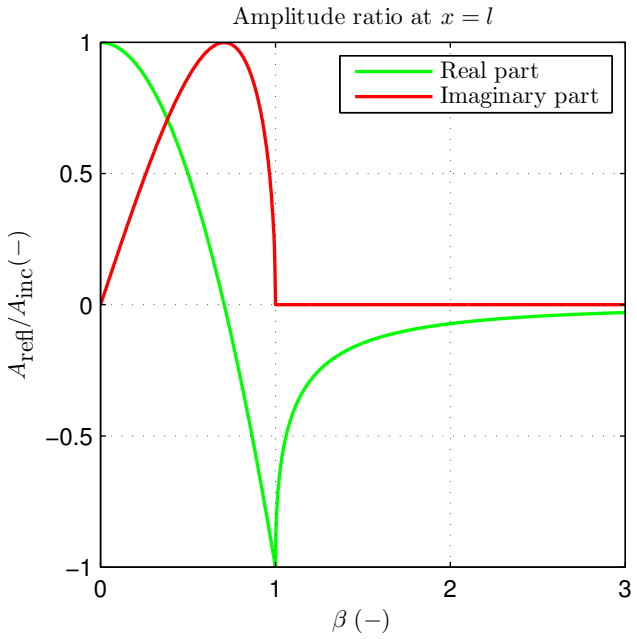

FIGURE 5.2: Ratio between the elevation amplitudes of the incoming and outgoing oscillations at the closed boundary.

boundary are found through $\frac{-g}{i\omega}\frac{\mathrm{d}N}{\mathrm{d}x}\big|_{x=l} = 0$:

$$\begin{aligned} U_{x=l} &= \frac{-g}{i\omega}\left[A_{\text{refl}}\Lambda_1 \exp(\Lambda_1[x-l]) + A_{\text{inc}}\Lambda_2 \exp(\Lambda_2[x-l])\right]_{x=l}, \\ &= A_{\text{refl}}\Lambda_1 + A_{\text{inc}}\Lambda_2 = 0. \end{aligned} \tag{5.13}$$

This leads to the following expressions for the ratio between the elevation amplitudes:

$$\frac{A_{\text{refl}}}{A_{\text{inc}}} = -\frac{\Lambda_2}{\Lambda_1} = \begin{cases} -\frac{\Lambda_r - i\Lambda_i}{\Lambda_r + i\Lambda_i} = \frac{\Lambda_i + i\Lambda_r}{\Lambda_i - i\Lambda_r} & \text{if } 0 \leq \beta \leq 1, \\ -\frac{\beta - \sqrt{\beta^2 - 1}}{\beta + \sqrt{\beta^2 - 1}} & \text{if } \beta \geq 1. \end{cases} \tag{5.14}$$

This ratio is plotted in figure 5.2, where four distinctive cases can be recognized.

- The first is for a prismatic channel, i.e. $\beta = 0$, such that $\Lambda_r = 0$. This leads to the situation that $A_{\text{refl}} = A_{\text{inc}}$, so that the amplitude ratio is 1.
- The second is at $\beta = \frac{\sqrt{2}}{2}$, such that $A_{\text{refl}}/A_{\text{inc}} = 0 + 1i$, which implies a phase shift of 90°.
- Next, if $\beta \to 1$ in the situation with critical convergence, $A_{\text{refl}} \to -A_{\text{inc}}$. This can be seen in figure 5.2, where the ratio is -1, which implies a phase shift of 180°. This can be interpreted in such a way that the reflected wave acts similar to the incoming wave, so that their velocities have the same direction. The result

of this is that the wavelength for which resonance occurs approaches infinity, as already shown in figure 5.1.

- Finally, the fourth case that can be distinguished is for strong supercritical convergence ($\beta \to \infty$), where the amplitude ratio is approaching zero. This is caused by the amplitude of the reflected oscillation, which is zero for infinite β, such that the elevation amplitude at the channel head is only caused by the incoming oscillation. This corresponds to what was found in the previous section.

5.3. Friction

This section will discuss the changes to the physical mechanism of a channel without secondary basin, due to the presence of bottom friction. In order to do this, the results shown in figure 5.1 will be compared to the frictional case, while the ratio between the two cases, $|N_{\text{fr}}/N_{\text{ref}}|$, will reveal the amplitude gain in this situation.

Figure 5.3 presents these cases, where panel *b* presents the frictional case. The difference that can be noticed between the cases, is that for subcritical convergence the resonance pattern damps out for increasing channel length. This is caused by wave dissipation, where tidal energy is lost due the influence of friction, so that the elevation amplitudes decreases. This is also visible in panel *c*, where for short channels almost no change in amplitude gain is shown (*green* areas). However, the effect of friction increases for increasing channel length. The second thing that can be mentioned is that opposed to weak convergence, less effects are visible for stronger convergent

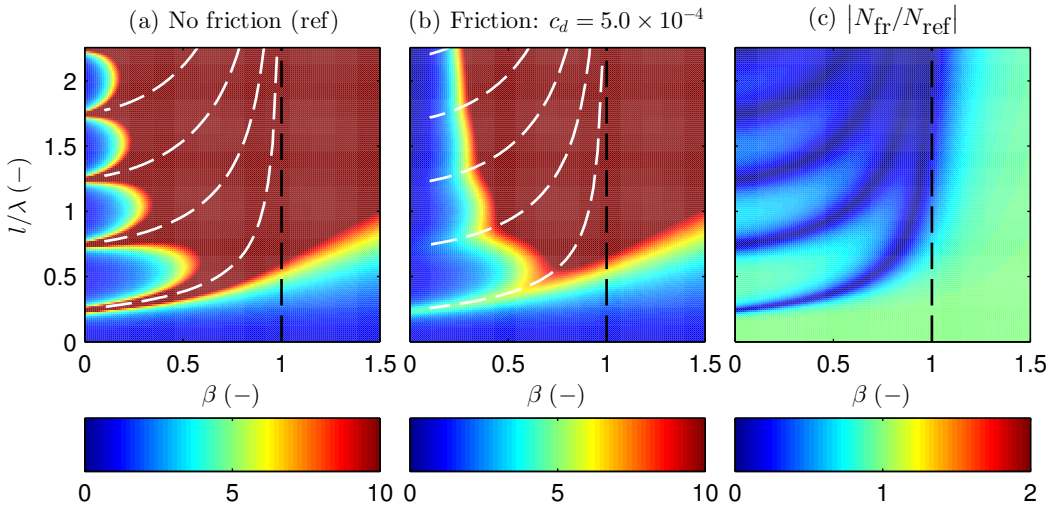

FIGURE 5.3: Effect of friction on the physical mechanism. (**a**) presents the frictionless case, (**b**) the case with normal friction conditions, while (**c**) presents the ratio $|N_{\text{fr}}/N_{\text{ref}}|$.

channels. Where the resonance pattern diminishes, the area of exponential increase remains high. This is best observed in supercritically convergent channels, where only for very large channel lengths, some amplitude reduction is noticeable in panel *c*. In the limit $\beta \to \infty$, the wavenumber k does not influence the elevation amplitude any more $\left(|N_{\mathrm{fr}}/N_{\mathrm{ref}}| = 1\right)$, while this is the parameter through which friction enters the system. As a result, no friction can be observed. This is again corresponds to the fact that in this limit, the channel elevation moves uniformly with the forcing amplitude.

The final remark that can be made from this case is that under the influence of bottom friction wavelengths tend to shorten slightly, which is easily mentioned when realising that figure 5.3a has only four resonance lines, while figure 5.3b displays five. This effect is larger for increasing friction.

Chapter 6

Parameter analysis

This chapter will present the results which are found through the analysis of the model parameters. As explained in chapter 1, the focus will be on the elevation amplitude at the channel head. In each of the following sections, one or more parameters will be varied to get a complete overview of the properties of the system, whereas the reference cases will be used as a starting point for each analysis. In order to keep this chapter as transparent as possible, several figures will be displayed in the appendices, which will be indicated accordingly.

6.1. Reference cases

The following section describes the cases that will be used as a reference throughout this chapter. Two cases will be discussed, one for a prismatic channel and one for a convergent channel.

6.1.1. Approach and parameters

Te determine the water levels in the channel, the complex amplitude N is defined. Since the interest here is in the effects of the different parameters, the amplification factor

$$A = N_{\text{head}}/N_{\text{head}}^{\text{ref}} \tag{6.1}$$

represents the ratio between the reference case and the case under research. Here, the value $|A|$ gives the *amplitude gain*, while $\arg(A)$ shows the phase shift.

TABLE 6.1: Overview of the model parameters, their reference values and secondary values. Capitals S, L and N denote 'small', 'large' and 'negative' basins, respectively.

Description	Symbol	Reference values	Alternative values
Forcing amplitude	N_{forc}	0.5 m	
Angular frequency M2-tide	ω	1.404×10^{-4} rad s^{-1}	
Main channel: length	l_{max}	700 km	
Main channel: depth	h	10 m	
Convergence	β	0, 0.25	0.1 – 2
Width channel mouth	B_0	1000 m	
Friction	c_d	2.5×10^{-3}	
Basin: area	A_j	20 km^2	S: 10 km^2, L: 100 km^2
Basin: channel length	$l_{b,j}$	1 km	N: 2 km
Basin: channel depth	$h_{b,j}$	5 m	N: 1 m
Basin: channel width	$b_{b,j}$	100 m	N: 50 m
Basin: eigenfrequency	$\omega_{0,j}$	4.95×10^{-4} rad s^{-1}	S: 7.00×10^{-4} rad s^{-1} L: 2.21×10^{-4} rad s^{-1} N: 0.50×10^{-4} rad s^{-1}

In order to expose the response of the basins as much as possible, the channel length will be varied in the range $0 < l < l_{\text{max}}$, while the basins position will be varied between $0 < x_1 < l$. The parameter values can be found in table 6.1. Furthermore, friction will not be considered in the reference cases, but will be analysed in section 6.6.

In both reference cases the basin characteristics will be kept fixed, so that the basin admittance $\tilde{Y}$ is similar in each case. The chosen parameter values for the basins are equal to that in the study of Roos and Schuttelaars (2015). The secondary values for the basins parameters will be used for the analysis of the basins characteristics.

6.1.2. Prismatic channel

The first reference case is that for a prismatic channel, which is represented by $\beta = 0$. Overall, this reference case is similar to the reference case described by Roos and Schuttelaars (2015), with the exception of the forcing.

For a constant width in a channel with one single section ($b_j = b_m$ and $k_j = k_{1,j;2,j} = k_m$), equation (4.25) can be solved to obtain the following result.

$$N_{\text{head}}^{\text{ref}} = \frac{N_{\text{forc}}}{\cos kl} \tag{6.2}$$

While equation (4.26) can be solved to obtain the result for one secondary basin.

$$N_{\text{head}} = \frac{N_{\text{forc}}}{\cos kl - \tilde{Y}_1 \sin(k[x_j - x_{j-1}]) \cos(k[x_{j+1} - x_j])} \tag{6.3}$$

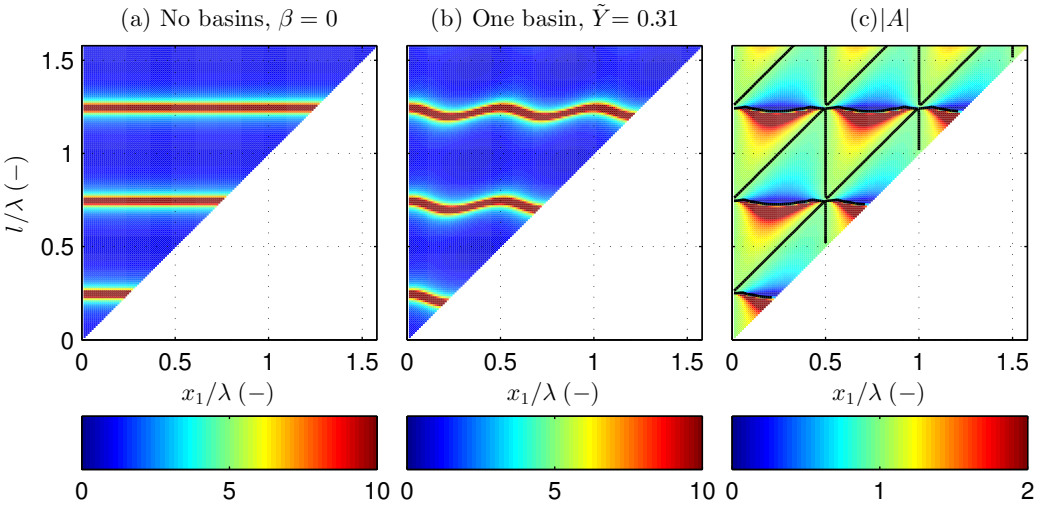

FIGURE 6.1: Reference case for prismatic channels, with the dimensionless elevation at the channel head $|N_{\text{head}}/N_{\text{forc}}|$ for a situation (**a**) without and (**b**) with one secondary basin at $x = x_1$. Panel (**c**) shows the amplitude gain $|A|$, where the *black* lines denote the unit contour lines. Channel length l and basin position x_1 have been scaled against the shallow water wavelength $\lambda \approx 443$ km.

Such that the amplification factor can be written as follows, which is similar to what was found by Roos and Schuttelaars (2015).

$$A = \left[1 - \frac{\tilde{Y}_1 \sin(k[x_j - x_{j-1}]) \cos(k[x_{j+1} - x_j])}{\cos kl}\right]^{-1} \tag{6.4}$$

Figure 6.1 presents this reference case, where panels a and b present the dimensionless elevation at the channel head for a situation with and without a secondary basin, respectively. Panel c shows the amplitude gain. To improve the interpretation of the results, the axis have been scaled against the frictionless shallow water wavelength $\lambda = 2\pi/k_0 \approx 443$ km.

The panel without a basin shows large amplification around $l/\lambda = \frac{1}{4}, \frac{3}{4}, ...$, the familiar quarter wavelength resonance. The effect of adding one basin becomes clear in the second panel, where a wavy resonance pattern can be observed. Eventually this leads to the pattern where locations for amplification and reduction appear, as shown in the third panel.

Compared to the reference case by Roos and Schuttelaars (2015), it should be noted that the pattern for amplification and reduction is slightly adjusted due to the absence of wave radiation.

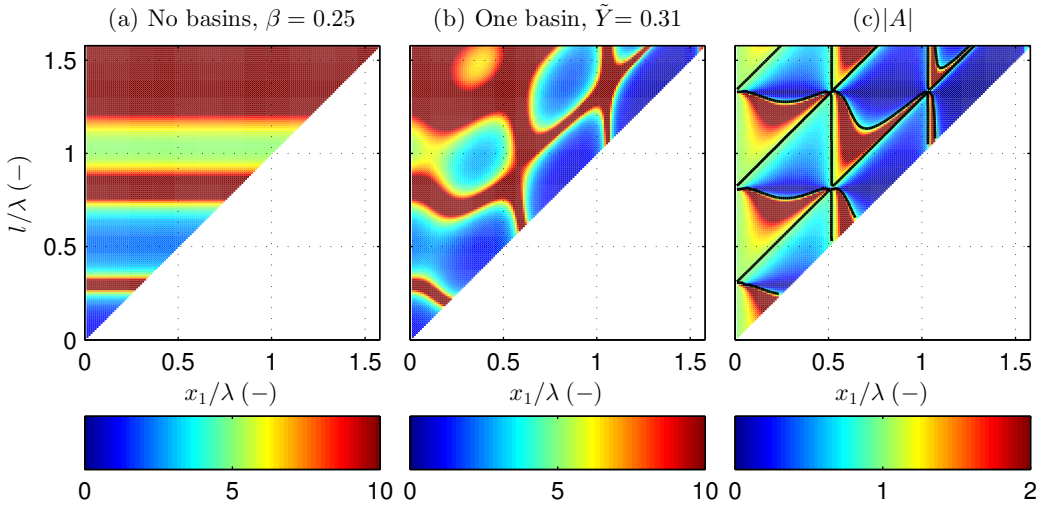

FIGURE 6.2: Similar to figure 6.1, but now for the convergent reference case ($\beta = 0.25$).

6.1.3. Convergent channel

The second reference case presents the effects of a single secondary basin in a convergent channel. To expose the changes which occur due to channel convergence as clear as possible, this case is characterised by a convergence factor of $\beta = 0.25$. As discussed in chapter 5, this is equivalent to a mildly convergent channel.

Opposed to the prismatic case, it is not possible to solve equations (4.25) to (4.27) by applying trigonometric identities, in order to obtain a 'simple' expression for the amplification factor. This is due to the fact that the oscillations in the channel do not behave like 'normal' sinusoidal waves. Therefore, the matrices are solved in MATLAB® using standard techniques.

Figure 6.2 presents this reference case, with a similar structure as in the prismatic case. Again, the quarter wavelength resonance can be observed, though, another process is visible here which is responsible for large amplification, which can be related to the channel convergence. This leads to a different response of a secondary basin as well (figure 6.2b), where large variations for the elevation amplitude can be seen. Although these reference cases differ much, the amplitude gain shows a fairly similar pattern of amplification and reduction. The main difference is that for basins placed further towards the channel head, the locations for which reduction occurs are increasing in area.

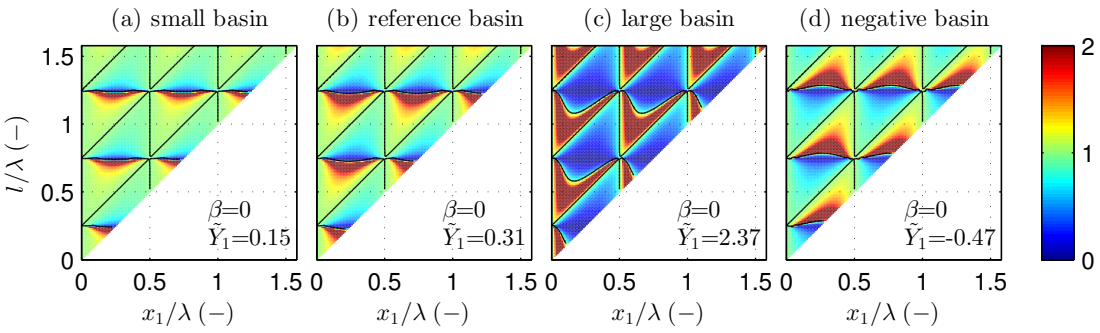

FIGURE 6.3: Responses of the amplitude gain $|A|$ to various basin sizes, here for a prismatic channel. The result is similar as that of Roos and Schuttelaars (2015), here slightly modified due to the absence of wave radiation. *Black* lines denote the unit contours, while the basin positions x_1 and x_2 have been scaled against the shallow water wavelength λ.

6.2. Basin characteristics

This section presents the effects of different basin dimensions on the elevation amplitude. The basin geometry is captured by the dimensionless basin admittance $\tilde{Y}$. The dimensionless parameter $\alpha_j = b_j/b_m$ controls the relative size of the basins to the width at the mouth, in such a way that the channel convergence has no effect on the basin admittance, as can be seen in the matrices on page 27. Thus, the dimensionless basin admittance involves the *local* channel width, however, by including parameter α, all basins are 'normalised' according to the width at the channel mouth.

Figures 6.3 and 6.4 show the results of implementing different basin geometries in both reference cases. For a prismatic channel, this result is similar to what has already been found by Roos and Schuttelaars (2015), here slightly modified due to a different sea representation. It can be seen that small basins have less effect on the amplitude change, while large basins show an intensified response. For certain configurations of

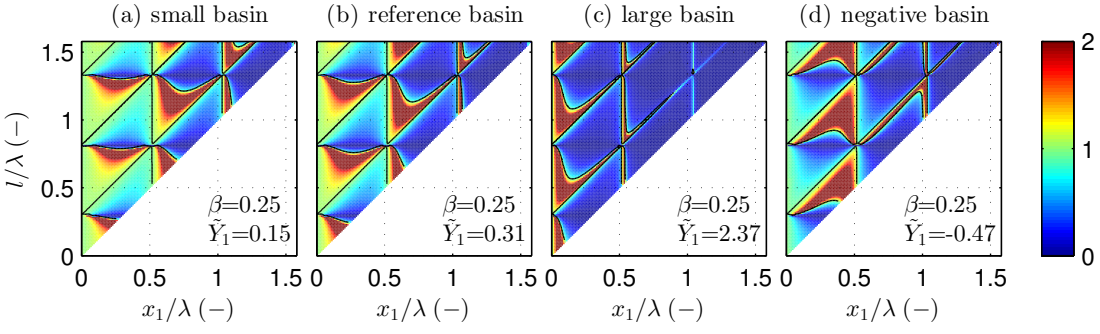

FIGURE 6.4: Similar to figure 6.3, but here for $\beta = 0.25$.

the basin, the system would shift from subcritically forced ($\tilde{Y} > 0$, 'positive' basin) to supercritically forced ($\tilde{Y} < 0$, 'negative' basin), which leads to a reversed pattern of amplification and reduction. 'Negative' basins may have long and shallow inlet channels for instance, but can also be found through other basin configurations.

In case of a convergent main channel, overall similar results are obtained. Small basins show a less intensive response, while larger basins are reacting more intensely. Also, in case of a 'negative' basin, the pattern of amplification and reduction reverses. Furthermore, it is evident that the magnitude of the response is stronger for 'negative' basins than for 'positive' basins.

6.2.1. Channel convergence

Now, it is interesting to see how these effects develop for increasing convergence. Appendix B gives an overview of the responses for other types of basins and for 'positive' basins the areas of amplification decay with increasing convergence, until there is only a distinction between basins close to the channel mouth and basins farther away. Moreover, this is also what can be seen for a 'negative' basin, only this leads to a rather interesting situation for supercritically convergent channels. Because the pattern of amplification and reduction reverses, in combination with an exponential oscillatory behaviour, supercritical channels combined with 'negative' basins will lead to a weakening of the elevation amplitude all throughout the domain. However, there is a clear difference in the intensity of the effect, with again the weakest reduction for a basin in the vicinity of the channel mouth.

6.3. Two basins

In the following section the effects will be discussed of two separate basins along the main channel. As an extension on the reference cases, a second basin is placed at an arbitrary point along the main channel. Since it is not possible to present more than two variable parameters in one figure, in this case the basin locations x_1 and x_2, channel length is chosen fixed, other than the presentation of the reference cases.

This can be seen in figures 6.5 and 6.6, where the effect of two basins, in combination with an increasing channel length, is given. The figures only differ for the convergence parameter β. The upper row (a-d) presents the amplitude gain $|A_{1+2}|$ of both basins combined, while the bottom row (e-h) presents the ratio Q, which represents the interaction between the basins:

$$Q = |A_{1+2}/(A_1 A_2)|. \tag{6.5}$$

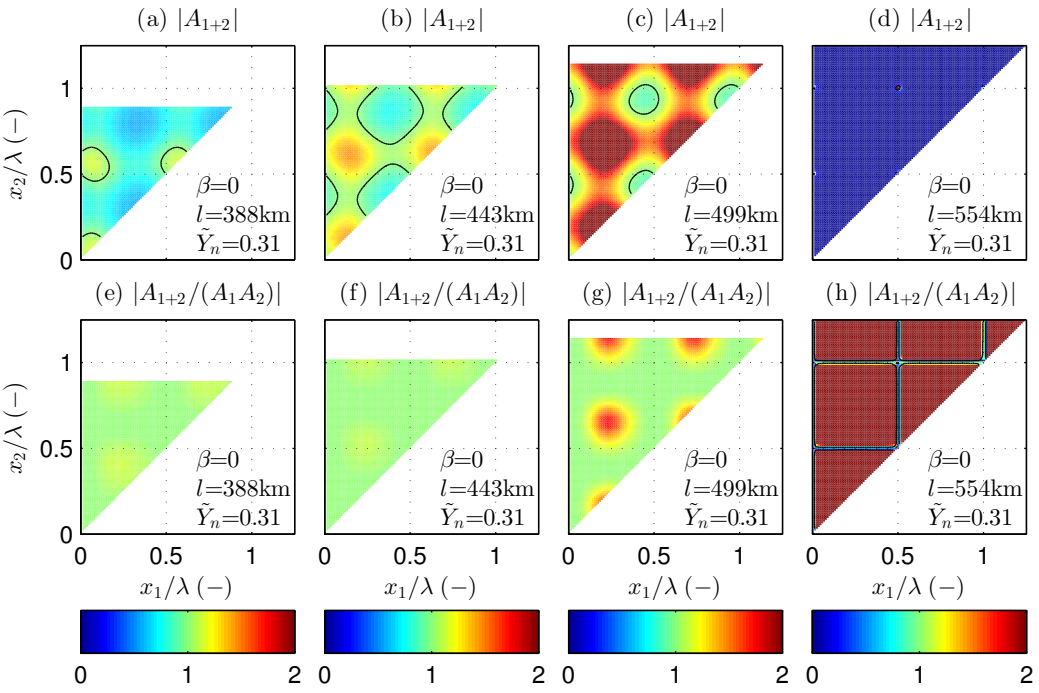

FIGURE 6.5: The top row represents the amplitude gain $|A|$ at the channel head in case of two similar basins for different channel lengths. The bottom row shows the ratio $Q = |A_{1+2}/(A_1A_2)|$, which represents the interaction between the basins. Note that *red* (*blue*) areas in the bottom row do not denote amplification (weakening) of the amplitude (as in the top row), but an amplified (weakened) response compared to the separate effects.

Here, $Q > 1$ indicates an amplified response (*red* areas) due to interaction between the basins, compared to the response of two non-interacting basins. Conversely, if $Q < 1$ the interaction between the basins leads to a weakened response (*blue* areas).

Prismatic channel Figure 6.5 presents the result for a prismatic channel, as already found by Roos and Schuttelaars (2015). The differences with their findings is explained due to the use of a different sea representation and different channel lengths. In general, similar results can be observed, with combinations for the basin locations where the elevation amplitude can be amplified or weakened. An overall pattern is visible where amplification occurs mainly around multiples of a half shallow water wavelength, and weakening is visible at a quarter shallow water wavelength and odd multiples of this. For the response of the subbasins separately, it is observed that the interaction between the basins leads to an amplified response in most of the domain. Figure 6.5*d*,*h* show a rather unique situation, where the channel length is chosen such that maximum resonance occurs in the channel. It can be seen that in the whole domain, the interaction between the basins leads to an amplified response. Other simulations, which are presented in figure C.1, show that for channel lengths near the

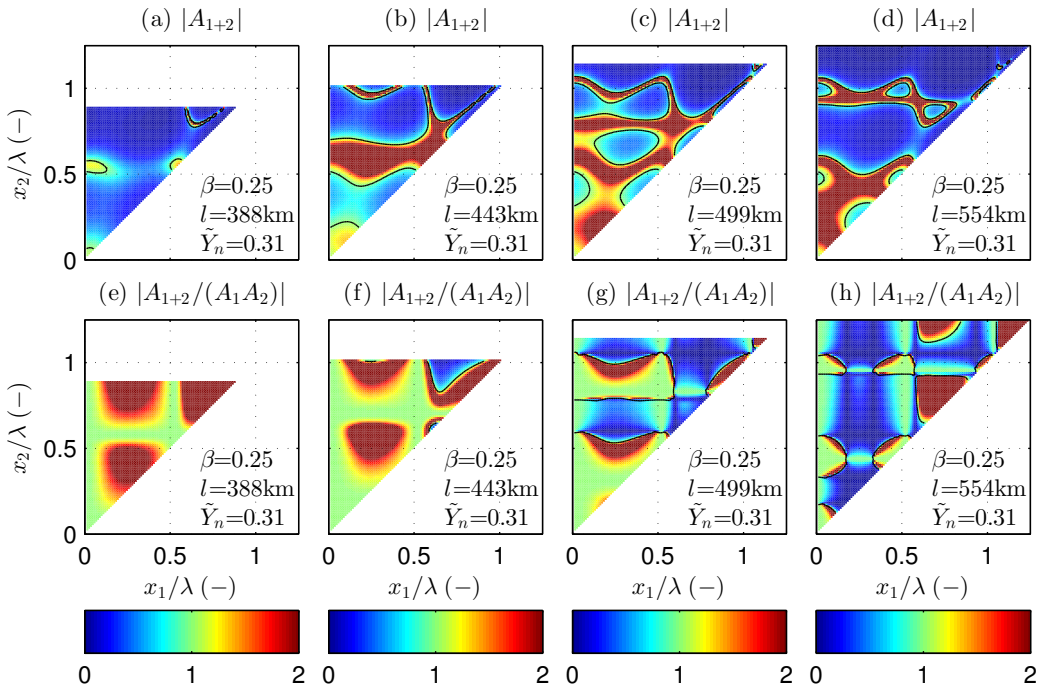

FIGURE 6.6: Similar to figure 6.5, but now for the convergent case ($\beta = 0.25$).

resonance length, both basins may bring the channel closer to resonance, as opposed to what was shown for the exact resonance length.

Convergent channel The result for a subcritically convergent channel can be observed in figure 6.6. Again, combinations of locations for which amplification or reduction occur are visible, while the transition between these situations is much less smooth than in a prismatic channel. Also, the pattern for which amplification or reduction occurs seems much less apparent. This result is the consequence of the deformed wavelengths in a convergent channel. For increasing convergence the wavelengths are increasing as well, which leads to different results in case of the same channel lengths. To adequately compare a convergent channel with a prismatic channel, different lengths have to be analysed.

This is done in figure 6.7, where the channel lengths have been chosen according to the same relative distance from the resonance peaks as in figure 6.5. Here, a similar result is obtained for where the channel length is equal to a resonance length. Both the individual basins, as well as the basins together lead to a weakening of the amplitude. For the remainder of the figures, no clear similarities can be observed.

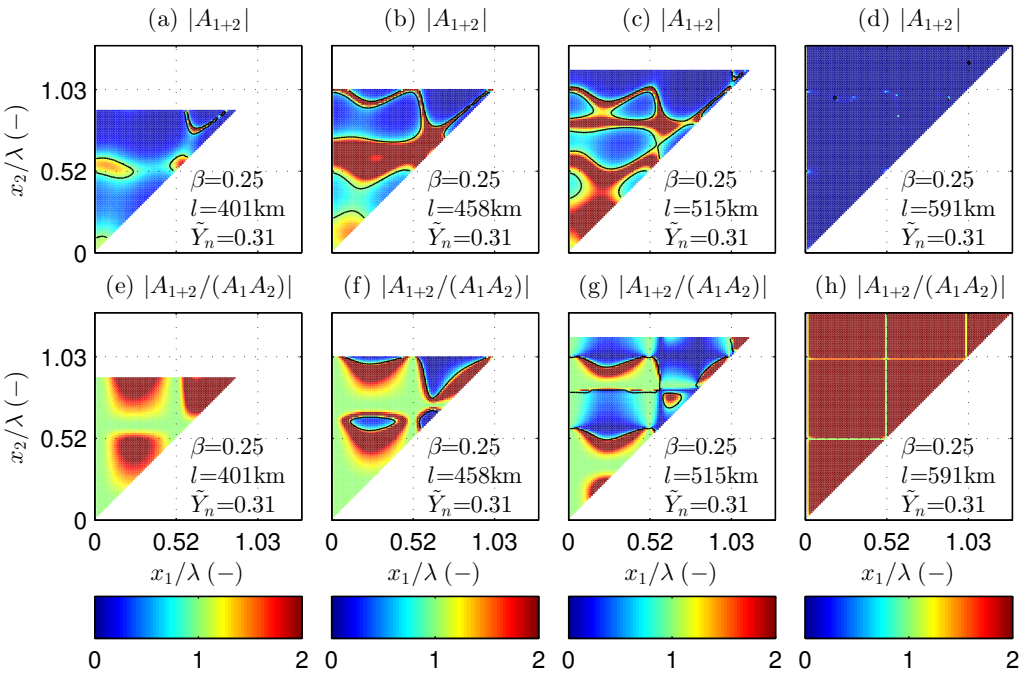

FIGURE 6.7: Similar to figure 6.6, but here adjusted for an increased wavelength due to convergence. The basin positions $x_{1,2}$ have been scaled against the shallow water wavelength λ in case of a prismatic channel. The axes tick marks denote the deformed wavelength in a convergent channel.

Stronger convergence In case of more strongly convergent channels, basins tend to have an overall dampening effect, while for supercritical convergence only basins placed near the channel mouth will lead to an amplification of the tide. This is shown in figures C.2 and C.3, where for an increasing β-value the effects of two basins are shown. Analogous to the response of a single basin in strongly convergent channels, two basins show a similar response, where this effect is even more increasing with increasing convergence.

Furthermore, it can be seen that for supercritically convergent channels, almost no interaction between the basins is observed ($Q = 1$). Only basins which are placed in close proximity to each other will lead to an amplified response, while a weakened response is not observed in supercritically convergent channels. The interaction between basins is even further decreasing for increasing convergence, until eventually no interaction is visible any more.

6.4. Three basins

For a situation with more than two basins, the visual representation is slightly different. For the same reason that the channel length was fixed in the previous section, also the location of the third basin will be fixed in each panel. Besides, since the third parameter to be varied along the sub-figures is here the location of the third basin, the channel length is kept constant. The location of the third basin will be systematically increased in eight steps until it reaches twice the shallow water wavelength λ.

The results for this analysis can be found in figures 6.8 and 6.10 and in appendix D. The panels in the sub-figures present the amplitude gain $|N_{\text{all}}/N_{\text{ref}}|$, which means that it is the total effect of the three basins together.

Prismatic channel Figure 6.8 shows the result for three basins in a prismatic channel, with an arbitrarily chosen channel length. Analogous to the results of one and two basins, we can distinguish locations for which the basins will bring the channel closer to resonance or vice versa. Furthermore, a pattern is visible in the figures. If the third basin is placed between a node and a landward located anti-node of the elevation,

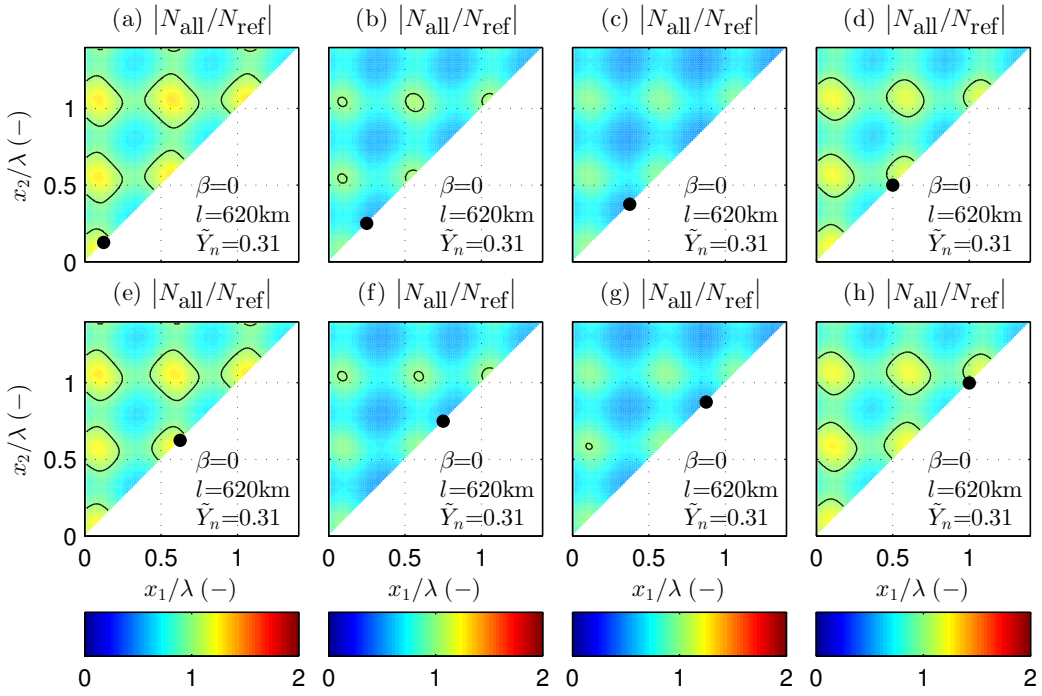

FIGURE 6.8: Amplitude gain $|N_{\text{all}}/N_{\text{ref}}|$ for the situation with three identical basins. *Red* areas indicate amplification of the amplitude, *blue* indicate dampening. The *black* dot represents the position of the third basin, where the first two are varied on the axes (scaled against the shallow water wavelength λ). *Black* lines represent the unit contours.

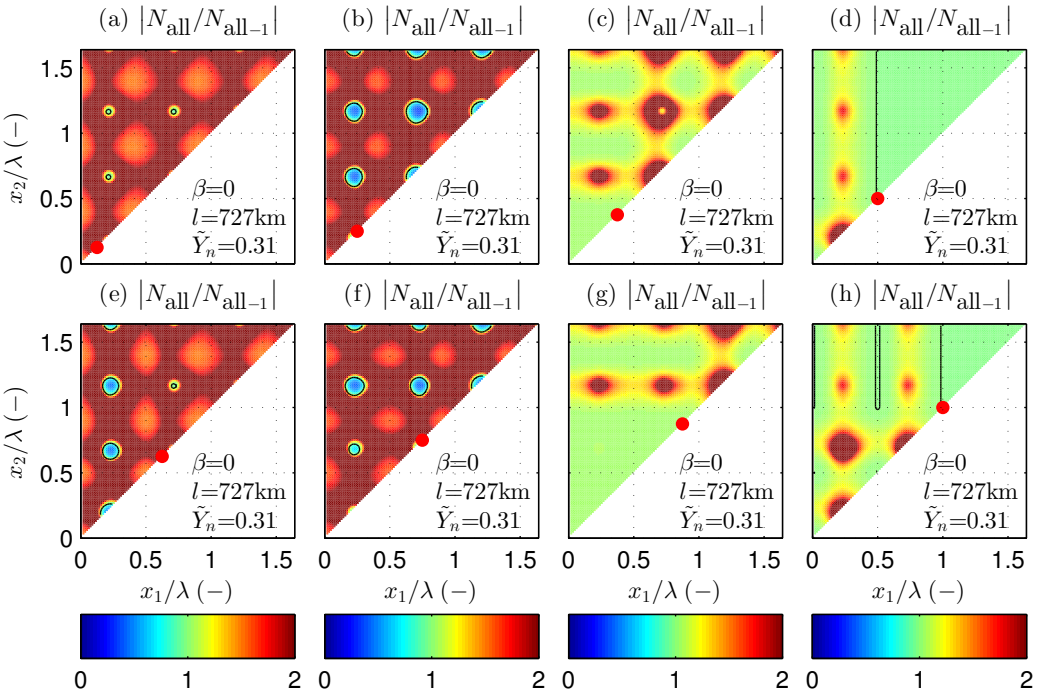

FIGURE 6.9: Separate effect of the third basin $|N_{\text{all}}/N_{\text{all-1}}|$ for the situation with three identical basins in a prismatic channel. The *red* dot represents the third basin.

amplification of the tide may occur. On the other hand, if the third basin is placed between an anti-node and a landward located node, the amplitude will be weakened throughout nearly the whole domain.

However, when this analysis is extended to different values for the channel length, this pattern is distorted. It is only visible in this way when the channel length is chosen to be between an anti-node and a landward located node. Conversely, when the channel length lies between a node and a landward located anti-node, all basins together will lead to an amplification of the tide almost on all locations. Only when the third basin is placed on a location in the above described pattern, some locations for which amplitude reduction occurs arise. This result can be found in figure D.1 in the appendix.

Particularly, it is interesting to analyse the separate effect of a third basin on the elevation amplitude. Figure 6.9 shows the separate amplitude gain of the third basin $|N_{\text{all}}/N_{\text{all-1}}|$, here for the same channel length as in the prior situation with amplification. *Red* areas indicate amplification of the amplitude, *blue* indicate dampening. The results clearly corroborate with the earlier findings, where large amplification is found when the third basin is placed between a node and a landward located anti-node. Furthermore, figure D.2 shows that reduction of the tide may occur when a basin is placed at the opposite locations of the channel, but only if the channel itself has a

TABLE 6.2: Summary of the results for three basins in a prismatic channel. Elevation *nodes* and *anti-nodes* are based on the length of the frictionless shallow water wave λ. For further explanation of these cases, see text.

	Channel length	
	Node $< l <$ *Anti-node*	*Anti-node* $< l <$ *Node*
Basin location		
Node $< x_3 <$ *Anti-node*	Large amplification	Minor amplification
Anti-node $< x_3 <$ *Node*	Minor reduction	Average reduction

length between an anti-node and a landward placed node. To summarize these findings, table 6.2 gives an overview of the situations for which amplification and reduction occur.

Convergent channel The pattern of amplification and reduction found in prismatic channels is not visible any more in convergent channels. Figure 6.10 shows the amplitude gain of all the basins together and it can be clearly observed that an overall reduction of the tidal amplitude is present, although small areas of amplification still

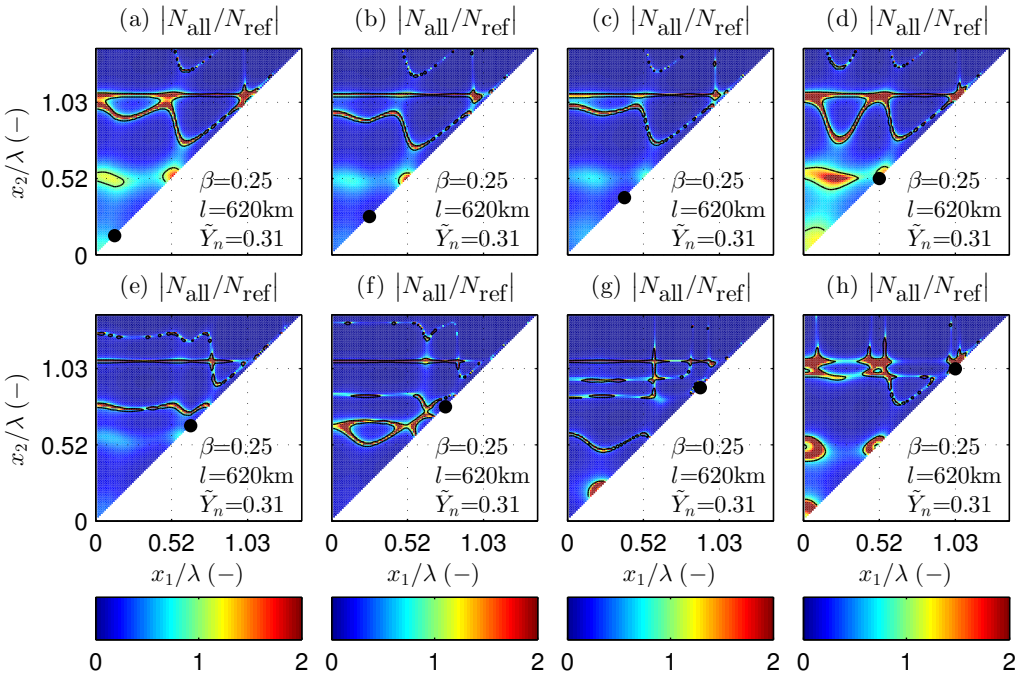

FIGURE 6.10: Amplitude gain $|N_{all}/N_{ref}|$ for the situation with three identical basins in a subcritical channel. The *black* dot represents the third basin, where the other two are represented by $x_{1,2}$. *Black* lines represent the unit contours. The increased tick marks on the axes indicate half multiples of the increased wavelength due to the convergence.

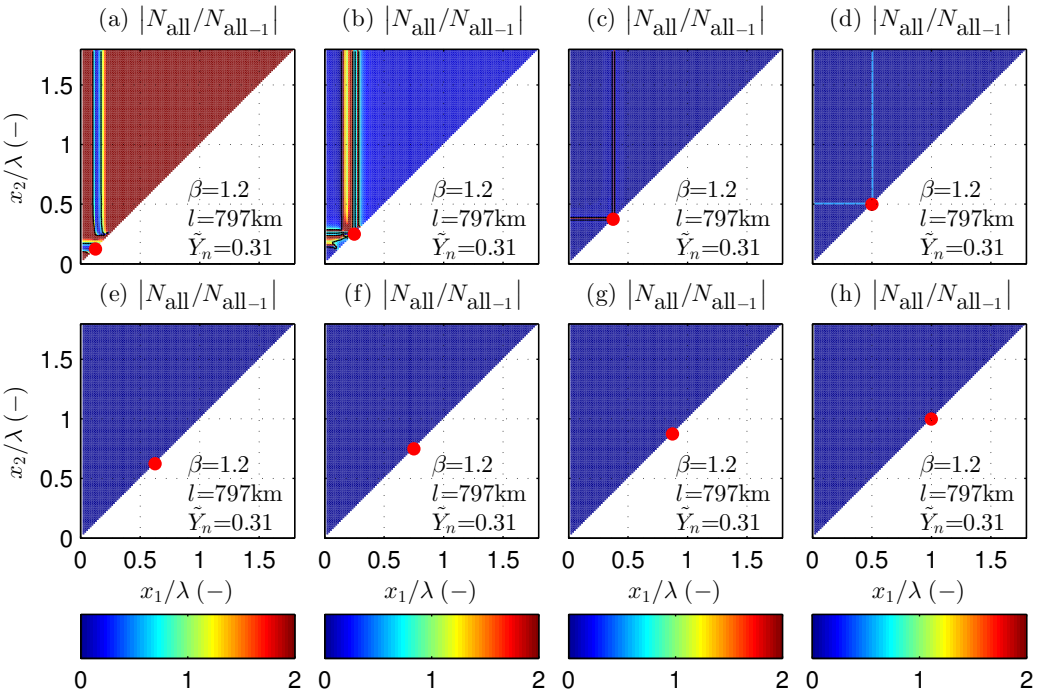

FIGURE 6.11: Separate effect of the third basin $|N_{all}/N_{all\text{-}1}|$ for the situation with three identical basins in a supercritical channel. The *red* dot represents the third basin. The axes tick marks are not adjusted to the increased wavelength any more, since no distinct waves are present in supercritical channels.

occur. Note that this situation is only valid for one specific length of the main channel. When this analysis is extended to various other values for this parameter, the opposite may happen as well, see appendix D.

When analysing the separate effect of one basin (figure D.3) the above findings are confirmed, nevertheless there is an indication that more amplification may occur when placing a basin near the mouth of the channel. So, no clear pattern can be found to predict the response, although there is one specific situation which can be observed. In panels *d* and *h* of figure D.3, it can be seen that when a basin is placed exactly on an elevation node, it has no upstream influence on the elevation amplitude. Revisiting the previous paragraph, the same situation exists for a prismatic channel (see figures 6.9 and D.2). This property can be explained through the physical mechanism, which will be discussed in detail in chapter 7.

Stronger convergence For supercritically convergent channels the effect of the third basin is rather evident, which directly follows from the understanding of the physical mechanism. Placing an extra basin at any place away from the channel mouth leads to a weakening of the tide. Only when the basin is placed in close vicinity of the

mouth, amplification occurs. This is demonstrated in figure 6.11, where the factor for the effect of a separate basin $|N_{\text{all}}/N_{\text{all-1}}|$ is shown. This result is also valid for other values of the channel length, which follows from other simulations not shown here.

6.5. More than three basins

When adding even more basins to the channel, the parameter space is increasing even more. In order to keep this chapter concise, the analysis is presented in appendix E. Overall, the results show that in convergent channels basins near the channel mouth might lead to an amplification of the tide, while basins placed further away tend to have a more dampening effect to the resonance. For increasing convergence, this effects becomes more apparent.

These result are in line with that of the situations with less basins. Moreover, it becomes clear that although a certain combination of basins shows an amplitude reduction, one of those basins might counteract this effect. Therefore, for practical application, it is important to analyse the effect of each basin separately.

6.6. Bottom friction

So far, all simulations have been carried out without bottom friction in order to expose the effects of channel convergence. This section repeats some of the more noticeable results from the previous sections, but now including friction. In the following simulations, friction is set to one-tenth of the values presented in appendix A, in order to optimally reveal the effects of bottom friction.

6.6.1. Reference cases

Th effect of friction can be well recognised in the reference cases, where the effect on a prismatic channel has already been shown by Roos and Schuttelaars (2015). They stated that due to dissipation of wave energy, the amplitude damps and the pattern resulting from the presence of a secondary basin changes. For convergent channels, a similar result can be observed. Figure 6.12 shows the effect of bottom friction on the second reference case, where corresponding results are visible. The wave dissipation is most noticeable in figure 6.12b, where the areas of high amplitudes are damping out, compared to the result in figure 6.2b. Furthermore, the effects to the amplitude gain are similar for convergent channels as for prismatic channels, where the pattern of amplification and reduction is distorted, more strongly for longer channels.

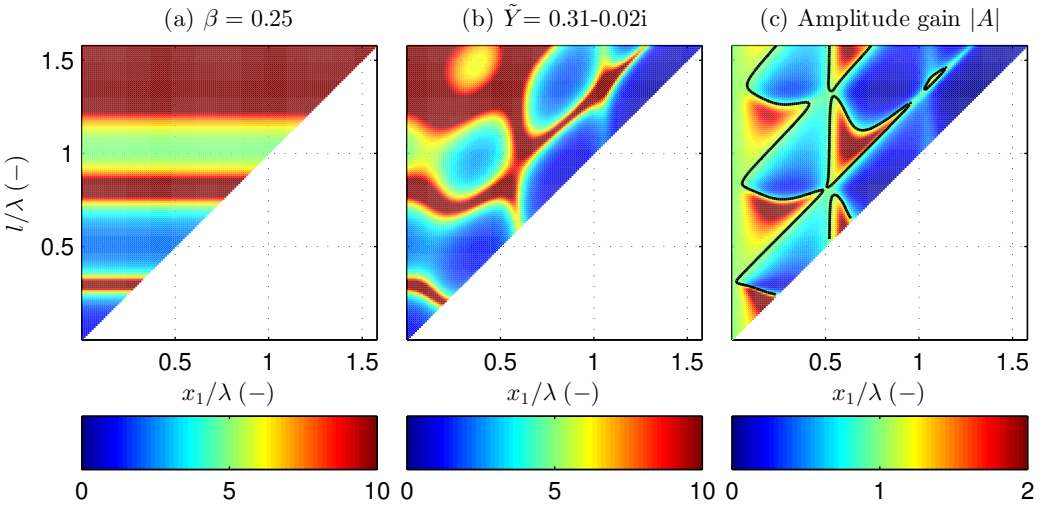

FIGURE 6.12: The effect of friction on the convergent reference case (figure 6.2). *Black* lines denote unit contours.

6.6.2. Basin characteristics

By including friction, not only the wave in the main channel will be subjected to dissipation of energy, also the water that flows through the inlet channel will feel the effects of friction. Figures 6.13 and 6.14 confirm this effect, where it can be seen that the basin admittance $\tilde{Y}$ changes due to the bottom friction (all other parameters are kept constant). The effect of bottom friction on the reference basin in a prismatic channel (figure 6.13b) has already been studied by Roos and Schuttelaars (2015), where they found that the amplitude gain weakens, while the observed pattern changes. This is also visible in this situation, where the differences are again the result of the choice for the sea representation. For larger basins, the pattern for amplification and reduction

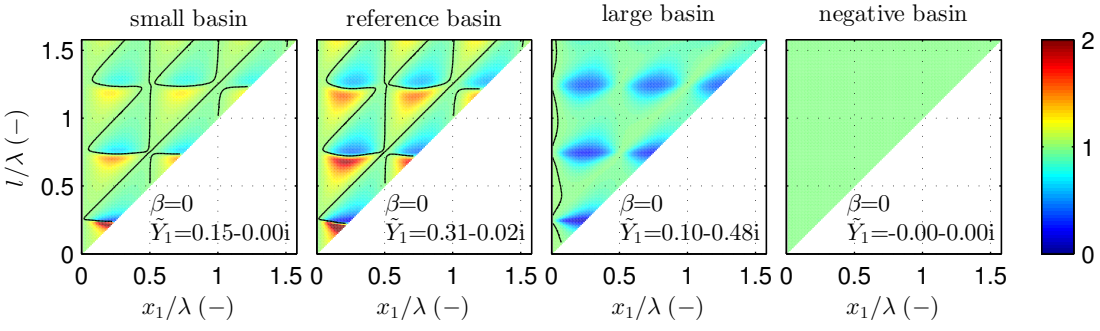

FIGURE 6.13: Responses of the amplitude gain to various basin sizes, here for a prismatic channel including moderate friction. Note that the admittance for the 'negative' basin has changed severely in comparison with the frictionless case (figure 6.3).

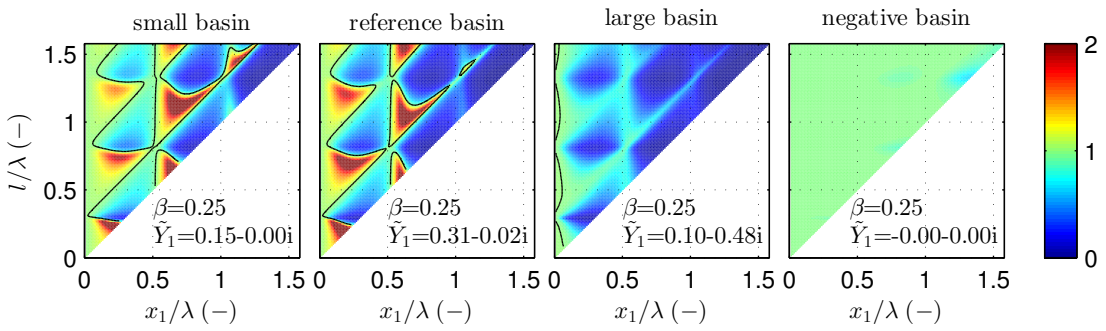

FIGURE 6.14: Effect of bottom friction to the response of basin of various sizes, here for $\beta = 0.25$.

changes severely, where almost everywhere in the domain the amplitude is weakened. This effect increases with increasing convergence, as can be seen in the convergent case.

Another interesting result here is that of the 'negative' basin, for which the amplitude gain is damped out throughout almost the whole domain. This follows from the basin admittance, which is close to zero. Figure 6.14 shows a similar behaviour, despite some small areas of reduction. Only for strong subcritical and supercritical convergence (see figure B.4) larger areas of elevation reduction arise, although the basin admittance remains nearly zero.

The response to all other basin configurations is in line with the earlier results, where the pattern for a frictionless channel is distorted.

6.6.3. Two basins

Although the previous revealed the effects of friction on retention basins, it is yet unclear which effect could be expected in a situation with more than one basin. Therefore this section will recall the cases in section 6.3, now including friction. Figures 6.15 (convergent channel) and C.4 (prismatic channel) present these cases, with the distinction between the overall amplitude gain (*top* row) and the interaction between the basins (*bottom* row).

For both cases it can be seen that due to wave dissipation the magnitude of the amplitude gain is less than in the frictionless cases, where the *red* and *blue* areas are less distinctive. Also the pattern of amplification and reduction is slightly adjusted, which is more apparent for the convergent case.

Regarding the interaction between the basins, the case with a prismatic channel (figure C.4) shows almost no interaction any more. Only for channel lengths close to the resonance lengths, the interaction becomes slightly more visible, which follows from

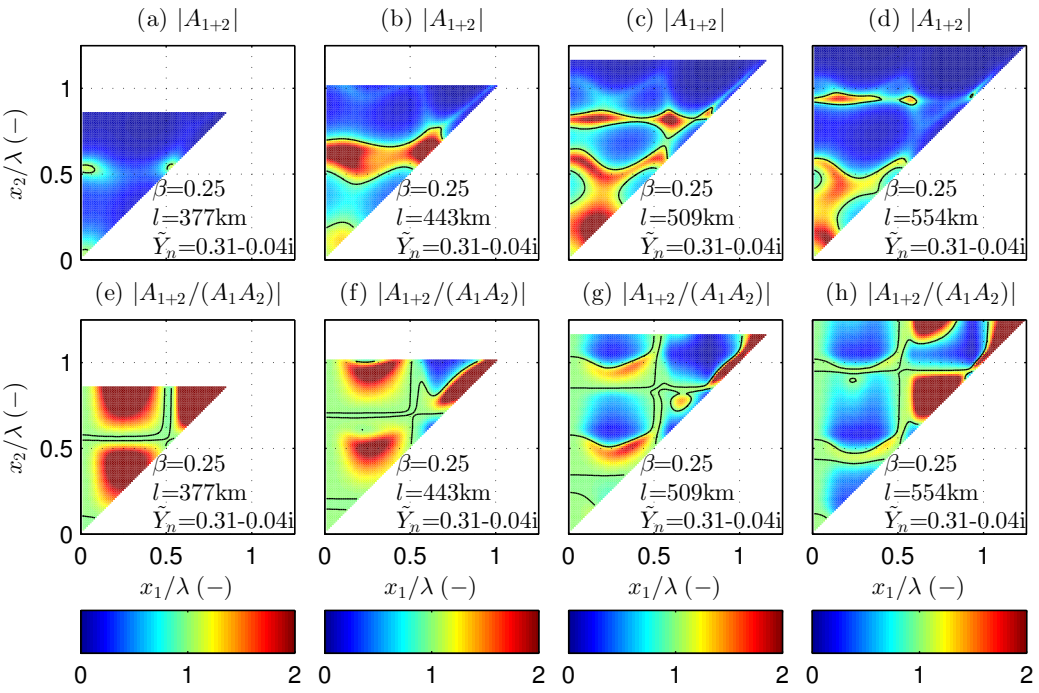

FIGURE 6.15: Effect of bottom friction on two basins along a convergent main channel with $\beta = 0.25$. The *top* row shows the amplitude gain, while the *bottom* row presents the quantity Q, which denotes the separate effect of both basins. *Black* lines show the unit contours. Axes have been scaled against the shallow water wavelength λ.

simulations not reported here. This effect does not appear in the convergent case, where the interaction between the basins is overall similar to that in the frictionless reference case. Areas of increased and decreased interaction may still occur, albeit less pronounced.

6.7. Summary

Appendix F gives a summary of results found in the previous sections. It presents the most noticeable outcomes of the performed simulations. Besides, it gives a comprehensive overview of the current knowledge of hydrodynamical effects in a convergent tidal channel with multiple secondary basins.

Chapter 7

Physical mechanism of retention basins

To understand the mechanism behind convergent channels with retention basins, this chapter will go into the physics behind these systems. Chapter 5 already showed the mechanism in a convergent channel without basins. For clarity, first the mechanism in a prismatic channel will be described, as already been discussed by Roos and Schuttelaars (2015).

7.1. Prismatic channel

The physical mechanism behind retention basins in a prismatic channel has been described by Roos and Schuttelaars (2015). Figure 7.1 shows this mechanism, where the left panel represents the reference case. It shows a standing wave in a main channel, which results in an amplitude N_1^{ref} somewhere along the channel ($x = x_1$).

Due to the presence of a secondary basin, additional waves are being triggered in the channel (Roos and Schuttelaars, 2015). This is caused by oscillations inside the basin as well as a volume transport through the inlet channel. The resulting waves in the main channel may develop in both directions of the inlet channel. The additional waves also have their own (unknown) elevation amplitude at $x = x_1$, here denoted as N_1'. This is shown in the right panel of figure 7.1, where the responding wave for deep sea conditions has been sketched. Since the conditions at the vertex point still have to be respected, the volume transport equation (4.21) can be rewritten to obtain the

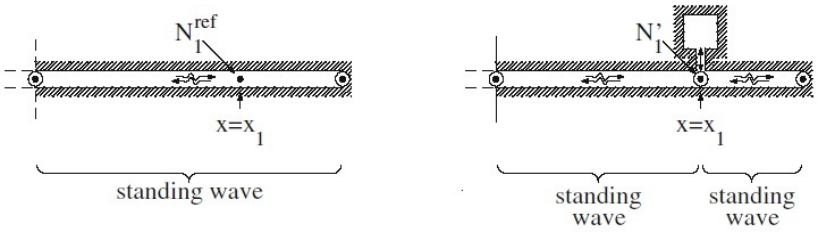

FIGURE 7.1: Physical mechanism in a prismatic channel (Roos and Schuttelaars, 2015). The left figure represents the reference wave, while the right figure shows the response of a single basin.

following expression:

$$\left(Y_{\mathrm{sw}} - Y_{\mathrm{lw}}\right) N_1' = Y_1 \left(N_1^{\mathrm{ref}} + N_1'\right). \tag{7.1}$$

Here, landward (Y_{lw}) and seaward (Y_{sw}) admittances have been introduced, which represent the admittances of the additional waves. Here, a positive $\tilde{Y}_{\mathrm{lw}}$-value means inflow towards the landward side of the vertex point. Equation (7.1) can be solved to obtain

$$\frac{N_1'}{N_1^{\mathrm{ref}}} = \frac{1}{(Y_{\mathrm{sw}} - Y_{\mathrm{lw}})/\tilde{Y}_1 - 1}, \tag{7.2}$$

expressed in terms of dimensionless admittances. Amplification occurs if $|N_1^{\mathrm{ref}} + N_1'| > N_1^{\mathrm{ref}}$, reduction if $|N_1^{\mathrm{ref}} + N_1'| < N_1^{\mathrm{ref}}$.

7.1.1. Cases without amplitude change

Furthermore, Roos and Schuttelaars (2015) describe three cases for which no amplitude change occurs, i.e. $|N_1^{\mathrm{ref}} + N_1'| = N_1^{\mathrm{ref}}$, and are explained below.

- *Case I*: At the position of the basin $x = x_1$, the reference wave displays a *node*, such that $N_1^{\mathrm{ref}} = 0$. The result is that the secondary basin does not encounter any forcing and no additional waves develop. This case develops in both deep sea conditions, as the channel extension case.
- *Case II*: The additional waves triggered by the secondary basin only lead to a phase shift at $x = x_1$. For deep sea condition, this is a phase shift of 180°. Besides, small basins lead again to the quarter wavelength resonance. Further, for the channel extension condition, this situation leads to the following resonance pattern, $[l - x_1]/\lambda = \frac{n}{2}$ with $n = 1, 2, ...$, which was already found by Alebregtse et al. (2013).

- *Case III*: This case only develops for deep sea conditions (which is the case in this study), where the additional waves are only present at the seaward side of the basin. This seaward wave displays a *node* at $x = x_1$, such that $N_1^{'} = 0$. Resonance now occurs if $x_1/\lambda = \frac{n}{2}$ with $n = 1, 2, ...$

7.2. Convergent channel

In this section the physical mechanism in convergent channels will be discussed. Similar to the situation for prismatic channel, this will be done for a single channel with and without basins.

In chapter 5 the response of the system to channel convergence has been shown, while here the focus will be on the response to a single secondary basin. Roos and Schuttelaars (2015) explained the physical mechanism responsible for the changes in elevation amplitude for a prismatic channel, which has been discussed in section 7.1.

7.2.1. Channel admittances

This paragraph describes the admittances for convergent channels. Since the reference standing wave only occurs for subcritical convergence, the focus here will be on this part of the domain.

The additional waves which are triggered by the secondary basins are of the form $N(x) = \exp(\Lambda_r x)\left[\hat{A}\cos(\Lambda_i x) + \hat{B}\sin(\Lambda_i x)\right]$, with constants $\hat{A}$ and $\hat{B}$. The roots read $\Lambda_r = \beta k$ and $\Lambda_i = k\sqrt{1-\beta^2}$.

The additional wave at the landward side of the vertex point is a standing wave, with an elevation *anti-node* at the boundary. Applying the landward boundary conditions $N(x_1) = N_1^{'}$ and $\frac{dN(l)}{dx} = 0$ gives an expression for $N_{\mathrm{lw}}^{'}(x)$ and $U_{\mathrm{lw}}^{'}(x)$:

$$N_{\mathrm{lw}}^{'}(x) = \frac{N_1^{'}\exp[\Lambda_r(x-l)]}{\exp[\Lambda_r(x_1-l)]}\frac{\Lambda_i\cos[\Lambda_i(x-l)] - \Lambda_r\sin[\Lambda_i(x-l)]}{\Lambda_i\cos[\Lambda_i(x_1-l)] - \Lambda_r\sin[\Lambda_i(x_1-l)]}, \tag{7.3}$$

$$U_{\mathrm{lw}}^{'}(x) = \frac{-iN_1^{'}}{\gamma}\sqrt{\frac{g}{h}}\frac{\exp[\Lambda_r(x-l)]}{\exp[\Lambda_r(x_1-l)]}\frac{k\sin[\Lambda_i(x-l)]}{\Lambda_i\cos[\Lambda_i(x_1-l)] - \Lambda_r\sin[\Lambda_i(x_1-l)]}. \tag{7.4}$$

The dimensionless landward admittance $\tilde{Y}_{\mathrm{lw}}$ now follows from equation (7.4):

$$\tilde{Y}_{\mathrm{lw}} = \frac{1}{\cot[\Lambda_i(l-x_1)]\sqrt{1-\beta^2}+\beta}. \tag{7.5}$$

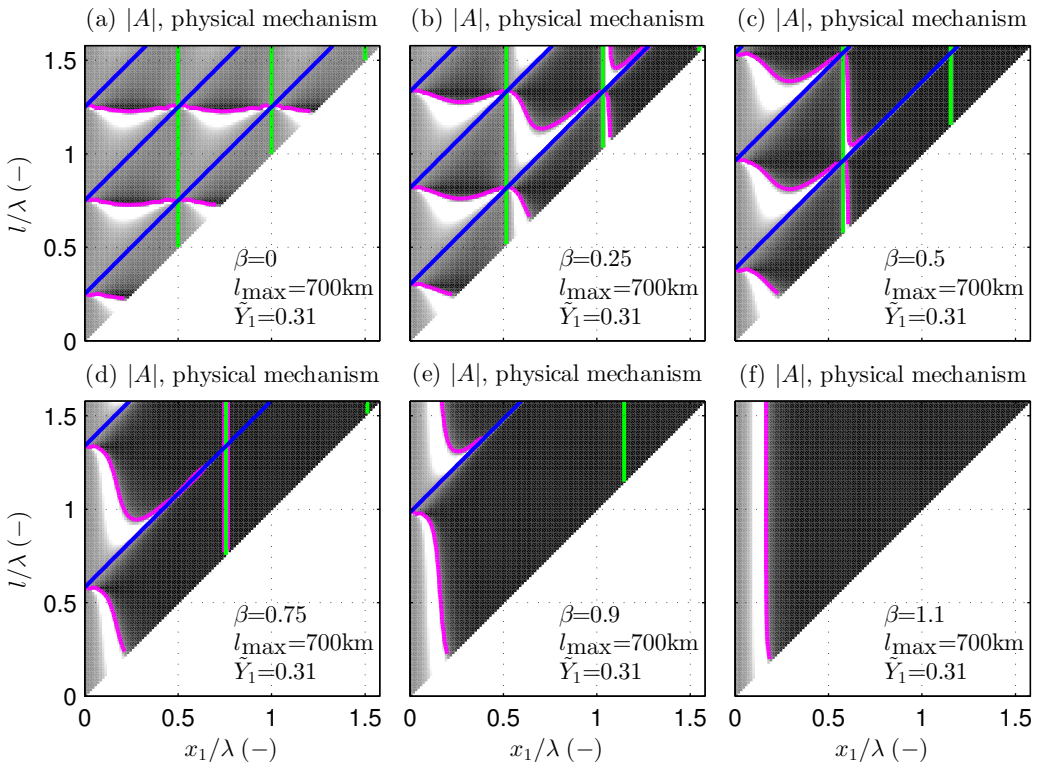

FIGURE 7.2: Physical mechanism for a convergent channel including one secondary basin. The figures show cases without amplitude change, where the *blue* lines denote *Case I*, the *green* lines *Case III*, while *Case II* is represented by the *pink* contour lines. Axes are scaled against the frictionless shallow water wavelength λ.

For the seaward wave, applying the boundary conditions $N(x_1) = N_1$ and $N(0) = 0$ gives an expression for $N'_{\mathrm{sw}}(x)$ and $U'_{\mathrm{sw}}(x)$:

$$N'_{\mathrm{sw}}(x) = \frac{N'_1 \exp(\Lambda_r x)\sin(\Lambda_i x)}{\exp(\Lambda_r x_1)\sin(\Lambda_i x_1)}, \tag{7.6}$$

$$U'_{\mathrm{sw}}(x) = \frac{iN'_1}{\gamma}\sqrt{\frac{g}{h}}\left(\frac{\exp(\Lambda_r x)\left[\Lambda_r \sin(\Lambda_i x) + \Lambda_i \cos(\Lambda_i x)\right]}{\exp(\Lambda_r x_1)k\sin(\Lambda_i x_1)}\right). \tag{7.7}$$

This leads to the dimensionless seaward admittance

$$\tilde{Y}_{\mathrm{sw}} = \frac{\sqrt{1-\beta^2}}{\tan(\Lambda_i x_1)} + \beta. \tag{7.8}$$

7.2.2. Cases without elevation change

Analogous to the situation for a prismatic channel, cases for which no elevation change occurs are present. These will be discussed in this paragraph.

- If the reference standing wave has a node at $x = x_1$, the secondary basins will be left unforced (*Case I*). No volume transport will be triggered, hence no additional waves will develop. This case occurs when $\tilde{Y}_{\mathrm{lw}} \to \infty$, i.e. $\Lambda_i \cos[\Lambda_i(x_1 - l)] - \Lambda_r \sin[\Lambda_i(x_1 - l)] = 0$, which leads to

$$\frac{l - x_1}{\lambda} = \frac{\pi n - \arctan(\frac{\sqrt{1-\beta^2}}{\beta})}{2\pi\sqrt{1-\beta^2}} \qquad \text{with } n = 0, 1, 2, ..., \tag{7.9}$$

  denoted by the *blue* lines in figure 7.2.

- Another case can be distinguished when the additional waves will only lead to a phase shift at $x = x_1$ and the channel head (*Case II*). For the deep sea limit in a prismatic channel, this occurs if $N_1'/N_1^{\mathrm{ref}} = -2$, i.e. $N_1' = -N_1^{\mathrm{ref}}$, which implies an 180° phase shift. It can be seen that this case does appear for convergent channels, but since the magnitude of the phase shift is unknown, no analytical solution can be found here. The *pink* lines in figure 7.2 denote this case, which are the unit contour lines.

- The third case for which no change occurs is when the additional seaward wave has a node at $x = x_1$, with the result that the volume transport triggered by the basins is fully accommodated by this wave and no additional wave at the landward boundary will be triggered (*Case III*). This situation occurs when $\tilde{Y}_{\mathrm{sw}} \to \infty$, i.e. $\sin(\Lambda_i x_1) = 0$, so that

$$\frac{x_1}{\lambda} = \frac{n}{2\sqrt{1-\beta^2}} \qquad \text{with } n = 1, 2, ..., \tag{7.10}$$

  which is shown by the green lines in figure 7.2. This situation only occurs in the deep sea limit, as already shown by Roos and Schuttelaars (2015).

Supercritical convergence From figure 7.2f it can be seen that the first two cases are not present any more. This supports the statement that in supercritical channels only an oscillatory movement will develop. Since oscillations do not display *nodes* and *anti-nodes*, the first two cases (*blue* and *green* lines) can simply not develop. The third case, which includes an unknown phase shift, does occur. Furthermore, it can be seen that in supercritical channels the channel length is not influencing the basins response any more.

Chapter 8

Application to the Ems River

Until now, only the theoretical part of the topic has been considered, which is of course the main application of such an idealised model. However, it is interesting to see to what extent this model can simulate the water motions in a real estuary, such as the Ems River. The data collection is described in the next paragraph, after which the model is calibrated based on historical observations.

8.1. Data collection and bathymetry

Since the model has the option to describe both the converging width as depth (through steps), this has been implemented in the model. In table 8.1 the bathymetry of the Ems River can be found. The data for the width convergence has been described by Chernetsky et al. (2010); Winterwerp (2013), whereas the depth data is described by Schuttelaars et al. (2011); Kumar et al. (2015). Figure 8.1 presents the geometry of the Ems River, based on these data.

TABLE 8.1: Sections in the Ems River (Chernetsky et al., 2010; Schuttelaars et al., 2011; Winterwerp, 2013; Kumar et al., 2015).

Width				**Depth**					
#	x [km]	L_b [km]	B_0 [km]	#	x [km]	h [m]	#	x [km]	h [m]
1	35	32	1088	1	0–5	10.5	8	35–40	5.5
2	50	27		2	5–10	10	9	40–45	5.2
3	64	33		3	10–15	8	10	45–50	4.8
				4	15–20	7.5	11	50–55	3
				5	20–25	7.2	12	55–60	2.5
				6	25–30	7	13	60–64	2
				7	30–35	6.5			

TABLE 8.2: Retention basins to be implemented along the Ems River, as presented by DHI-WASY (2012); Donner et al. (2011, 2012).

#	Location	x [km]	Area [km^2]	Depth [m]	Width [m]	Length [km]	Scenario A	B	C1	C2
1	Sautelertief L	25.2	3.00	2	136	0.4			*	
2	Sautelertief S	25.2	2.00	2	136	0.4		*		
3	Ledamundung	34.7	0.50	2	132	0.4				*
4	Weekeborg	36.7	4.00	2	122	0.4		*	*	
5	Westoverledingen	37.7	1.40	2	117	0.4				*
6	Hornhusen L	39.7	0.80	2	108	0.4				*
7	Hornhusen S	39.7	0.50	2	108	0.4			*	
8	Grotegaste	40.2	0.50	2	105	0.4				*
9	Mittingen	44.7	0.50	2	105	0.4				*
10	Nesseburg	46.2	1.50	2	99	0.4			*	*
11	Tunxdorf	50.7	2.50	2	82	0.4	*		*	
12	Stapelmoor	50.7	5.00	2	82	0.4	*			
13	Papenburg	51.2	1.50	2	81	0.4				*
14	Brual	52.2	1.00	2	84	0.4				*
15	Brahe	54.2	0.75	2	83	0.4				*
16	Rhede L	55.7	2.50	2	78	0.4	*			
17	Rhede S	55.7	0.50	2	78	0.4			*	

Table 8.2 presents the dimensions of all the proposed secondary channels in the Ems-Dollard estuary, as described by DHI-WASY (2012); Donner et al. (2011, 2012). The depth of the inlet channels has been kept constant for all basins and is estimated on the basis of the presented data. The width of the inlet channels is between 50-80% of the channel width, depending on the location along the channel. The length of the channel is reported to be several hundreds of meters long, so this is set to be 0.4 *km*. All other

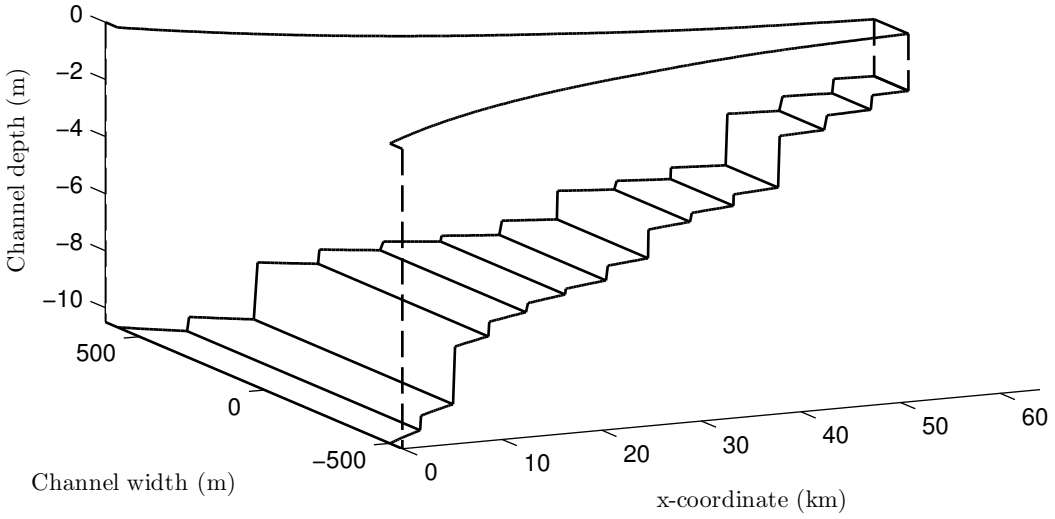

FIGURE 8.1: Schematic representation of the Ems River, based on the values provided in table 8.1.

parameters are directly described in the sources and have been adopted accordingly. Finally, the last column indicates which basin is present in which scenario.

8.2. Calibration

8.2.1. Method

For the calibration of the model, water levels from 2001/2005 have been used (Talke and de Swart, 2006). The parameter for bottom friction is the only 'unknown' in the model and therefore this parameter has been adjusted in such a way that the model approaches the observed water levels (figure 8.2) as close as possible.

To this end, friction may vary in three different sections of the channel, a downstream section (0 – 25 km), a middle section (25 – 50 km) and an upstream section (50 – 64 km). This last section is chosen in such a way that it coincides with the part of the river which is upstream of Papenburg. Here, large floodplains are present along the river, which may influence friction.

To determine the best 'fit' for the model, standard regression analysis is used, where the goal is to minimise the sum of the squared errors. The R^2-value denotes this 'fit', with values between 0 (bad) and 1 (good). Through an iterative process, the best combination of friction values have been found, which are presented hereafter.

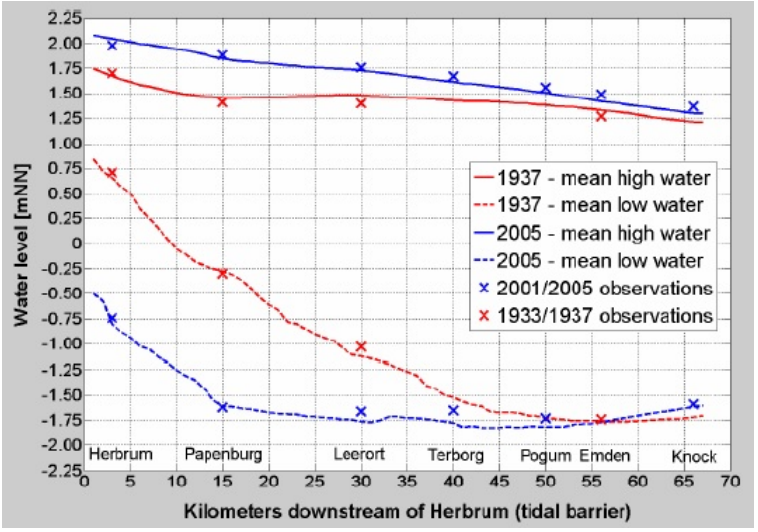

FIGURE 8.2: Observed water levels in the Ems-Dollard estuary in 2001/2005 (Talke and de Swart, 2006).

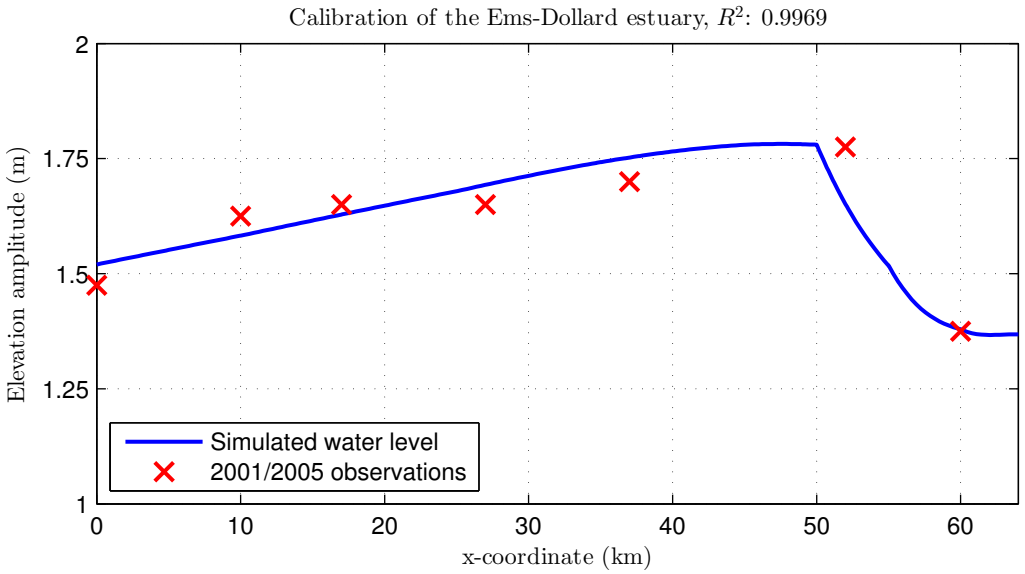

FIGURE 8.3: Calibration results. Friction parameters are $c_{d,1} = 1.1 \times 10^{-3}$, $c_{d,2} = 0.8 \times 10^{-3}$ and $c_{d,3} = 2.8 \times 10^{-3}$ for the downstream, middle and upstream section respectively. Note that the x-axis has been mirrored compared to figure 8.2.

8.2.2. Result

The result of the calibration is presented in figure 8.3 and it can be seen that the model predicts the water levels in the channel fairly well, showing an R^2-value of almost 1. Note that this is based on only 7 measurements along a river of 64 km, so that this result does not necessarily describe the water levels in the Ems in a 'perfect' way. The friction parameters for the three sections are $c_{d,1} = 1.1 \times 10^{-3}$, $c_{d,2} = 0.8 \times 10^{-3}$ and $c_{d,3} = 2.8 \times 10^{-3}$. Especially in the first two sections, relatively low friction can be observed. This corresponds to what has been found in literature, where high sediment concentrations were related to fluid mud layers (Schrottke and Bartholomä, 2008; Winterwerp, 2011). As already shown in figure 2.4, the highest concentrations of sediment in the Ems River can be measured in the middle section.

It has to be noted that the model produces only elevation amplitudes and that the observations are based on high and low water levels. As can be seen in figure 8.2, the difference in between high and low water is not symmetrical, while this is obviously the case for the model.

TABLE 8.3: Dimensionless admittances for the proposed basins.

#	Location	Eigenfrequency [rad/s]	Eigenperiod [h]	$\tilde{Y}$ [-]
1	Sautelertief L	0.002	0.87	0.036 - 0.0088i
2	Sautelertief S	0.0011	1.59	0.025 - 0.0027i
3	Ledamundung	0.002	0.87	0.006 - 0.0000i
4	Weekeborg	0.002	0.87	0.040 - 0.0215i
5	Westoverledingen	0.0014	1.25	0.018 - 0.0012i
6	Hornhusen L	0.0009	1.94	0.010 - 0.0003i
7	Hornhusen S	0.0012	1.45	0.006 - 0.0001i
8	Grotegaste	0.0016	1.09	0.006 - 0.0001i
9	Mittingen	0.0023	0.76	0.006 - 0.0001i
10	Nesseburg	0.0023	0.76	0.019 - 0.0021i
11	Tunxdorf	0.0023	0.76	0.027 - 0.0123i
12	Stapelmoor	0.0023	0.76	0.014 - 0.0269i
13	Papenburg	0.0024	0.73	0.019 - 0.0034i
14	Brual	0.0012	1.45	0.013 - 0.0012i
15	Brahe	0.0025	0.7	0.010 - 0.0005i
16	Rhede L	0.0018	0.97	0.019 - 0.0158i
17	Rhede S	0.0015	1.16	0.006 - 0.0002i

8.3. Effect of scenarios

Four different scenarios have been presented by DHI-WASY (2012); Donner et al. (2011, 2012), which include several retention basins along the Ems River. The dimensions of these basins are given in table 8.2, including the mentioned scenarios. For each basin, the admittance has been calculated (see table 8.3) from where it follows that in comparison to the basins used in the analysis, these basins can best be classified as 'small'. As shown in section 6.2, these types of basins tend to have only a small effect on the elevation amplitude. This appears in the results as well, which can be observed in figure 8.4. The response of the basins to the reference situation is only in the order of a few *mm*, where the scenarios (with the exception of scenario *A*) show an undesired effect on the elevation amplitude, which is increasing.

A possible cause for this can be the location of the basins. Table 8.2 shows that the basins in scenario *A* are placed farther towards the channel head than (most) of the other basins. Since the total sum of the retention areas is fairly similar among the scenarios, it appears that basins more upstream have a more favourable effect on the water levels.

Another explanation may be found in table 8.3, where it can be noticed that each of the basins is subcritically forced. From the analysis it was clear that 'positive' basins in a supercritically convergent estuary can only weaken the response if they are not placed in the vicinity of the channel mouth. Since the results show that the

Ems is indeed supercritically convergent, this channel appears too short for basins to effectively decrease the elevation amplitude.

To explain the fact that the scenario A does show a decrease of the elevation amplitude, the *local convergence factor* can be defined.

$$\beta_j' = \frac{\beta_j}{\mu_j} \tag{8.1}$$

This factor takes the depth transitions into account, which may lead to a different local convergence. The analysis shows that, especially towards the end of the channel, the local convergence is decreasing ($\beta' = 0.5$ at the channel head), such that the channel here can best be described as a mildly convergent channel. From the analysis it was clear that for these types of channels only an indication can be given for the expected response, opposed to supercritically convergent channels. Areas of amplification and reduction may occur everywhere along the channel, although areas of reduction are more likely to be present towards the channel mouth. Thus, it is possible that some of the proposed basins are located in an area of amplification.

8.4. Alternative scenarios

In order to accomplish a reasonable reduction of the amplitude, different options can be explored. Based on the understanding of the mechanism, three alternatives will be considered. The first is the creation of 'negative' basins, since the analysis showed that these types of basins may lead to a reduction of the amplitude in strongly convergent

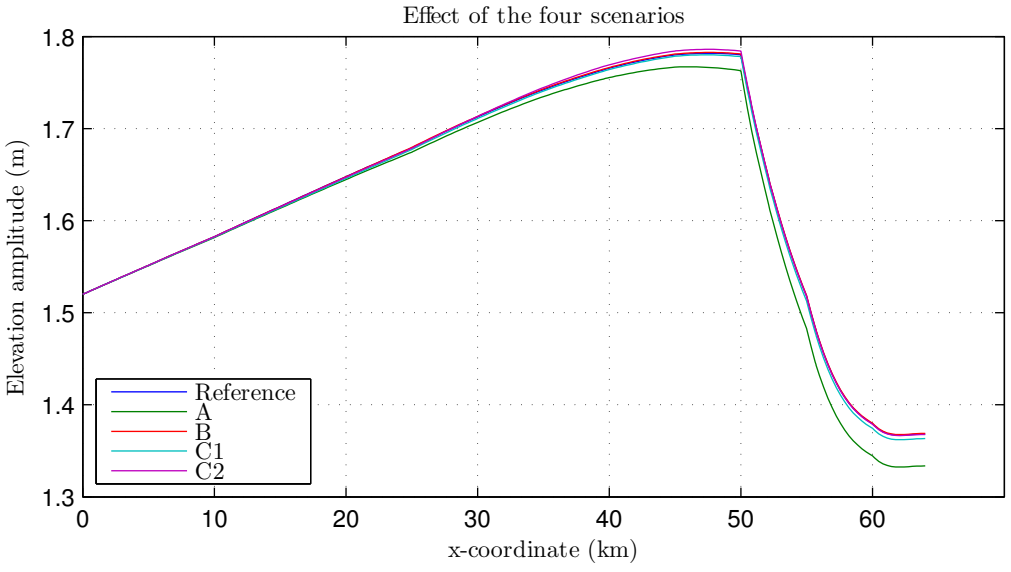

FIGURE 8.4: Responses of channel elevation to the four scenarios.

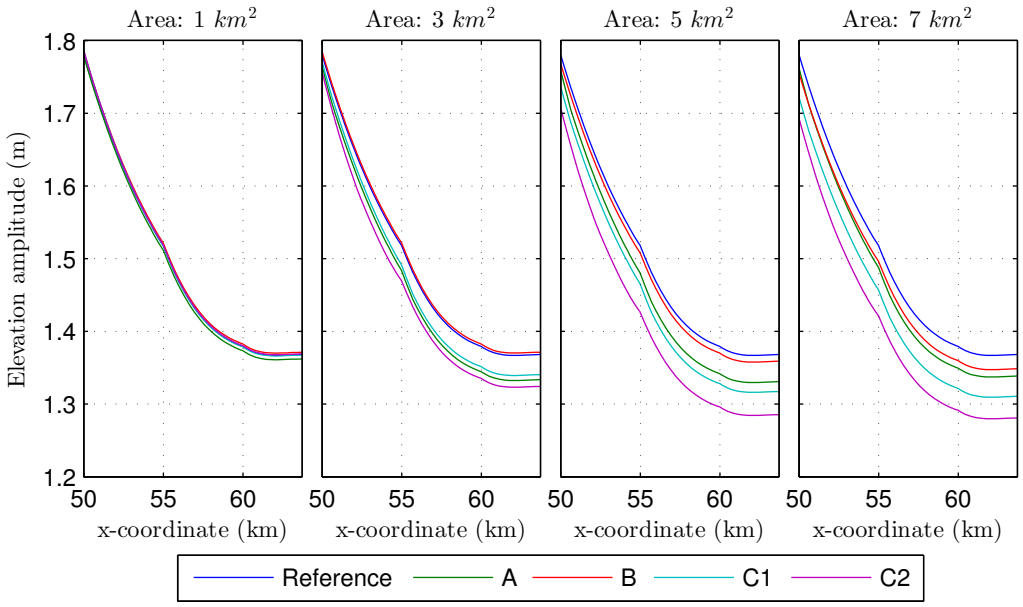

FIGURE 8.5: Effect of different basin areas on the elevation amplitude. For clarity, only the upstream part of the channel is shown, since here the effects are most apparent.

channels. The second alternative includes 'large' basins, as they may also lead to amplitude reduction, while the third alternative focusses on the locations of the basins. Additionally, a fourth alternative will be considered, which is the adjustment of the friction parameter of the inlet channels.

8.4.1. 'Negative' basins

The idea here is to implement 'negative' basins, since these are more likely to result in a positive effect for short channels. Though, this only holds for basins in supercritically convergent channels due to the influence of friction (figure B.4).

Now, the analysis shows that for the basin admittance to become 'negative', unrealistic dimensions would have to be used. For instance, the length of the inlet channel would have to be increased up to 4 *km*. Regarding the practical applicability, it can thus be concluded that this alternative is not viable.

8.4.2. 'Large' basins

Roos and Schuttelaars (2011) already showed that 'large' basins may show significant reduction in elevation amplitude and from chapter 6 it follows that under the influence of friction, these types of basins show a favourable result almost for every location.

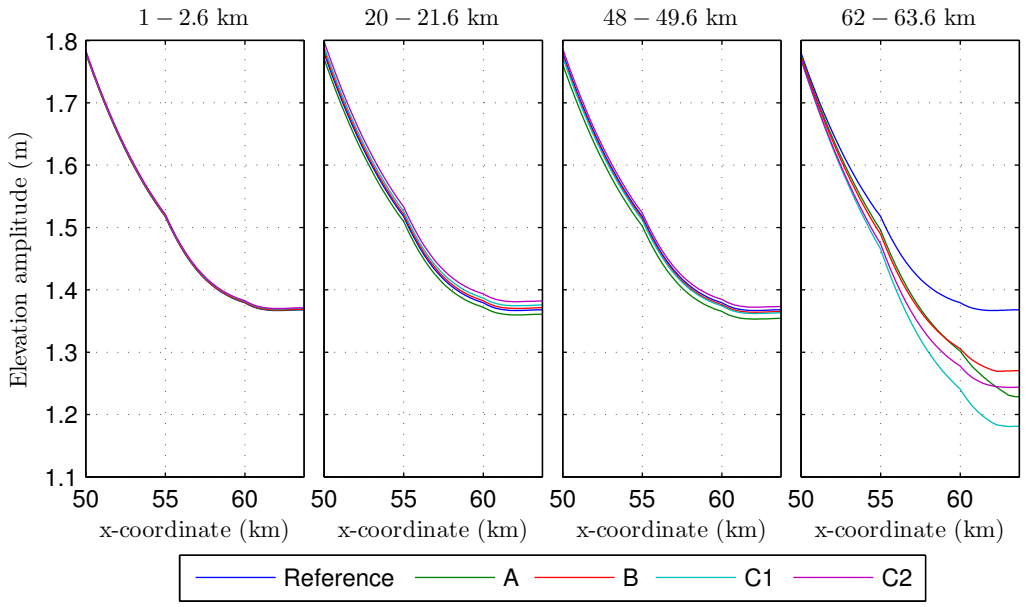

FIGURE 8.6: Similar to figure 8.5, but now for different locations of the basins. (Note the changed scale of the y-axis.)

Figure 8.5 shows the result for these alternative basin areas, where indeed larger amplitude reduction is visible for larger basin areas, which is most apparent for scenario *C2*. From other simulations, it turns out that this is not a continuing process. If basins areas are increased even more, the effects tend to weaken again. Although the amplitude reduction at the channel head is increasing with the basin area, this effect is much less present for other locations along the channel.

8.4.3. Locations

Another alternative is to relocate the basins in the proposed scenarios. The locations in the current plans are selected from a practical point of view, but these locations may not be the most effective in the sense of reducing the elevation amplitude. To this end, the basins have been grouped (100 m apart) and are placed at four locations along the channel; near the mouth (1 – 2.6 km), near Terborg (20 – 21.6 km), near Papenburg (48 – 49.6 km) and near the channel head (62 – 63.6).

Figure 8.6 shows the resulting elevation amplitude for these alternatives, where the result in panel *d* is the most distinctive. For basins placed near the channel head, significant amplitude reduction is visible. For basins at other locations along the channel almost no change appears. Furthermore, the reduction as seen in figure 8.6d is not visible further downstream, so this is only a local effect.

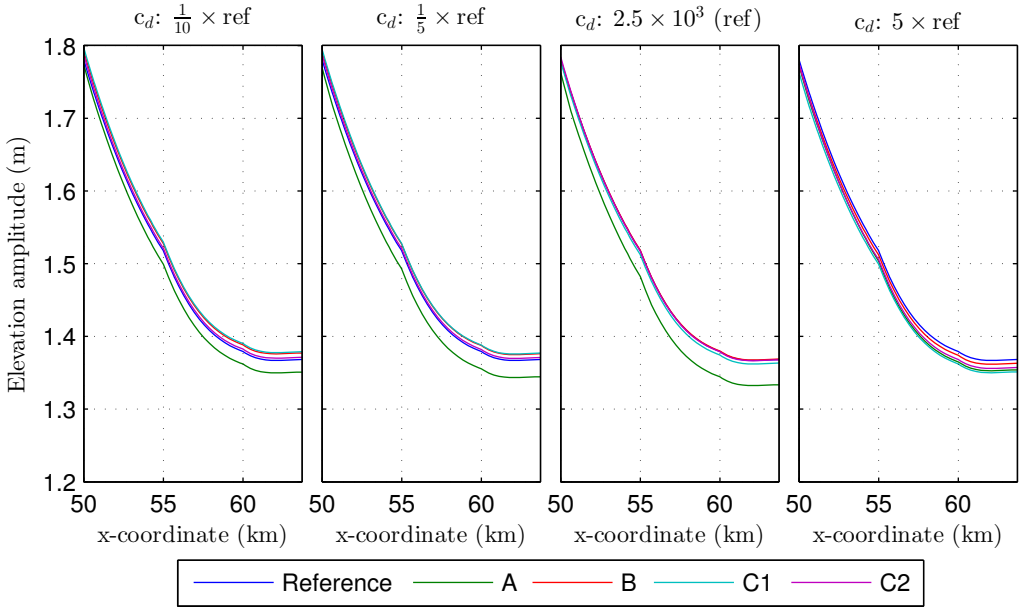

FIGURE 8.7: Similar to figure 8.5, but now for different friction values of the inlet channels.

8.4.4. Friction

The final alternative that is considered here, is the adjustment of bottom friction in the inlet channel. Through the friction parameter c_d this can be adjusted, while three scenarios will be reviewed. For those scenarios, friction is set to $\frac{1}{10}$, $\frac{1}{5}$ and 5 times the reference value.

From figure 8.7 it appears that friction in the inlet channel has only a minor influence on the elevation amplitude in the main channel. Especially for larger friction values, almost no effects can be noticed any more. Moreover, the largest reduction is realised in the reference case.

8.5. Combined alternatives

The result presented in figure 8.8 shows the combined alternative where basins with an area of 5 km^2 are placed between km 55 and the channel head, all 0.5 km apart. It can be seen that these measures together lead to an amplitude reduction of more than 40 cm (for scenario *C2*) at the channel head. For other locations along the channel, amplitude reduction is also visible, albeit less magnified. Although the model including the original basins does not show significant decrease of the tidal amplitude, these measures give a good indication of possible improvements of the current plans.

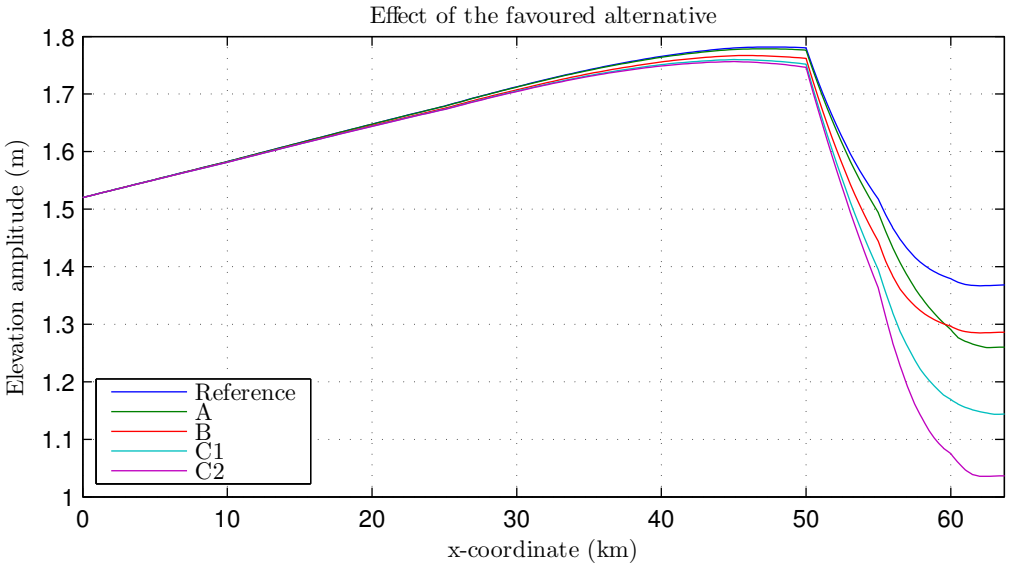

FIGURE 8.8: Response to the favoured alternative, with basins with an area of 5 km^2 located 0.5 km apart between km 55 and 64 . All other dimensions are equal to the original scenarios.

8.6. Other models

Compared to the results in DHI-WASY (2012); Donner et al. (2011, 2012), the proposed scenarios in this model show a different effect. In the mentioned studies most of the scenarios were found to lead to a significant improvement of the present situation. Figure 8.9 shows this result for scenario *C1* and *C2*, where a reduction of the tidal range (which is twice the elevation amplitude) of around 1,5 meter is visible.

To some extent these differences may be related to the design of the scenarios. As discussed in chapter 2, the measures which are included in the scenarios are not only retentions basins, but do include other implementations as well. These other adjustments to the main channel are properties which can not be included in this idealised model.

Although this model is unable to reproduce the results obtained by the more complex 3D models, it does show some interesting ideas which could be considered in the design of such retention basins. For instance, relocating the basins towards the channel head may improve the results significantly.

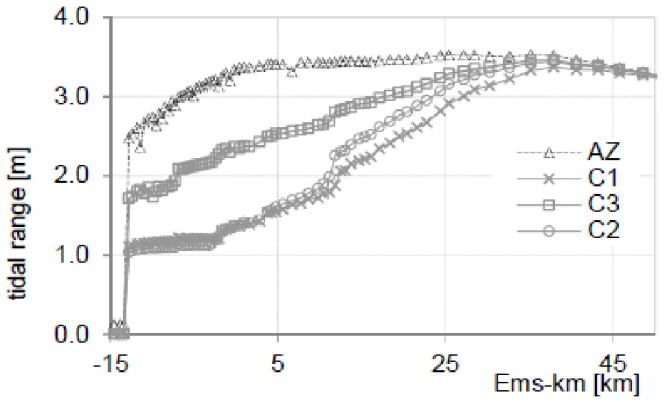

FIGURE 8.9: Tidal range for scenarios *C1*, *C2* and *C3* (not discussed here) and the reference level *AZ*, as presented by Donner et al. (2012). (Note the adjusted x-axis, with Papenburg at Ems-km 0.)

Chapter 9

Discussion

This chapter will discuss the findings from the earlier chapters. First it will go into the role of main channel, followed by the role of the basins characteristics in the system. Finally, the practical applicability of the model will be discussed.

9.1. Main channel geometry

The main objective of the study was to unravel the effect of a convergence on the elevation amplitude in a tidal channel. It appears that convergence has a large influence on the observed elevations amplitudes, as it causes an exponential increase in water levels towards the channel head. Besides, wavelengths tend to increase, until no real waves can be seen any more. This is where the channel is called supercritically convergent. The convergence parameter β represents this, where $\beta = 1$ stands for the boundary between subcritical and supercritical convergence. Due to the increase in wavelengths, the familiar quarter wavelength resonance is not visible any more for stronger convergent channels, which only holds for prismatic channels, as seen in Roos and Schuttelaars (2015) for instance.

Although this idealised model includes a converging width, the channel follows a straight line from mouth to head. Many tidal rivers show some sort of meandering pattern, which leads to different flow patterns which can not occur in cross-sectionally averaged models. A more advanced approach would be to allow for a three-dimensional water motion, so that the effects of an arbitrary geometry can be investigated. Such an approach would also allow to effectively expose the behaviour of bottom friction throughout the channel, as this parameter was found to be of large influence. Winterwerp (2011) already explained that, due to fluid mud layers, bottom friction may

decrease in the channel, which again could have a large influence on the vertical flow structure. Another option is to include a different method for determining bottom friction, such as the approach presented by Roos and Schuttelaars (2011).

Since idealised modelling is not very suitable to describe a three-dimensional water motion including many different processes, complex numerical models are used for this purpose. It should be clear that this does not allow for an extensive parameter analysis, so that processes like convergence can not be understood well. To bridge this gap between idealised and numerical modelling, Kumar et al. (2015) have developed a semi-idealised model to investigate the influence of an arbitrary geometry. They found that by using a more realistic geometry, results were more favourable than by using solely an exponential function, as used in this study. However, even when a semi-idealised model is used, it is not possible to analyse the processes in such detail as it has been done in this study.

9.2. Secondary basins

The influence of the secondary basins in the model is described by the basin admittance $\tilde{Y}_j$. It controls the response of the elevation amplitude to the dimensions of the basin. Already shown by Roos and Schuttelaars (2015), the admittance depends on the geometry of the basin and inlet channel, relative to that of the main channel. For frictionless prismatic channels, they also showed that a distinction can be made between super- ('negative') and subcritically ('positive') forced basins. This study has shown that by including bottom friction, this pattern is distorted. Especially for 'negative' basins, it was found that their response was greatly weakened and for some dimensions they even shifted to the subcritical regime.

From the analysis, it appears that in order to create such negative basins under the influence of bottom friction, highly unlikely dimensions would have to be used. In fact, 'negative' basins are not reported to occur in nature, so that the creation of such a basin would be totally man-made. Moreover, the Ems case showed that the due to the small basin admittances the observed effects were small as well. Alternatively, the basin admittance $\tilde{Y}$ could also be derived from a model that allows for a more complex geometry, though this model has to be linear due to the linear relationship in equation (4.21). Such a complex model could reveal realistic dimensions for which the basins would be more effective and possibly even supercritically forced.

9.3. Practical application

For the practical application of this model, the case of the Ems-Dollard estuary has been considered. Currently, plans to construct retention basins along the tidal river are in an advanced state. Complex 3D models have simulated the hydro- and morphodynamics in the system, revealing several scenarios that will reduce tidal range and sediment concentration in the estuary. However, these models do not allow for an extensive parameter analysis. To this end, this idealised model has been developed.

Although this model has a simplified geometry, it performs quite well in simulating the water levels in the Ems River. However, the model only shows some minor effects due to the implementation of retention basins. Therefore, it seems that this model, in its current idealised setting, is unable to reproduce the effects of retention basins obtained by the more complex 3D models. On the other hand, the model did reveal that placing the secondary basins further towards the channel head leads to more favourable results. Naturally, these results will have to be confirmed by complex numerical models, but this outcome may have important implications for the further development of these scenarios in the Ems River.

An important advantage of this model is that it is ready to be implemented in other estuaries. For instance, the Loire in France is also subject to distorted tidal dynamics. Since this estuary can also be characterised as a (strongly) convergent channel, the possible implementation of retention basins could be analysed by this model as a first step. Furthermore, in the (convergent) Western Scheldt there are currently plans for de-poldering the Hedwigepolder to compensate nature for the deepening of the estuary. Such plans could also be quickly reviewed using this idealised model, giving an indication of the expected outcomes.

Chapter 10

Conclusions and Recommendations

This thesis presents a study into the tidal dynamics in convergent estuaries. Through the use of a developed idealised model, the effects of retention basins and channel convergence have been studied. The first section will present the conclusions that can be drawn from this study, where each of the research questions will be answered separately. Next, an overview of the recommendations which follow from this study will be given.

10.1. Conclusions

Q1. What are the main problems that can be observed in the Ems-Dollard estuary nowadays and which model studies focus on addressing these problems through the use of retention basins?

Over the past centuries the Ems has faced many natural and anthropogenic changes. Due to the changes, the tidal range has dramatically increased over the past decades, while suspended sediment concentrations have increased in the whole estuary. Nowadays, the estuary is marked as highly polluted, with large 'dead' parts throughout the river. To address these problems, recently four scenarios have been developed which consist of the construction of several retention basins along the tidal river.

Many researchers have tried to explain the effects of retention basins on tidal dynamics. Recently, Roos and Schuttelaars (2015) developed an idealised model and they showed that the effect of retention basins depends on geometries of the sea and main channel,

as well as the basin characteristics and bottom friction. However, they limited their study to prismatic channels, which marks the main interest of this study; convergent tidal channels.

Q2. What are the effects of multiple retention basins on hydrodynamics in convergent tidal channels?

To analyse the effect of channel convergence in combination with retention basins, an idealised model has been developed. The interest is in the amplitude gain at the channel head, which may imply amplification, reduction, or no change at all.

2.1. *What is the effect of channel convergence on the hydrodynamics of tidal rivers?*

Convergent channels can be distinguished in their degree of convergence through the parameter β, ranging from prismatic, to subcritically, critically and supercritically convergent channels. Starting with prismatic channels ($\beta = 0$), the (quarter) wavelength for which resonance occurs increases with increasing (subcritical) convergence, until these wavelengths are infinitely long when approaching the critical boundary ($\beta = 1$). In a supercritically convergent channel, no waves can be distinguished any more. Here, the elevation amplitude is oscillating in phase with the forcing amplitude and is exponentially increasing towards the channel head. In the limit $\beta \to \infty$, the elevation amplitude at the channel head is moving uniformly with the forcing amplitude.

2.2. *Which effects can be observed when adding one or more retention basins along the main channel?*

Adding a single basin along a convergent channel will trigger additional waves in the main channel, which can lead to amplitude reduction and amplification. For prismatic channels, this is an evenly distributed pattern, but in convergent channels this pattern is distorted. In convergent channels the basins tend to have stronger effects on the amplitude gain, whereas the areas of amplitude reduction increase in size. For increasing convergence, the areas of amplitude reduction continue to grow until in the supercritical regime. In this regime, only basins placed in the vicinity of the mouth will lead to amplification; all other locations show a reduction of the elevation amplitude.

This striking property can be observed for channels with more secondary basins as well, where basins in supercritically convergent channels will always lead to a reduction of the amplitude when placed away from the channel mouth. In this regime, channel length has no influence on the amplitude gain any more. Furthermore, interaction between basins in supercritically convergent channels is found to lead to an even more favourable result. Basins placed in close proximity of each other strengthen each other's individual response.

2.3. *How does the basin geometry interact with channel convergence?*

From the definition of the *dimensionless basin admittance* $\tilde{Y}$, Roos and Schuttelaars (2015), already showed that 'large' basins may significantly weaken the elevation amplitude, where this study confirms this effect for convergent channels as well. They also explained that 'negative' basins display a reversed response. Together with the mentioned response in the supercritical regime this leads to an interesting result; all throughout the domain amplitude reduction can be observed.

2.4. *To what extent does bottom friction counteract the effects of the channel convergence?*

Bottom friction affects each of the processes in the system. Regarding the physical mechanism, it is found that due to friction, wavelengths shorten slightly. Furthermore it can be seen that bottom friction leads to an overall decrease of the elevation amplitude. This is the opposite of the effect of convergence, so for some extent these parameters are indeed counteracting each other. Furthermore, it can be seen that for strong supercritically convergent channels, bottom friction does not influence the elevation amplitude any more.

Another effect of bottom friction is that the response of 'negative' basins almost decreases to zero. Moreover, 'large' basins are now the preferably basins, showing amplitude reduction all throughout the domain. Again, this effect increases with increasing convergence.

Q3. To what extent can the acquired knowledge be applied to the Ems-Dollard estuary?

In order to explore the practical applicability, the model has been calibrated according to historical water levels in the Ems-Dollard estuary. This calibration shows that the model is able to predict the water levels in the convergent channel in a fairly good way.

To study the effect of the retention basins on the elevation amplitude in the estuary, the proposed scenarios have been implemented in the model. It appears that all the basins can be characterised as 'small', such that the expected effect is minor. This follows from the results as well, where the response of the basins only leads to an effect in the order of a few mm. This opposed to complex numerical studies into this matter, which showed an amplitude decrease of 50 – 100 cm. It is likely that other processes play an important role in the effects of retention basins in tidal channels, which are excluded in this idealised model.

However, this model proved suitable for exploring new alternatives and adjustments to the current scenarios. For the Ems case, the placement of basins more towards the

channel head showed some promising results. This exemplifies the usefulness of this idealised model, where its most important application is to expose the processes that play a vital part in the understanding of the system.

10.2. Recommendations

10.2.1. Model development

- **Complex basin geometry**
  The retention basins in this study are represented as Helmholtz basins. This is convenient because these are simple to implement, but effective in simulating the effects of secondary channels. However, it appears that, especially in the practical application, the basin admittance is much smaller than what could be expected from numerical models. Therefore, the advice is to develop a separate model to determine the basin admittance in a more realistic way, provided that this model is linear.

- **Friction determination**
  This study has exposed the physical mechanism for convergent channels, with and without retention basins. To this end, friction has been discarded for most of the analysis. However, by including friction all the processes were affected, which had a significant influence on the results. Therefore, the recommendation is to further look into the behaviour of friction in the model. For this, a different approach could be used, as for instance the method discussed by Roos and Schuttelaars (2011).

10.2.2. Retention basins in the Ems River

- **Basins close to the channel head**
  For the practical application of the model to the Ems case, it has been shown that basins close to the channel head lead to more amplitude reduction than basins that are not. This could have major implications for the design of the considered basins. Since this is found in an idealised setting, the advice is to implement these changes into numerical models to confirm these results.

- **Basins in close proximity**
  Similar to basins placed farther towards the end of the channel, this study has shown that (in strongly convergent channels) basins in close proximity of each other tend to strengthen each other's response. Also these findings should be implemented into numerical models for confirmation of the results.

Bibliography

Alebregtse, N. C. and de Swart, H. E. (2014). Effect of a secondary channel on the nonlinear tidal dynamics in a semi-enclosed channel: a simple model. *Ocean Dynamics*, 64(4):1–13.

Alebregtse, N. C., de Swart, H. E., and Schuttelaars, H. M. (2013). Resonance characteristics of tides in branching channels. *Journal of Fluid Mechanics*, 728:R3.

Bioconsult (2006). Zur Fischfauna der Unterems. Kurzbericht über die Erfassungen 2006. Report prepared for LAVES, Hildesheim, IBL, Oldenburg, Ingenieurbüro Grote, Papenburg.

Bos, D., Büttger, H., Esselink, P., Jager, Z., de Jonge, V., Kruckenberg, H., Van Maren, B., and Schuchardt, B. (2012). De ecologische toestand van het Eemsestuarium en mogelijkheden voor herstel. Der ökologische Zustand des Emsästuars und Möglichkeiten der Sanierung. Technical report, Leeuwarden/Veenwouden.

Chernetsky, A. S., Schuttelaars, H. M., and Talke, S. A. (2010). The effect of tidal asymmetry and temporal settling lag on sediment trapping in tidal estuaries. *Ocean Dynamics*, 60(5):1219–1241.

Cleveringa, J. (2008). Ontwikkeling sedimentvolume Eems-Dollard en het Groninger wad. Overzicht van de beschikbare kennis en gegevens. Technical Report December, Marknesse.

DHI-WASY (2012). Perspektive lebendige Unterems. Teilprojekt wasserbau. Kurzbericht von Juni 2012. Technical report.

Donner, M., Ladage, F., and Stoschek, O. (2012). Impact and retention potential of tidal polders in an estuary with high suspended sediment concentrations. In *Conference Proceedings of ICHE, Florida*.

Donner, M., Ladage, F., Stoschek, O., and Nguyen, H. H. (2011). Methods and Analysis Tools for Redevelopments in an Estuary With. *Coastal Engineering Proceedings management*, 1(33):1–13.

Esselink, P., Bos, D., Oost, A. P., Dijkema, K. S., Bakker, R., and de Jong, R. (2012). Verkenning afslag Eems-Dollardkwelders. Technical report, Vries.

Groenendijk, H. and Bärenfänger, R. (2008). Gelaagd Landschap. Veenkolonisten en kleiboeren in het Dollardgebied. Technical report, Bedum.

Habermann, C. (2003). Morphologischer Nachlauf nach Baggermaßnahmen in Tideästuaren. Technical report.

Hallas, M. (2015). Quantum of the Seas Float Out and Ems Conveyance. URL: http://quantumoftheseas.blogspot.nl/. Date accessed: 01-07-2015.

Höpner, T. (1994). Auswirkungen der Ästuarvertiefung in der Emsmündung. *Hrsg., Blackwell-Wiss.Verlag Berlin*, pages 171–175.

Jager, Z. and Vorberg, R. (2008). Effecten van de door Nederland voorgenomen ontrgondingen en verspreiding van baggerspecie in de Eems op garnalen en vis. Literatuurstudie in opdracht van RWS Waterdienst. Technical report.

Jensen, J., Frank, T., and Mudersbach, C. (2002). Synoptic field measurements in the context of hydrological changes in the Ems estuary. In *Low-lying Coastal Areas – Hydrology and Integrated Coastal Zone Management (International Symposium Bremerhaven 9.-12.9.2002)*, volume 13, Koblenz. Deutsches IHP/OHP Nationalkomitee.

Jensen, J. and Mudersbach, C. (2002). Analysis of tidal water levels along the German North Sea coastlines. In *Proceedings of the fifth conference MEDCOAST 01*, pages 29–36, Tunesia.

Jensen, J. and Mudersbach, C. (2005). Recent sea level variations at the north sea and baltic sea coastlines. *ICEST*.

Jensen, J., Mudersbach, C., and Blasi, C. (2003). Hydrological Changes in Tidal Estuaries Due to Natural and Anthropogenic Effects. In *6th International MEDCOAST 2003 Conference*, Ravenna, Italy.

Jonge, de, V. N. (1983). Relations Between Annual Dredging Activities, Suspended Matter Concentrations, and the Development of the Tidal Regime in the Ems Estuary. *Canadian Journal of Fisheries and Aquatic Sciences*, 40(S1):s289–s300.

Kuehl, H. and Mann, H. (1973). Untersuchungen zur Hydrobiologie der Unteren Ems. *Arch. Fischereiwiss*, 23:243–268.

Kumar, M., Schuttelaars, H. M., and Roos, P. C. (2014). Understanding the Influence of Retention Basin on Tidal Dynamics in Tidal Estuaries. In *Proceedings of the 17th Physics of Estuaries and Coastal Seas (PECS) Conference*, volume 16, page 14254, Porto de Galinhas, Pernambuco, Brazil.

Kumar, M., Schuttelaars, H. M., Roos, P. C., and Moller, M. (Submitted, 2015). Three-Dimensional Semi-Idealized Model for Tidal Motion in Tidal Estuaries, An application to the Ems estuary. *Ocean Dynamics*.

Lighthill, J. (1978). Waves in fluids. *Cambridge University Press*.

Lorentz, H. A. (1922). Het in rekening brengen van den weerstand bij schommelende vloeistofbewegingen. *De Ingenieur*, 37:695.

NAM (2010). Bodemdaling door Aardgaswinning, NAM-gasvelden in Groningen, Friesland en het noorden van Drenthe-statusrapport 2010 en prognose tot het jaar 2070. Technical Report September, Assen.

Niemeyer, H. D. and Kaiser, R. (2000). Evaluation of Design Water Levels and Design Wave Run-Up for an Estuarine Coastal Protection Master Plan. *Coastal Engineering (2000)*, pages 118–118.

NLWKN (2012). Gewässergütekarte (regionalspezifisch) der Ems. URL: http://www.nlwkn.niedersachsen.de/portal/live.php?navigation_id=8521&article_id=42302&_psmand=26. Date accessed: 10-12-2014.

Rollenhagen, K. (2011). Untersuchungen zur Minderung des Schlicheintrags in die Unterems.

Roos, P. C. and Schuttelaars, H. M. (2011). Influence of topography on tide propagation and amplification in semi-enclosed basins. *Ocean Dynamics*, 61(1):21–38.

Roos, P. C. and Schuttelaars, H. M. (2015). Resonance properties of tidal channels with multiple retention basins: role of adjacent sea. *Ocean Dynamics*, 65(3):311–324.

Schrottke, K. and Bartholomä, A. (2008). Detaillierte Einblicke in die ästuarine Schwebstoffdynamik mittels hochauflösender Hydroakustik. Technical report, Koblenz.

Schuttelaars, H. M., de Jonge, V. N., and Chernetsky, A. (2013). Improving the predictive power when modelling physical effects of human interventions in estuarine systems. *Ocean and Coastal Management*, 79(0):70–82.

Schuttelaars, H. M., de Jonge, V. N., and Chernetsky, A. S. (2011). Influence of the length of an estuary on tidal motion and sediment trapping. page 32.

Siefert, W. and Lassen, H. (1986). Development and Course of Storm Surges in the Ems, Weser and Elbe (Final Report of a KFKI Project) [ENTWICKLUNG UND ABLAUF VON TURMFLUTEN IN EMS, WESER UND ELBE (ABSCHLUSSBERICHT EINES KFKI-PROJEKTES)]. Technical report.

Steen, D. (2003). Planungen und Eingriffen im Dollartraum nach 1945. Zwischen Weser und Ems. Technical report, WSD, Aurich.

Stratingh, G. A. and Venema, C. A. (1855). *De Dollard. Geschied-, aaerdrijks-, en natuurkundige beschrijving van dezen boezem der Eems.* Verenging tot Behoud van de Waddenzee, Harlingen en Stichting Het Groninger Landschap, Groningen.

Talke, S. A. and de Swart, H. E. (2006). Hydrodynamics and Morphology in the Ems/Dollard estuary: Review of Models, Measurements, Scientific Literature, and the Affects of Changing Conditions. *Civil and Environmental Engineering Faculty Publications and Presentations*, (Paper 87).

Welle, van der, J. and Meire, P. (1999). Levende Eems, herstelplan voor Eems en Dollard. Technical Report 1999/08, Instituut voor Natuurbehoud, gezamenlijke natuurbeheersorganisaties, Groningen/Harlingen/Brussel.

Werkgroep Dollard (2001). Literatuurstudie over het storten van baggerspecie in de Mond van de Dollard. Technical report, Haren.

Winterwerp, J. C. (2011). Fine sediment transport by tidal asymmetry in the high-concentrated Ems River: Indications for a regime shift in response to channel deepening. *Ocean Dynamics*, 61(2-3):203–215.

Winterwerp, J. C. (2013). On the response of tidal rivers to deepening and narrowing. *Deltar*, (March).

Zimmerman, J. T. F. (1982). On the Lorentz linearization of a quadratically damped forced oscillator. *Physics Letters A*, 89(3):123–124.

Appendix A

Model formulation: friction

In all the parts of the model friction is specified to Lorentz' linearisation (Lorentz, 1922; Zimmerman, 1982). The friction coefficients in equations (3.3) and (3.9) can be determined as follows.

$$r = \frac{8c_d\hat{u}}{3\pi} \qquad\qquad r_j = \frac{8c_d\hat{v}_j}{3\pi} \tag{A.1}$$

Where $c_d = 2.5 \times 10^{-3}$ is a drag coefficient and $\hat{u}$, $\hat{u}_s$ and $\hat{v}_j$ are typical scales for the velocities in the system, which are further specified below.

For the main channel and the sea, the velocity scale is equal to the velocity amplitude of a frictionless shallow water wave with an elevation amplitude of N_{forc}. For the Helmholtz basins this is the channel velocity amplitude as it were frictionless and forced by an elevation amplitude N_{forc}.

$$\hat{u} = \hat{u}_s = N_{\text{forc}}\sqrt{g/h} \qquad\qquad \hat{v}_j = \frac{g\omega N_{\text{forc}}}{l_j\left|\omega^2 - \omega_{0,j}^2\right|} \tag{A.2}$$

With eigenfrequency $\omega_{0,j} = \sqrt{gb_jh_j/A_jl_j}$.

Appendix B

Results: basin characteristics

Frictionless channel

This section presents the additional results for the basin characteristics in a frictionless channel.

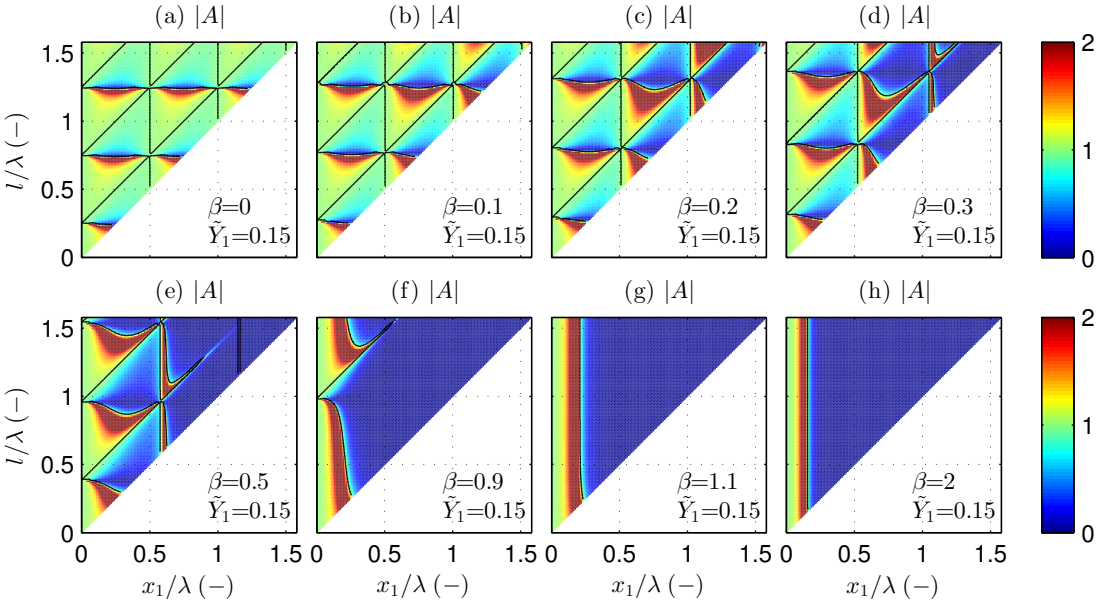

FIGURE B.1: Responses of channel elevation to the presence of a 'small' basin, here for various convergence lengths. Axes are scaled against the frictionless shallow water wavelength λ, *black* lines denote the unit contours.

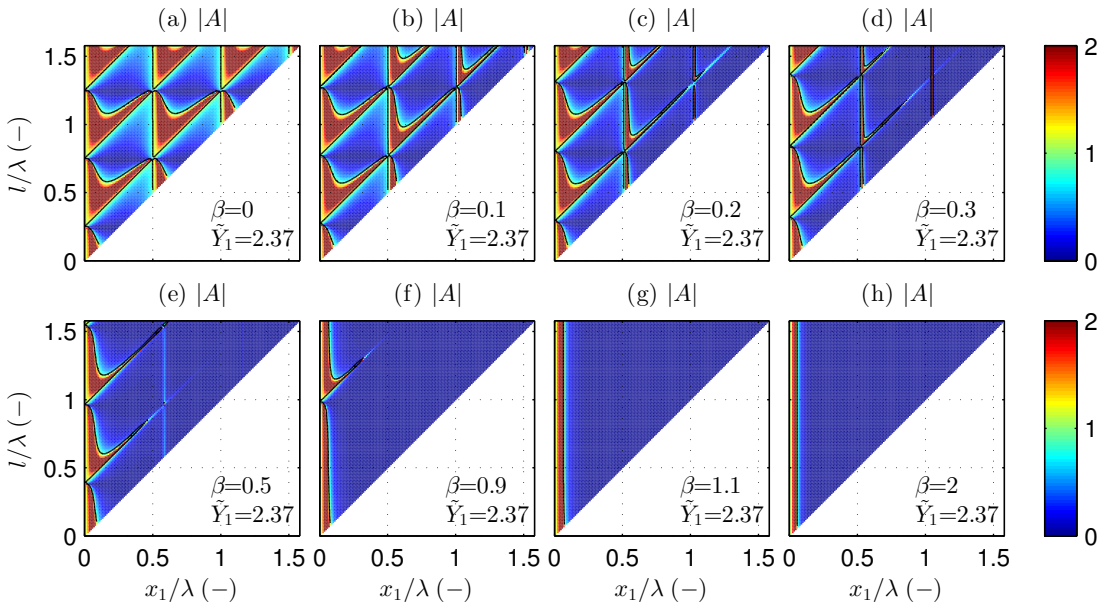

FIGURE B.2: Similar to figure B.1, but now for 'large' basins.

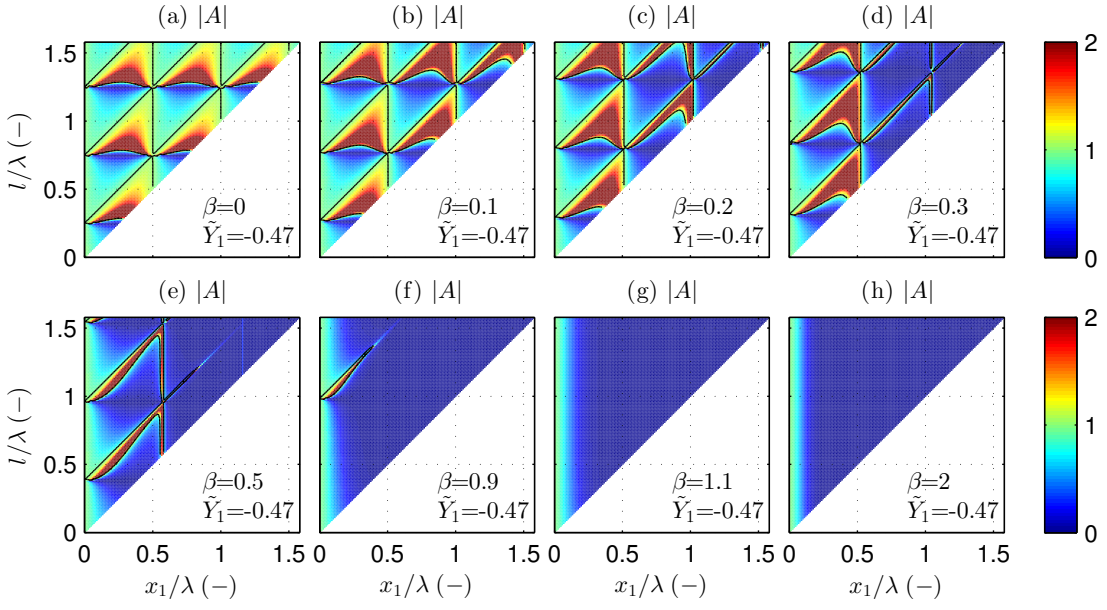

FIGURE B.3: Similar to figure B.1, but now for 'negative' basins.

Friction

This section presents the additional results for the basin characteristics, here combined with bottom friction.

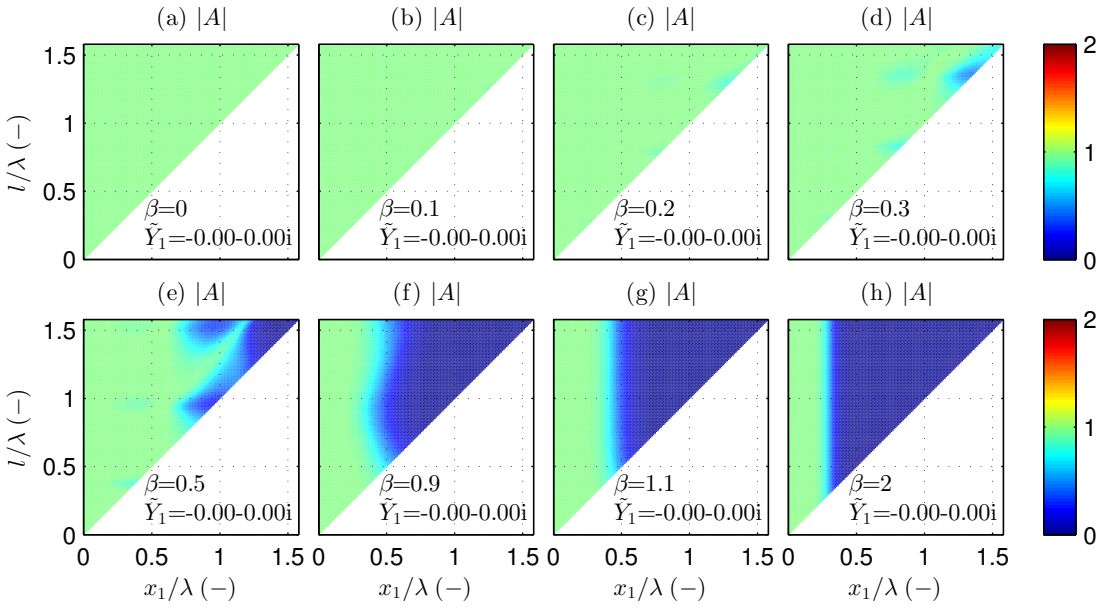

FIGURE B.4: Responses of channel elevation to the presence of a 'negative' retention basin under the influence of bottom friction, here for various convergence lengths. Axes are scaled against the frictionless shallow water wavelength λ.

Appendix C

Results: two basins

This appendix presents the additional results for cases with two basins.

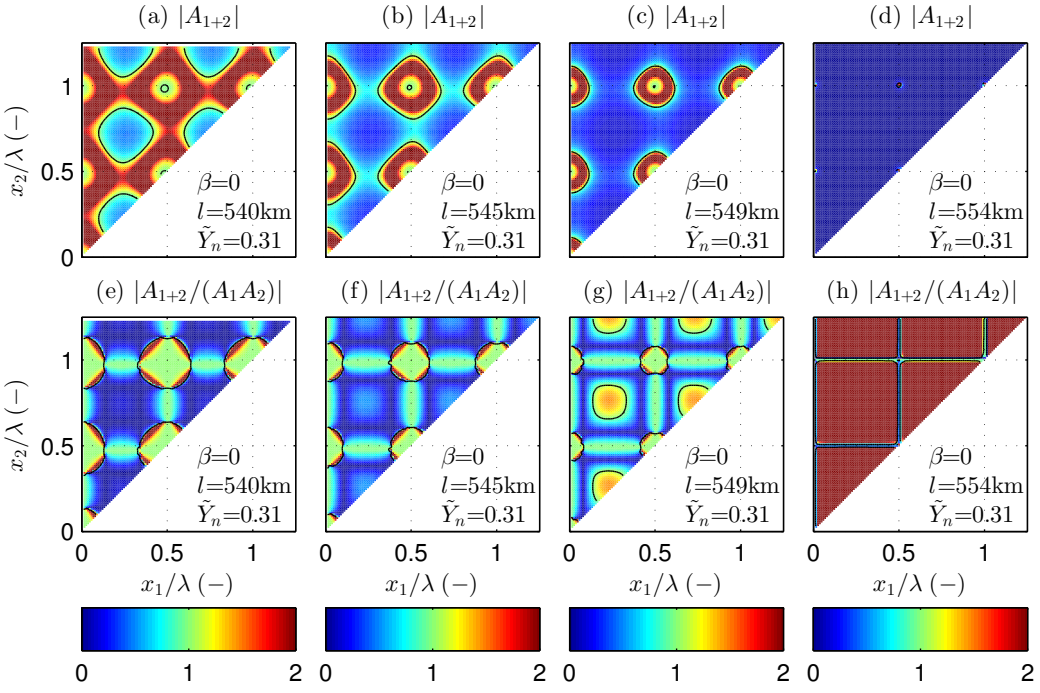

FIGURE C.1: Amplitude gain for the situation with two basins in a prismatic channel, with channel lengths such that they approach maximum resonance. The *top* row represents the amplitude gain $|A|$ at the channel head in case of two similar basins for different channel lengths. The *bottom* row shows the ratio Q, which represents the interaction between the basins. *Black* lines represent the unit contours.

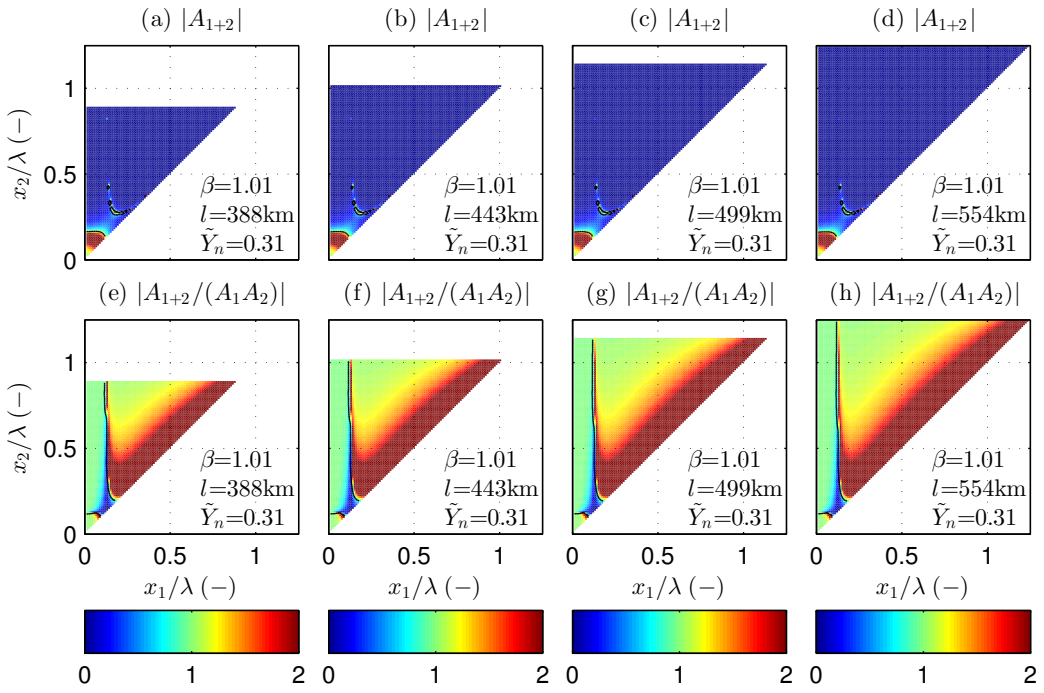

FIGURE C.2: Amplitude gain for the situation with two basins in a supercritical channel ($\beta = 1.01$). The *top* row represents the amplitude gain $|A|$ at the channel head in case of two similar basins for different channel lengths. The *bottom* row shows the ratio Q, which represents the interaction between the basins. Basin position x_1 and x_2 have been scaled against the shallow water wavelength.

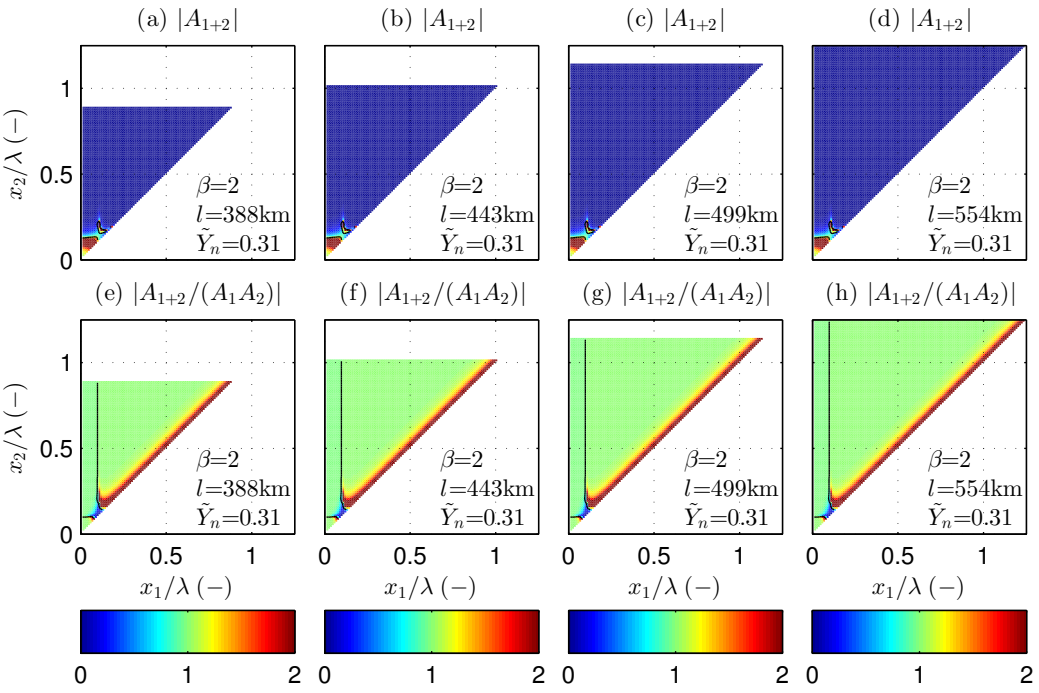

FIGURE C.3: Similar to figure C.2, but now for stronger convergence ($\beta = 2$).

Friction

This section shows the result for the frictional case.

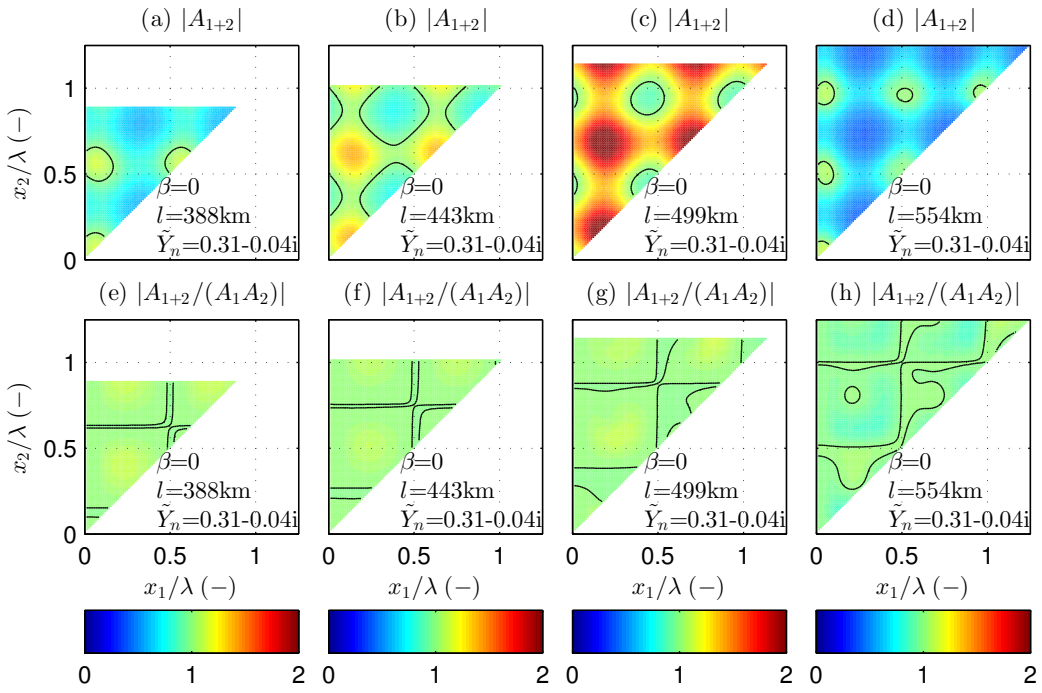

FIGURE C.4: Amplitude gain for the situation with two basins in a prismatic channel, here including friction and for various channel lengths. The *top* row represents the amplitude gain $|A|$ at the channel head in case of two similar basins for different channel lengths. The *bottom* row shows the ratio Q, which represents the interaction between the basins.

Appendix D

Results: three basins

This appendix presents the additional results for cases with three basins.

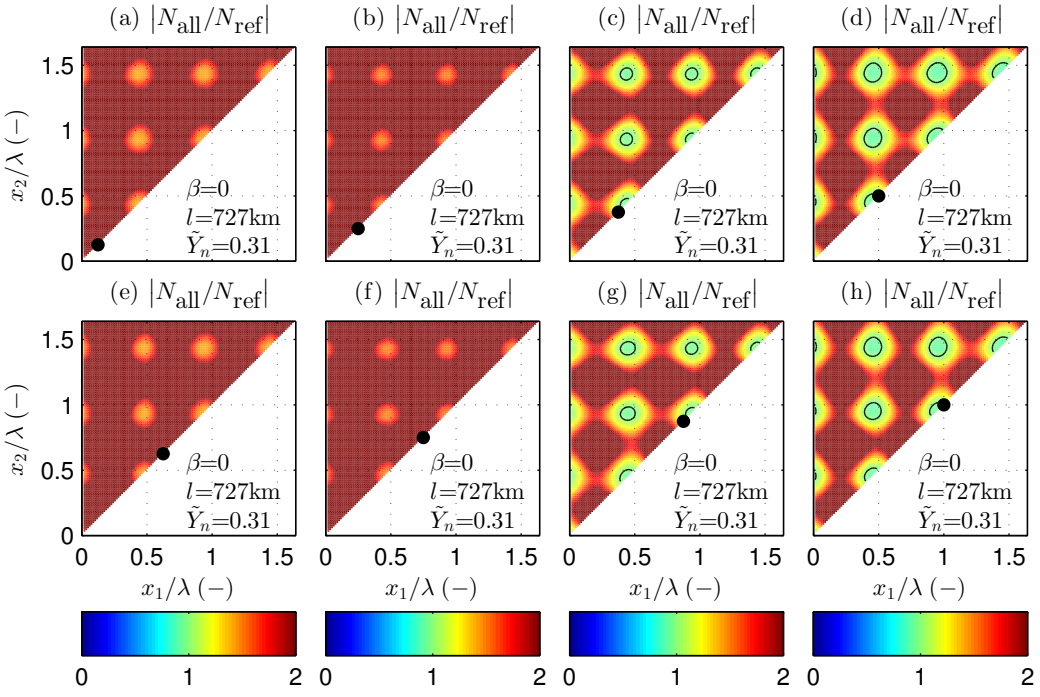

FIGURE D.1: Amplitude gain for the situation with three identical basins. The *black* dot represents the third basin, where the first two are varied on the axes. Channel length is chosen to lie between a node and a landward located anti-node.

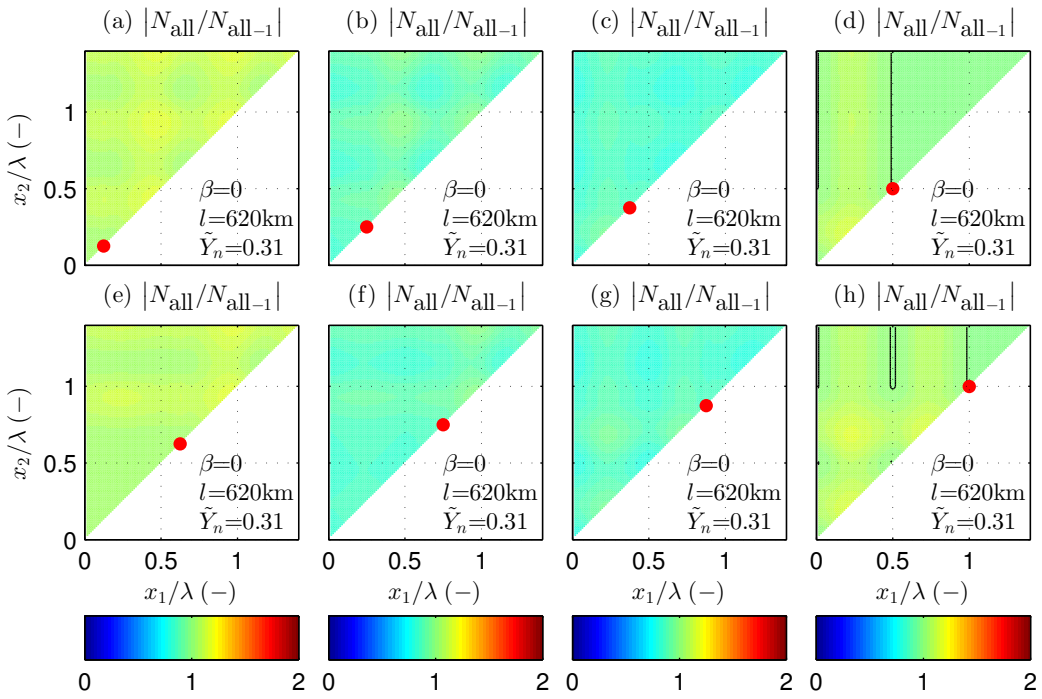

FIGURE D.2: Separate effect of the third basin $|N_{\text{all}}/N_{\text{all-1}}|$ for the situation with three identical basins. The *red* dot represents the third basin, where the first two are varied along the axes, which are scaled against the shallow water wavelength λ. Channel length lies between an anti-node and a landward located node, while it can be seen that reduction occurs when a basin also lies between an anti-node and a landward located node.

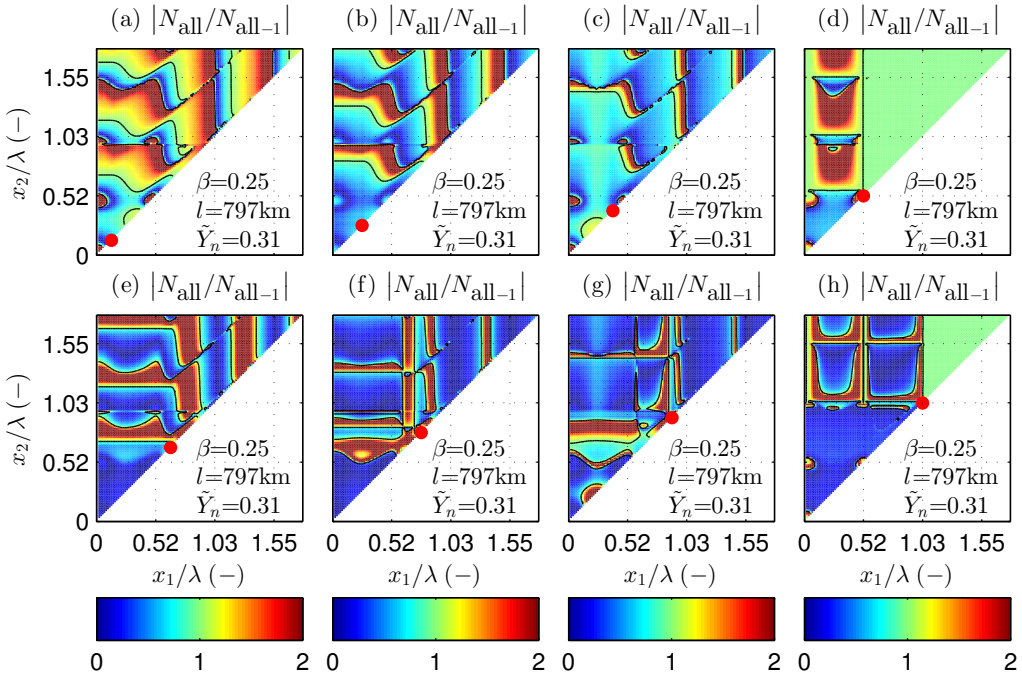

FIGURE D.3: Separate effect of the third basin (*red* dot) for the situation with three identical basins, while the position of the third basin has been adjusted for increasing convergence. A basin located exactly on a node does not trigger a wave at the landward side (**d** and **h**).

Appendix E

Results: multiple basins

This appendix presents the result for the case with multiple basins. Similar to the situation with three basins, the channel length is chosen to be constant, while any basins more than the two variable ones, will be on a fixed position. This analysis is further characterised by an arbitrarily chosen location for the fixed basin, in opposition to the previous section.

To analyse the effect of the basins on the amplitude the factor for the amplitude gain of a separate basin $|N_{\text{all}}/N_{\text{all-1}}|$ will be used solely. It is less relevant to consider the total effect of all the basins together, since it would be unclear which additional basin is responsible for the observed effects. By using only this indicator, the focus is on one specific basin in every simulation.

E.1. Four basins

The following presents the result for the situation with four identical basins along the main channel, here with $\beta = 0.4$. Since this implies that the channel convergence is becoming more important, it can be expected that there should be a clear difference between basins near the mouth and basins near the head. The results in figure E.1 corroborate this, where it can be seen that the effect of the fourth basin is considerably dependent on the location along the channel.

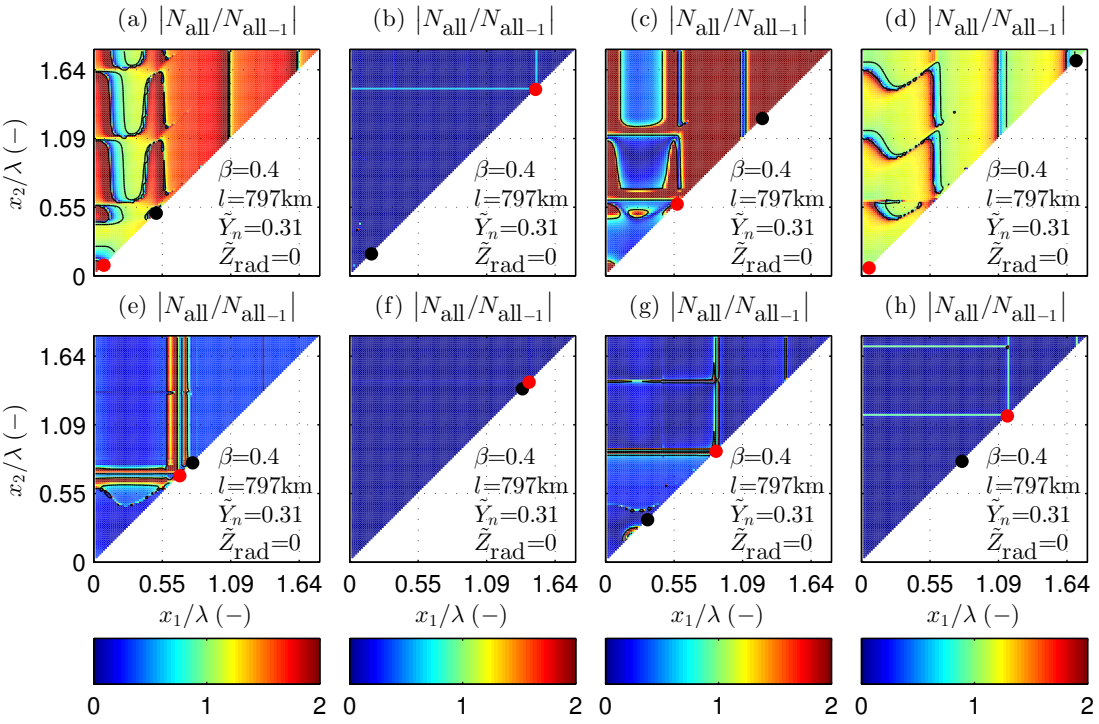

FIGURE E.1: Separate effect of adding a fourth basin $|N_{all}/N_{all\text{-}1}|$ for a channel with $\beta = 0.4$. The *red* dot represents the basin under consideration, while the *black* dot represents the third basin. The axes tick marks are adjusted to the increased wavelength due to convergence.

When analysing the same situation in channels with other convergence properties (see figures E.2 to E.4), it is evident that this feature is even more obvious for increasing convergence, which is in line with the other results. For a prismatic channel, no clear pattern is visible, which is probably the result of the interaction with the other fixed basin. Though, it is clear that the magnitude of the effects are stronger in convergent channels than in prismatic channels.

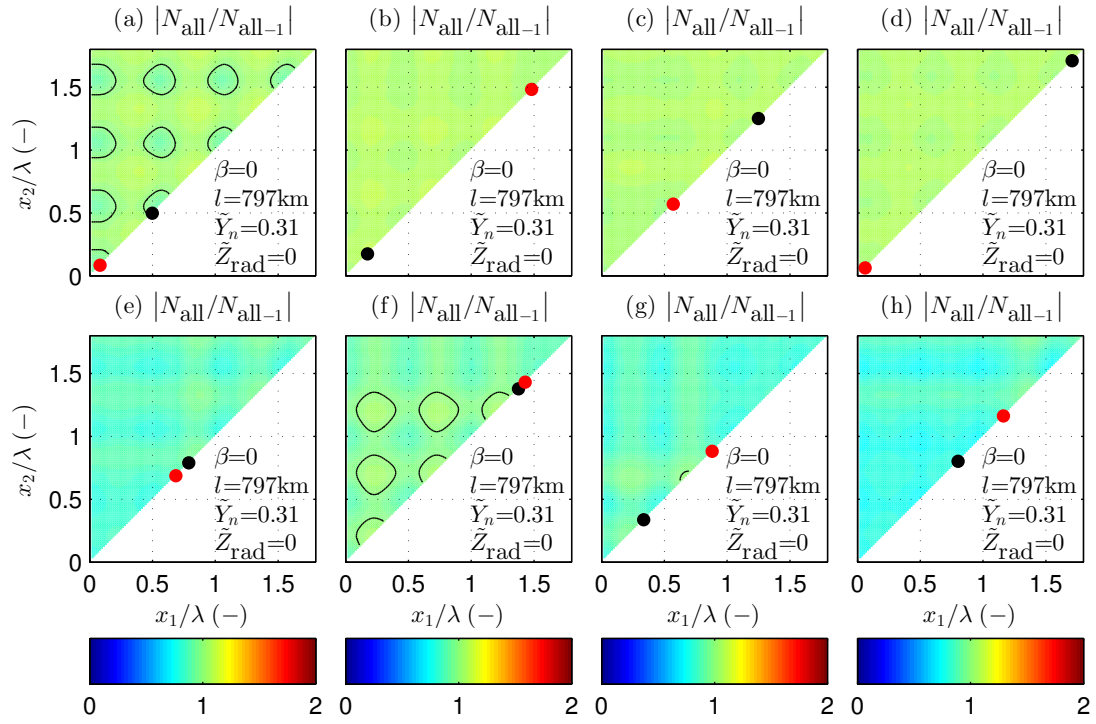

FIGURE E.2: Effect of a fourth basin (*red* dot) on the amplitude gain, where while the *black* dot represents the third basin. Axes are scaled against the frictionless shallow water wavelength λ.

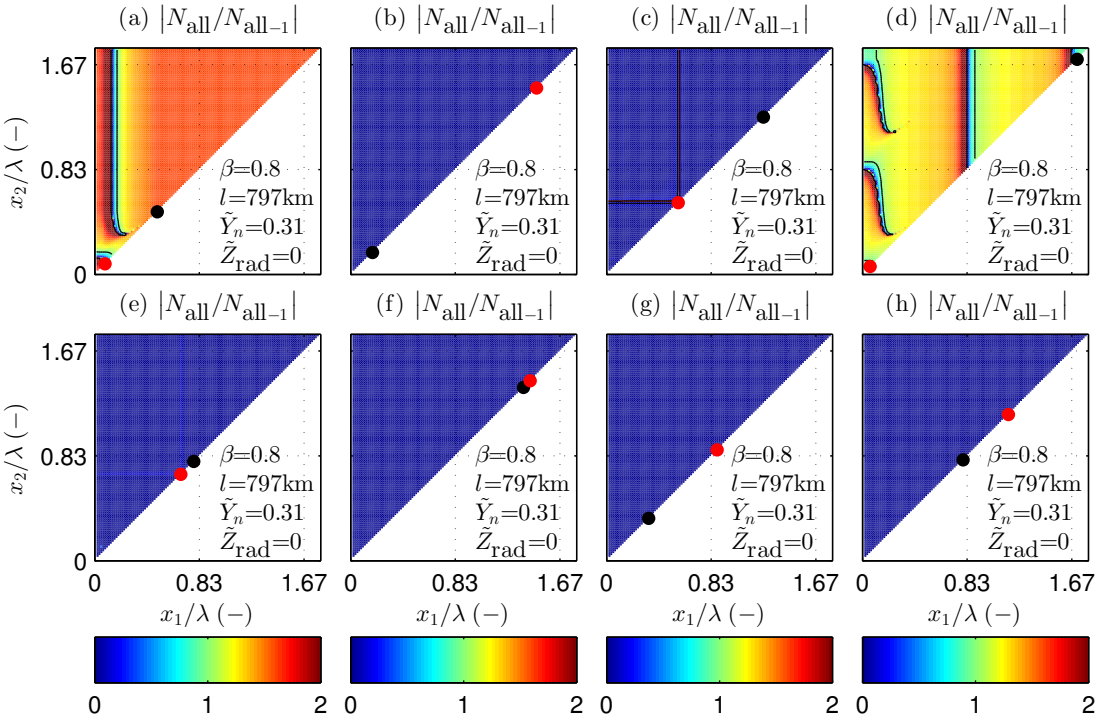

FIGURE E.3: Similar to figure E.1, but now for $\beta = 0.8$.

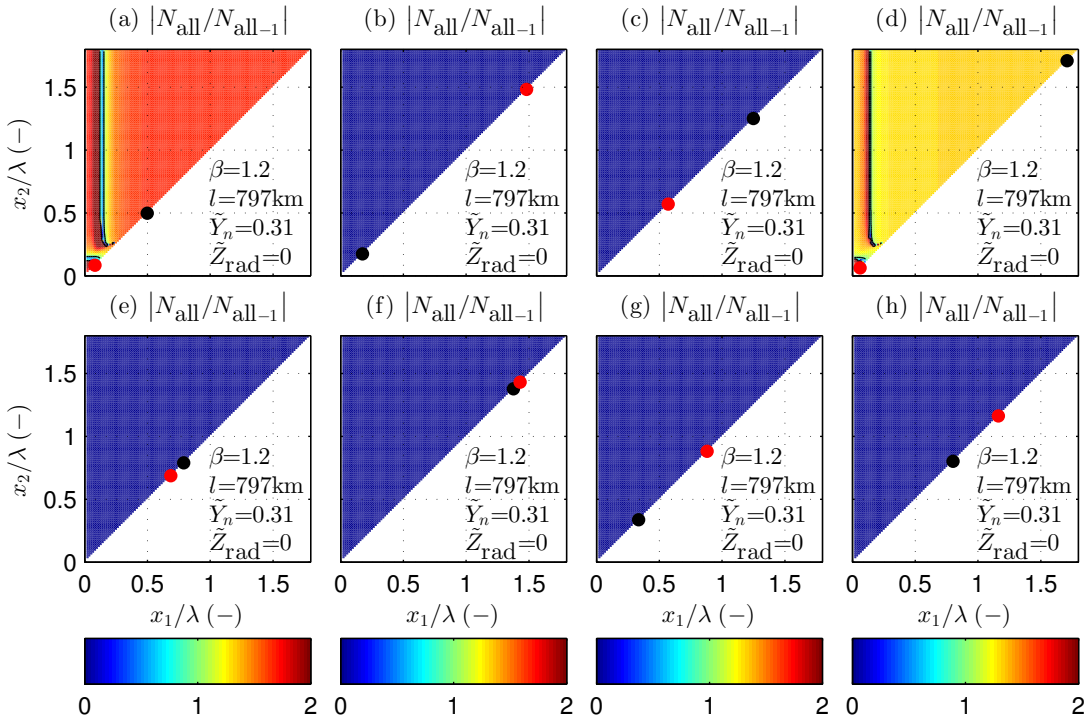

FIGURE E.4: Similar to figure E.2, but now in a supercritically convergent channel.

E.2. Eight basins

It is particularly interesting to find out if the effects found in the previous sections can still be distinguished for a situation with even more basins. Therefore, the results for a channel with eight retention basins are presented here, where each basin has the exact same dimensions. For the effect of adding an eighth basin along a convergent channel with $\beta = 0.4$, see figure E.5. Again, it is clearly visible that basins near the channel mouth might lead to an amplification of the tide, while basins placed further away tend to have a more dampening effect to the resonance.

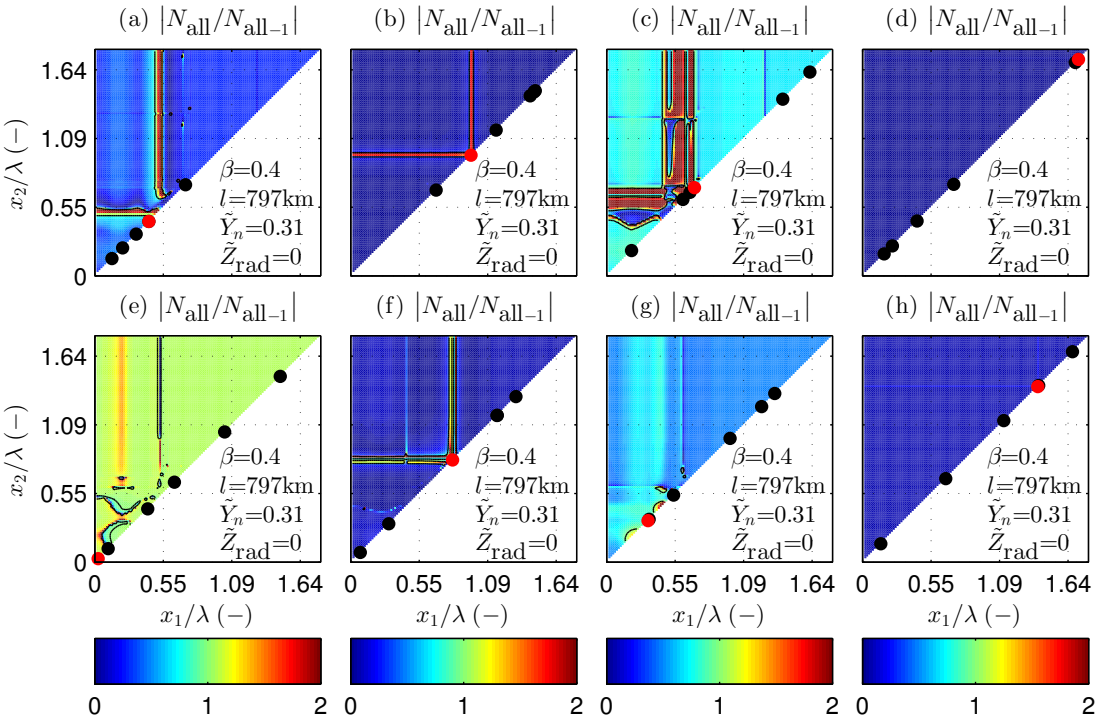

FIGURE E.5: Similar to figure E.1, but now for eight basins. Some basins might seem to overlap each other, but for to modelling purposes these are always more than *0.5 km* apart.

Figures E.6 to E.8 show these results for other convergence configurations. Again, similar results are obtained as for the previous simulations. Similar to the situation with $\beta = 0.4$, the magnitude of the effects is less evident as well for a prismatic channel, in comparison to convergent channels.

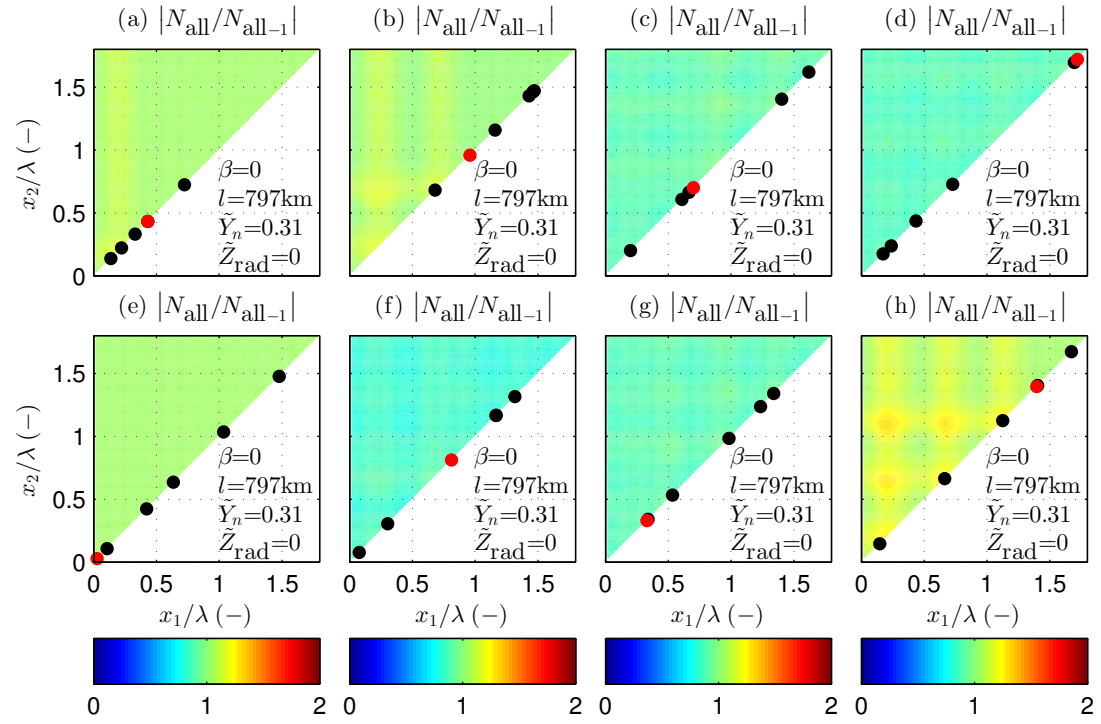

FIGURE E.6: Similar to figure E.5, but now for a prismatic channel.

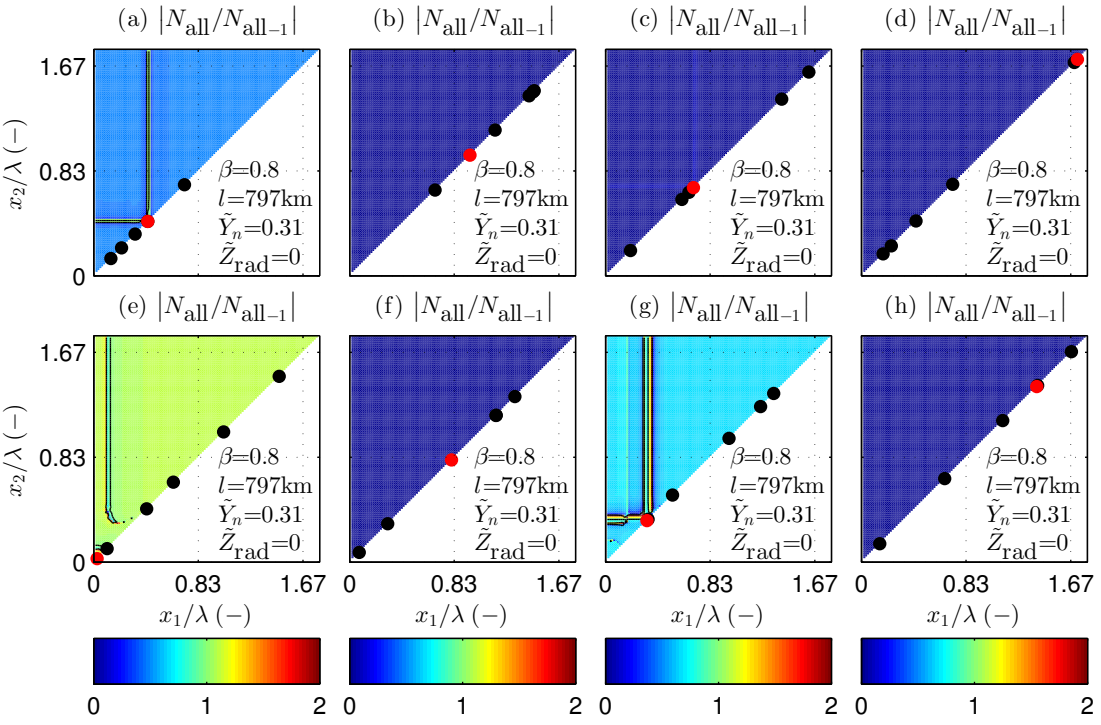

FIGURE E.7: Similar to figure E.5, but now for $\beta = 0.8$.

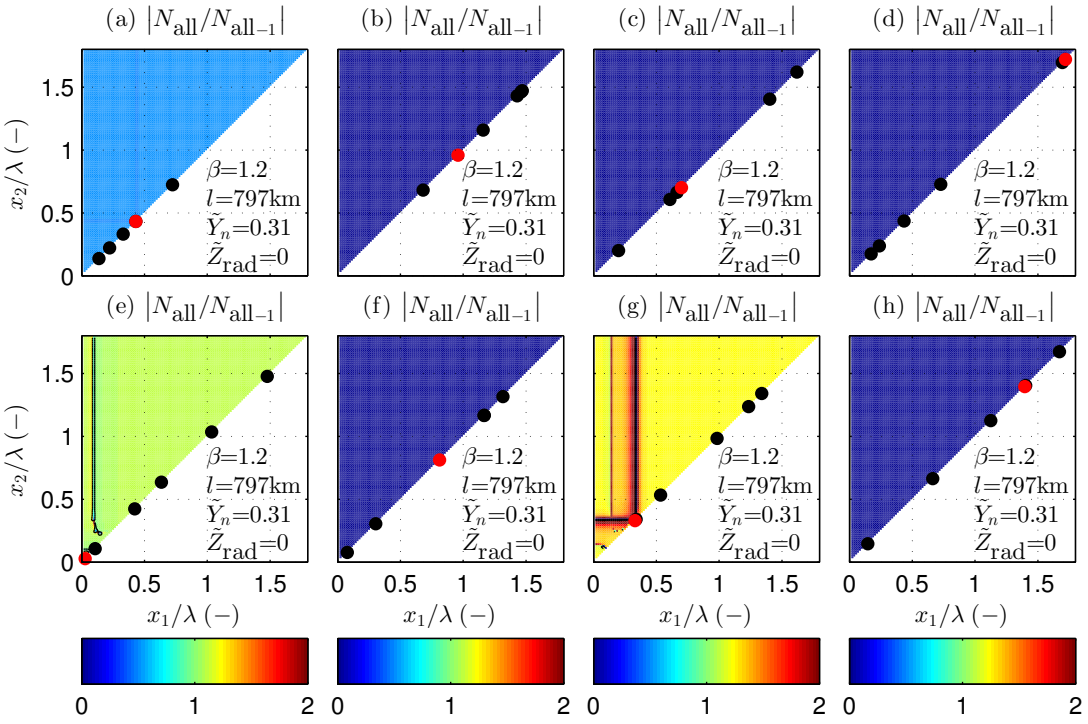

FIGURE E.8: Similar to figure E.5, but now in a supercritically convergent channel.

Appendix F

Overview of current knowledge

On page 108 the results found in this study have been summarised. It presents the most noticeable outcomes of the performed simulations and the analysis of the physical mechanism. Besides, it gives a comprehensive overview of the current knowledge of hydrodynamical effects triggered due to the placement of retention basins along a tidal channel.

Analysis	Prismatic channel		Subcritical convergence		Supercritical convergence	
Physical mechanism	**No basins** Resonance at a quarter (shallow water) wavelength and odd multiples of this.	**One basin** Additional waves develop due to the presence of basins. Different cases of no amplitude change can be found. For small basins and CESD-limit: Amplification of the tide when placed between a node and a successive located seaward node.	**No basins** Wavelength for which resonance occurs increases with convergence. Exponential amplification becomes more important.	**One basin** Cases for which no amplitude change occurs are similar to a prismatic channel. Case II occurs with an unknown phase shift. Areas of amplitude amplification are decreasing with increasing convergence.	**No basins** Resonance does not occur any more, only exponential amplification. Strongly convergent channels move uniformly with the forcing amplitude.	**One basin** Placement near the mouth leads to amplification, placement at all other locations leads to a weakening of the tide. Channel length is not influencing the response of the basin any more.
Two basins	Different amplification and reduction patterns are visible. Interaction between basins may occurs, which can lead to an amplified as well as a weakened response. Larger basins show stronger interactions. Channel length and sea geometry have a large influence on the effects.		For weakly converging channels, the response patterns are not spatially uniform anymore, but show a chaotic pattern for amplification and reduction. For stronger (subcritical) convergence, amplitude amplification only occurs near the channel mouth.		Supercritical converging channels show an overall reduction of the amplitude, except when placed near the channel mouth. Interaction between basins only occurs in close proximity, here the basins show an amplified response. For increasing convergence this interaction decreases.	
Adding one extra basin	The effects of adding an extra basin are according to the described physical mechanism. Interaction between the basins leads to a deviant response.		Overall similar patterns are visible as described above. As opposed to the effects for a prismatic channel, channel length is less important.			
Multiple basins	Overall similar patterns are visible as described above. Multiple basins can lead to a significant reduction (or amplification) of the elevation amplitude.					
Basin geometry	Larger basins show stronger responses than smaller basins. Supercritical forced basins show a reversed pattern of amplification and reduction.		A similar amplification and reduction pattern is visible as for a prismatic channel, here combined with the effects of adding more basins.		Again a similar pattern is visible. Almost no distinction can be made anymore between super- and subcritically forced basins, all types of basins lead to a weakened response.	
Depth transitions	Similarities with width convergence. With a decreasing depth, the shallow water wavelength decreases as well.		Together these properties show an even more pronounced effect.			
Friction	Wave dissipation leads to a dampening of the amplitude. Longer channels shows higher wave dissipation.		Friction leads to a weak shortening of wavelengths, which counteracts channel convergence. Some areas of amplification may occur due to a phase shift.		Since the oscillation has no sinusoidal character anymore, friction only leads to a decrease of the elevation amplitude.	